

Control for Micro-Assembly of Heterogeneous MEMS Microrobots through Common Control Signal

BY

VAHID FOROUTAN

B.S., Central Tehran Branch, Islamic Azad University, Tehran, Iran, 2006

M.S., Science and Research Branch, Islamic Azad University, Tehran, Iran, 2008

Ph.D., Science and Research Branch, Islamic Azad University, Tehran, Iran, 2011

THESIS

Submitted as partial fulfillment of the requirements
for the degree of Doctor of Philosophy in Electrical and Computer Engineering
in the Graduate College of the
University of Illinois at Chicago, 2018

Chicago, Illinois

Defense Committee:

Danilo Erricolo, Chair and Advisor

Milos Zefran

Michael Strocio

Sabri Cetin, Mechanical and Industrial Engineering

Reza Tafreshi, Texas A&M University

Mohammad Elahinia, University of Toledo

Copyright by
VAHID FOROUTAN
2018

To my Mother, Father and Sister.

TABLE OF CONTENTS

<u>CHAPTER</u>	<u>PAGE</u>
1 INTRODUCTION	1
1.1 Microrobots	1
1.2 Multi-Microrobotic Systems	7
2 STRESS-ENGINEERED MICROROBOT	11
2.1 Stress-Engineered Microrobot (MicroStressBot)	12
2.2 GCSR: A Strategy for Multi-Microrobots Control and Assembly	16
3 CLUSTER SYSTEM I: ENABLING GCSR THROUGH CON- TROL SIGNAL DIFFERENTIATION	24
3.1 String-Cluster System	24
3.2 SATurated-Cluster System (SAT-C)	39
3.3 Hardware Experiments	47
3.3.1 Robots with two direct-drive wheels	47
3.3.2 Hardware system	47
3.3.3 Single-shape assembly	50
3.3.4 Robustness against disturbance	52
3.3.5 multiple-shapes assembly	53
4 CLUSTER SYSTEM II: ENABLING GCSR THROUGH CON- TROL SIGNAL DIFFERENTIATION	61
4.1 Cluster-String System	61
4.2 Symmetric Electromechanical SATurated - 1 System (SeSAT-1)	71
4.3 Hardware Experiments	78
4.3.1 Robots with two direct-drive wheels	78
4.3.2 Hardware system	79
4.3.3 Assembly	79
4.3.3.1 Robustness against disturbance	80
5 CONCLUSION	86
APPENDICES	90
CITED LITERATURE	95
VITA	103

LIST OF TABLES

<u>TABLE</u>		<u>PAGE</u>
I	COMPARISON OF THE CONTROL VOLTAGE BANDWIDTH REQUIREMENTS AND CONTROL PULSE EFFICIENCY OF NHG, STRING, SESAT, STRING-CLUSTER AND SAT-C SYSTEMS . .	46
II	EXPERIMENTALLY RECORDED AVERAGES OF THE FORWARD SPEED AND THE TURNING RATE FOR EACH ROBOT IN THE SYSTEM. $(D_1, D_2) = (C_1(D_1), C_1(D_2))$, $(D_3, D_4) = (C_2(D_1), C_2(D_2))$, $(D_5, D_6) = (C_3(D_1), C_3(D_2))$ and finally $(D_7, D_8) = (C_4(D_1), C_4(D_2))$	51
III	EXPERIMENTALLY RECORDED TIME FOR THE ASSEMBLY.	55
IV	COMPARISON OF THE CONTROL VOLTAGE BANDWIDTH REQUIREMENTS OF NHG, STRING, SESAT, R-CLUSTER-STRING AND SESAT-1 SYSTEMS	78

LIST OF FIGURES

<u>FIGURE</u>		<u>PAGE</u>
1	Micro/nano scale robots: (a) Polymer-Based Wireless Resonant Magnetic Microrobot [2] © [2014] IEEE, and (b) Magnetic nano robot [4] © [2012] IEEE.	2
2	Scanning-electron micrograph of two types of stress engineered microflyers [5].	3
3	Optical micrograph of a stress-engineered microflyer attached to a transfer frame [6] © [2008] IEEE, which allows the flyer to be transported and deposited onto the heater. The frame chassis contains attached shadow masks, which protects it during the deposition of the stressor layer [5].	4
4	Tip height of a tethered hinged (i) test structure during the activation of an underlying heater [5]. Inset shows the test structure before (left) and after (right) elevation close to its maximum height.	5
5	Two separate successful levitation experiments using two different types of microflyers (top and bottom) [5]. The optical micrographs show the flyers before (a), during (b) and after (c) levitation. Red arrow indicates the displacement of the flyers during the experiment.	6
6	The kinematics of the MicroStressBots. a) Trajectory with raised steering arm, b) Trajectory with lowered steering arm [6] © [2008] IEEE.	13
7	SEM image of a MicroStressBot [6] © [2008] IEEE.	14
8	Snap-down and release voltages of the MicroStressBots.	15
9	The control and power-delivery waveform for a single MicroStressBot. (a) Turning, (b) Straight-line motion.	21
10	Trajectories of MicroStressBots D_1 and D_2 during partial microassembly [6] © [2008] IEEE.	22

LIST OF FIGURES (Continued)

<u>FIGURE</u>		<u>PAGE</u>
11	(a) Transition voltages for a STRING system of two microrobots, and (b) Control primitives that access three of the hysteresis states for the system.	23
12	Cluster Structure. $V_{dl} = \text{Min}(V_{d1}, V_{d2})$, $V_{dh} = \text{Max}(V_{d1}, V_{d2})$, $V_{ul} = \text{Min}(V_{u1}, V_{u2})$ and $V_{uh} = \text{Max}(V_{u1}, V_{u2})$. Snap-down and release voltages are shown as circles and rectangles.	26
13	String-Cluster system.	27
14	String-Cluster system. Showing the proof of the base condition of Lemma 1.	31
15	String-Cluster system. Showing the proof of the inductive step of Lemma 1.	32
16	Illustration of control cycle in String-Cluster system. (control primitive $P_j(S)$, where $S = 1$)	37
17	Example of an SAT-C system with $k = 4$ and $l = 4$	43
18	a) Schematic of the Robot, b) Kinematics of the Robot.	48
19	Block diagram of the system.	48
20	Transition control points (snap-down and release points).	49
21	Four Clusters: C_1 (yellow), C_2 (pink), C_3 (blue) and C_4 (black) in the system.	50
22	Cross type of target shapes.	52
23	Experimental assembly data using four Clusters (eight robots). (a) Arbitrary initial configuration. (b) Forming the seed shape (ϕ_{k1}) using $C_4(D_1)$ and $C_4(D_2)$ while the rest are confined to the circular trajectories. (c) Forming the second intermediate shape (ϕ_{k2}) using $C_3(D_1)$ and $C_3(D_2)$ while the rest are confined to the circular trajectories, (d) Generating the third intermediate shape (ϕ_{k3}) using $C_2(D_1)$ and $C_2(D_2)$ while the rest are confined to the circular trajectories, and finally (e) Generating the final shape ($\phi_{k4} = \phi_k$) using the $C_1(D_1)$ and $C_1(D_2)$. .	56

LIST OF FIGURES (Continued)

<u>FIGURE</u>		<u>PAGE</u>
24	Experimental assembly data using four Clusters (eight robots). (a) Arbitrary initial configuration, (b) Forming the seed shape (ϕ_{k1}) using $C_4(D_1)$ and $C_4(D_2)$ while the rest are confined to the circular trajectories, (c) Forming the second intermediate shape (ϕ_{k2}) using $C_3(D_1)$ and $C_3(D_2)$ while the rest are confined to the circular trajectories, (d) Generating the third intermediate shape (ϕ_{k3}) using $C_2(D_1)$ and $C_2(D_2)$ while the rest are confined to the circular trajectories, and finally (e) Generating the final shape ($\phi_{k4} = \phi_k$) using the $C_1(D_1)$ and $C_1(D_2)$. .	57
25	Robustness against disturbance experiment using two Clusters (four robots). (a) Arbitrary initial configuration, (b) Generating the final shape ($\phi_{k4} = \phi_k$) using the $C_2(D_1)$ and $C_2(D_2)$ followed by $C_1(D_1)$ and $C_1(D_2)$, (c) Disassembly due to disturbance, (d) Forming the seed shape (ϕ_{k1}) using $C_2(D_1)$ and $C_2(D_2)$ while the rest are confined to the circular trajectories, and finally (e) Generating the final shape ($\phi_{k2} = \phi_k$) using the $C_1(D_1)$ and $C_1(D_2)$	58
26	Multiple shapes assembly (four shapes) using four Clusters (eight robots). (a) Arbitrary initial configuration. (b) Forming the first target shape (ϕ_{k1}) using $C_4(D_1)$ and $C_4(D_2)$ while the rest are confined to the circular trajectories, (c) Forming the second target shape (ϕ_{k2}) using $C_3(D_1)$ and $C_3(D_2)$ while the rest are confined to the circular trajectories, (d) Generating the third target shape (ϕ_{k3}) using $C_2(D_1)$ and $C_2(D_2)$ while the rest are confined to the circular trajectories, and finally (e) Generating the fourth final shape (ϕ_{k4}) using the $C_1(D_1)$ and $C_1(D_2)$	59
27	Multiple shapes assembly (two cross shapes) using four Clusters (eight robots). (a) Arbitrary initial configuration. (b) Forming the first seed shape (ϕ_{k1}) using $C_4(D_1)$ and $C_4(D_2)$ while the rest are confined to the circular trajectories, (c) Forming the second seed shape (ϕ_{k2}) using $C_3(D_1)$ and $C_3(D_2)$ while the rest are confined to the circular trajectories, (d) Generating the first target shape (ϕ_{k3}) using $C_2(D_1)$ and $C_2(D_2)$ while the rest are confined to the circular trajectories, and finally (e) Generating the second final shape (ϕ_{k4}) using the $C_1(D_1)$ and $C_1(D_2)$	60
28	R-Cluster Structure. $V_{dl} = \text{Min}(V_{d1}, V_{d2})$, $V_{dh} = \text{Max}(V_{d1}, V_{d2})$, $V_{ul} = \text{Min}(V_{u1}, V_{u2})$ and $V_{uh} = \text{Max}(V_{u1}, V_{u2})$. Snap-down and release voltages are shown as circles and rectangles.	63

LIST OF FIGURES (Continued)

<u>FIGURE</u>		<u>PAGE</u>
29	R-Cluster-String system. Showing the proof of the inductive step of Lemma 1.	65
30	Illustration of control cycle in R-Cluster-String system. a) Control primitive $P_{12}(S)$, where $S = 0$, b) Control primitive $P_{12}(S)$, where $S = 1$, c) Control primitive $P_{12}(S)$, where $S = 2$, and d) Control primitive $P_{12}(S)$, where $S = 3$	81
31	Illustration of control cycle in <i>R-Cluster-String</i> system. a) Control primitive $P_i(S)$, where $S = 0$ and $i = 3$, and b) Control primitive $P_i(S)$, where $S = 1$ and $i = 3$	82
32	Illustration of Nested Group (<i>NG</i>)	82
33	Example of a SeSAT-1 system with $K = 4$ and $L = 4$	83
34	a) Schematic of the Robot, b) Kinematics of the Robot.	83
35	Experimental assembly data using eight robots. a) Arbitrary initial configuration, b) Forming the seed shape, c) Forming the intermediate shape, and finally d) Generating the final shape.	84
36	Robustness against disturbance experiment using four robots. a) Arbitrary initial configuration, b) Generating the final shape, c) Disassembly due to disturbance, d) Forming the intermediate shape, and finally e) Generating the final shape.	85
37	Permission for Chapter 1 Reference 2	91
38	Permission for Chapter 1 Reference 4	92
39	Permission for Chapter 1 Reference 5	93
40	Permission for Chapter 1 and Chapter 2 Reference 6	94

SUMMARY

We present a new efficient control framework for controlling groups of heterogeneous stress-engineered MEMS microrobots for accomplishing the micro-assembly process. The objective is to maximize the number of controllable microrobots in the system while keeping the number of external global signals as low as possible (highly underactuated system). This work proposes a theoretical control strategy that could complete multiple-shapes microassembly from arbitrary initial configuration where all the control primitives can be accompanied with a constant number ($O(1)$) of control pulses of the power delivery waveform. We show that with the new control strategy not only we can have a highly underactuated system but also we will have a robust controllable system which could complete the microassembly started from arbitrary initial configuration. These control methods are sufficient to implement a system that is robust against disturbance.

The main contributions of the proposed control strategy is that 1) it can accomplish the process of the microassembly from arbitrary initial configuration, 2) it can control a highly underactuated microrobotic-system which allows maximizing the number of simultaneously individually controllable robots, 3) the size of the programming waveform does not grow with population size (i.e. size of the control primitive is $O(1)$), 4) it is robust against disturbance and finally, 5) the assembly can be efficiently nucleated with arbitrary number of seed shapes.

We focus on microrobotic systems that can be modeled as nonholonomic unicycles. We validate the control policy with hardware experiments for implementing planar assembly using

SUMMARY (Continued)

multiple robots with direct drive wheels. These results lay the foundation for developing new methods to control of a large number of MEMS microrobots.

CHAPTER 1

INTRODUCTION

*(Some parts of this chapter are copied from my published paper with the following citation:
V. Foroutan, R. Majumdar, O. Mahdavi pour, S. P. Ward, and I. Paprotny, " Levitation of
untethered stress-engineered microflyers using thermophoretic (Knudsen) force," in Tech. Dig.
Hilton Head Workshop 2014: A Solid-State Sensors, Actuators and Microsystems Workshop,
Jun. 2014, pp. 105 – 106)*

Authors contributions: Vahid Foroutan performed the experiments and data analysis; Ratul Majumdar performed the device fabrication and stress-engineering; Omid Mahdavi pour helped in writing the manuscript and drawing the figures; Spencer Ward performed the theoretical modeling and calculations; Igor Paprotny conceived the idea and supervised the project.

1.1 Microrobots

Micro/nano robots are micro/nano-scale, complex devices designed to perform a specific task or repeatitive tasks with accuracy. Microscale robotic systems have many applications in areas such as biomedicine [8], surveillance [9], or microassembly [10]. Magnetic micro/nano robots [1, 2,4,11,12], thermal microflyers [13], miniature (unmanned aerial vehicles) UAVs systems [14–16], omnicopter micro aerial vehicle [17], the scratch-drive micro-robot [18], optically controlled bacteria [3], the electric-field-controlled paramecium [19,20] and the magnetic-field-controlled

bacteria [21,22] are the examples of such microrobots. Figure 1 shows some of these micro/nano robots.

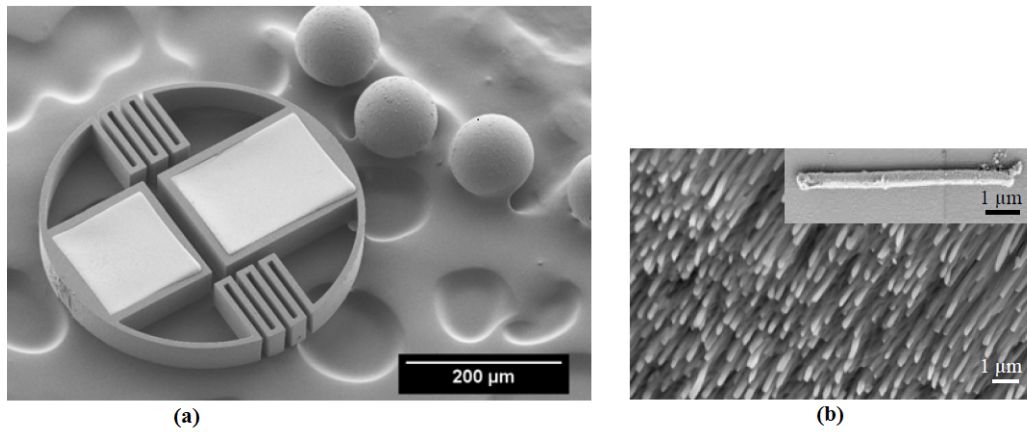


Figure 1: Micro/nano scale robots: (a) Polymer-Based Wireless Resonant Magnetic Microrobot [2] © [2014] IEEE, and (b) Magnetic nano robot [4] © [2012] IEEE.

The first experimental validation of successful untethered levitation of $300\mu\text{m} \times 300\mu\text{m}$ sized microscale structures (microflyers) was shown in [5]. As shown in [5], the device is actuated (levitated) by thermal force generated by an underlying microfabricated heater. This is the first validation of potentially a new type of actuation mechanism for MEMS structures, which may pave way for new class of free-flying microscale robots. The microflyer chassis was fabricated

using a surface micromachining process. To stabilize the device during flight, the chassis was curved out-of-plane using an in-situ masked MEMS stress-engineering process.

The initially planar microrobot chassis was fabricated from polycrystalline silicon (polysilicon) using a multi-user MEMS fabrication process. The flyers and the heaters were released in hydrofluoric acid (49% HF), and out-of-plane curvature was generated using a novel post-release stress engineering process. Figure 2 shows a scanning-electron micrograph of two of the stress-engineered microflyers that were successfully levitated during the experiments.

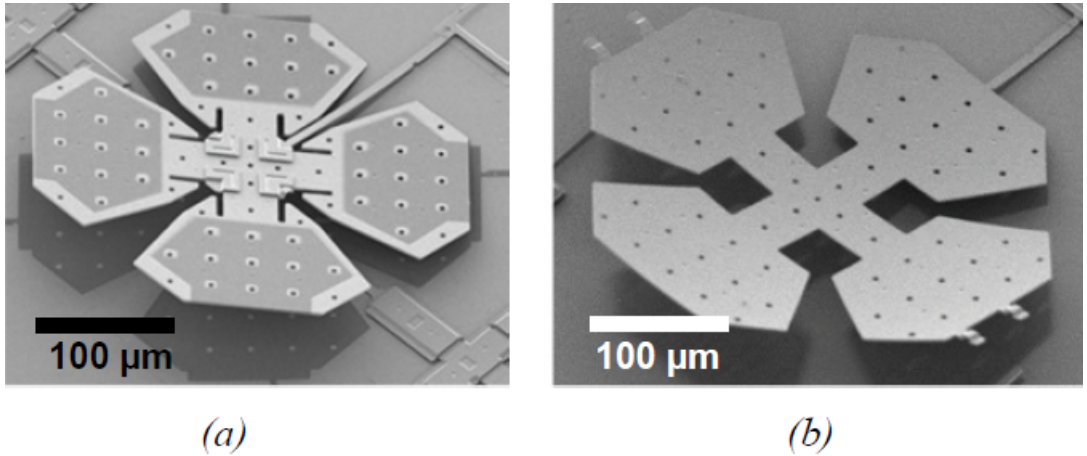


Figure 2: Scanning-electron micrograph of two types of stress engineered microflyers [5].

The microflyers were fabricated attached to the transfer frames [6] to enable successful transfer and placement on the heater prior to levitation. Figure 3 shows an optical micrograph

of a transfer frame. Microprobes inserted into the hinges of the transfer frame can be used to transport the microflyers between their location on the die and the fabricated heater.

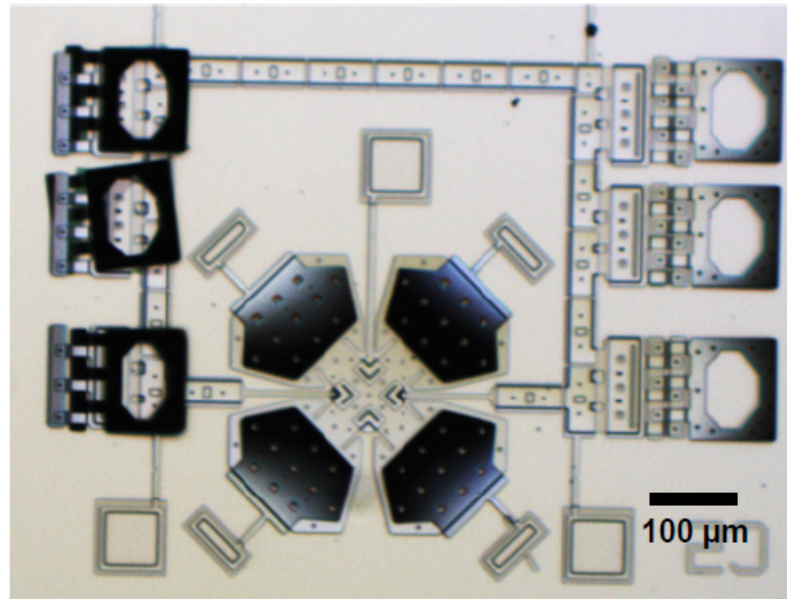


Figure 3: Optical micrograph of a stress-engineered microflyer attached to a transfer frame [6]
 © [2008] IEEE, which allows the flyer to be transported and deposited onto the heater. The frame chassis contains attached shadow masks, which protects it during the deposition of the stressor layer [5].

It has been demonstrated in [5] both the actuation of microfabricated test structures using the thermal force, as well as the levitation of the untethered microrobot. Figure 4 shows the

elevation of a tethered hinged test structure (as shown in the inset optical micrographs) using thermophoretic force generated by an underlying heater. These experimental results confirm our theoretical modeling of the thermophoretic force.

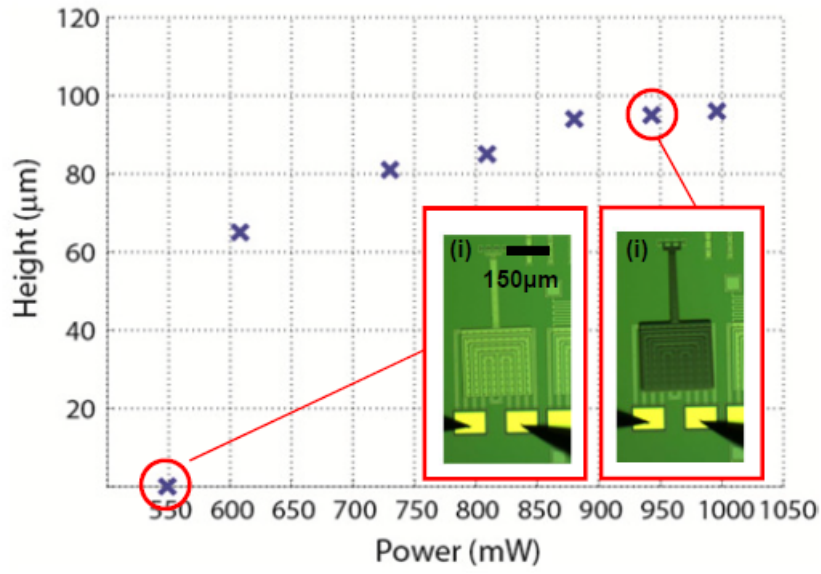


Figure 4: Tip height of a tethered hinged (i) test structure during the activation of an underlying heater [5]. Inset shows the test structure before (left) and after (right) elevation close to its maximum height.

Figure 5 shows images of microflyers prior to take-off, mid-flight, and after landing, in two separate levitation experiments. Because the heater was approximately the same size as the

microflyer, the device would always translate towards its periphery. As expected, landing would occur as soon as significant part of the microflyer chassis would transit outside of the heated area.

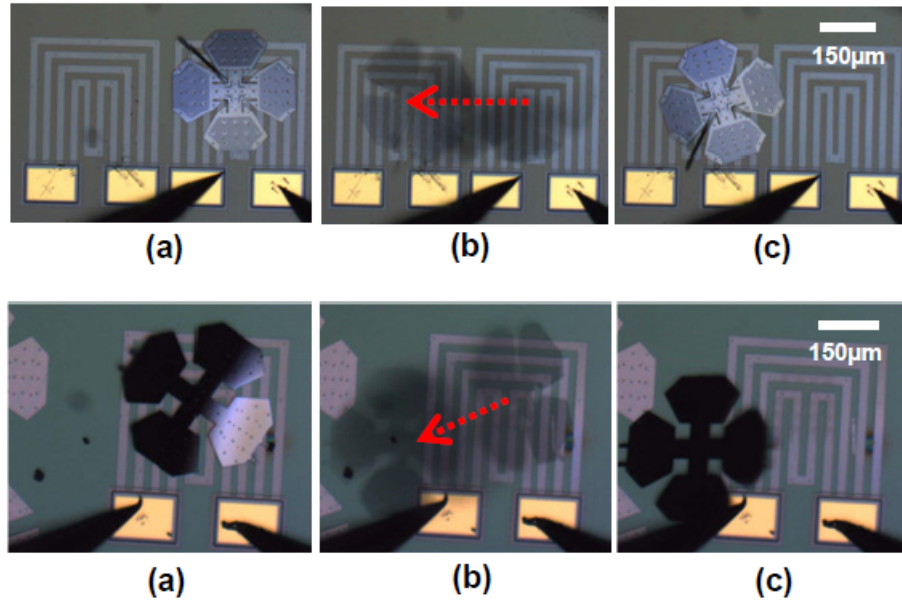


Figure 5: Two separate successful levitation experiments using two different types of microflyers (top and bottom) [5]. The optical micrographs show the flyers before (a), during (b) and after (c) levitation. Red arrow indicates the displacement of the flyers during the experiment.

1.2 Multi-Microrobotic Systems

A group of centimeter-scale robots with enough on-board capabilities such as on-board power and communication has been built and controlled in [23,24]. As it has been shown in [25], even the swarm of millimeter scale robots have been successfully developed with enough on-board battery, tactile sensing capabilities and ICs for control. Controlling large swarm of simple microrobots is challenging due to communication and onboard-computation constraints. New control strategies have to be devised to provide time-efficient independent control of individual microrobot within a large population. One of the strategies could be dedicated sources of power and actuation [26–28] for each robot. This could be done by creating local magnetic fields with an array of microcoils [29, 30] or electrically insulating the subsystems from one another [31–33] or using resonant frequencies of vibration for a specific component [34] or using selective transmittance windows made from photonic band gap materials [35]. Another strategy could be controlling the system by global external signals [36–42]. Researchers have developed different techniques for external global control signals for the group of micro-scale robots in the system such as Multi-microrobotic system using optical energy [43–47], Multi-microrobotic using magnetic fields [48–52] and/or Multi-microrobotic system utilizing physiological energy [53–57].

Traditional control approaches consider specific control signals for each robot [58, 59], but these techniques suffer from the linear increase in control and communication bandwidth by the increase in robots population. This becomes more challenging as the size of the microrobot decreases.

In [60,61], controlling a distributed system of many devices that differ in behavior falls under the concept of Ensemble Control (EC). In Ensemble Control (EC), the robots are modeled as nonholonomic unicycles with inhomogeneity in turning and linear velocity. By using state feedback control policy, a globally asymptotically stable ensemble of unicycles controlled by uniform control inputs is achieved. It has been shown in [61] that the ensemble of nonholonomic unicycles is asymptotically stable by using a suitable Lyapunov function. Although EC provides promising control policy to any number of robots in theory, in practice it is not successful for more than ten robots due to the control error (system noise), which cancels the inhomogeneity effect. Also, EC needs a perfect state estimation, and the controllers require at worst a matrix inversion and at best a summation over all robot states which is not practical for a large number of robots. In [61], the control policy is based on the robots local coordinate, and the trajectory of each robot is independent and disregards collision, which is impractical for any microrobotic system due to stiction effects.

Recently microrobots with physical heterogeneity are produced. They respond differently to a global control signal. Stress-engineered MEMS microrobot (MicroStressBots) [6,7,62,63], independently controllable magnetic structures with different cross-sections [64], and microrobots with different resonant frequencies in a global magnetic field [65] are the examples of such microrobots. The manipulation control primitives based on heterogeneity increase linearly with the size of the population, making their control challenging. Global Control Selective Response (GCSR) is a strategy to control and maneuver robots to complete the microassembly. GCSR uses design-induced heterogeneity of stress-engineered MEMS microrobot (MicroStressBots)

and causes differences between their trajectories to maneuver the robots from an initial to a target goal configuration. As stated in [7], GCSR uses the control matrix to control the single robot sequentially while the other robots are confined to circular trajectories. Although GCSR could reduce the control signal bandwidth requirements to $O(\sqrt{n})$ where n is the number of microrobots in the system, it is not an efficient control theory for completing microassembly from arbitrary initial configuration. As stated in [7], GCSR could only control one microrobot at each iteration of the microassembly process freely while electrostatically anchored the others, making their independent control from arbitrary initial configuration difficult. Control strategies in [7] are not able to control two MicroStressBots simultaneously. Hence, creating the seed-shape for starting the microassembly process could only be possible from specific initial configurations of microrobots. As it has been shown in [7], the number of control primitives increases linearly with the number of microrobots, which shows that the control theory cannot be implemented for a large population of microrobots in the system.

In [66], control strategies for physical homogeneous robots (identical robots) are proposed. Although it is shown that the manipulation primitives can be accomplished with a constant number of commands, this system is not controllable in an obstacle free environment and also is impractical for any microrobotic system due to stiction effects.

In this dissertation, we propose a general microassembly control theory for the highly underactuated system based on physical heterogeneity in an obstacle free environment where all the control primitives can be accompanied with a constant number ($O(1)$) of control pulses of the power delivery waveform. We show that with the new control strategy not only we

can have a highly underactuated system but also we will have a robust controllable system which could complete microassembly started from arbitrary initial configuration. First section of chapter 2 focuses on Stress-Engineered Microrobot (MicroStressBot). We discuss the kinematics, fabrication and the power delivery techniques for stress-engineered MEMS microrobot (MicroStressBots). Second section of chapter 2 discusses the Global Control Selective Response (GCSR) strategy for controlling multiple Microrobots. Chapter 3 focuses on the Cluster System I control theory for the highly underactuated system based on physical heterogeneity in an obstacle free environment. In chapter 4, we introduce the Cluster System II that is robust against disturbance and capable of accomplishing microassembly from arbitrary initial configurations. Chapter 5 concludes our discussion.

CHAPTER 2

STRESS-ENGINEERED MICROROBOT

(Some parts of this chapter are copied from my paper with the following citation: Vahid Foroutan, Farhad Farzami, Danilo Erricolo, Ratul Majumdar, and Igor Paprotny, "SAT-C: An Efficient Control Strategy for Assembly of Heterogenous Stress-Engineered MEMS Microrobots," International Conference on Robotics and Automation (ICRA), 2018.

Authors contributions: Vahid Foroutan conceived the idea, proved it, developed the macroscale platform for experiments and wrote the paper; Farhad Farzami helped in setting up the experimental platform and drawing the figures; Danilo Erricolo supervised the project; Ratul Majumdar helped in drawing some figures; Igor Paprotny defined the project, supervised and led the paper writing.

(Some parts of this chapter are copied from my paper with the following citation: Vahid Foroutan, Farhad Farzami, Danilo Erricolo, and Igor Paprotny, "Efficient Constant-Time Addressing Scheme for Parallel-Controlled Assembly of Stress-Engineered MEMS Microrobots," International Conference on Control, Automation and Robotics (ICCAR), 2018.

Authors contributions: Vahid Foroutan conceived the idea, proved it, developed the macroscale platform for experiments and wrote the paper; Farhad Farzami helped in setting up the experimental platform and drawing the figures; Danilo Erricolo supervised the project; Igor Paprotny supervised the paper writing.

2.1 Stress-Engineered Microrobot (MicroStressBot)

Figure 6 shows the schematic of the stress-engineered MEMS microrobot (MicroStressBot). This robot includes an untethered scratch drive actuator (USDA) and an out-of-plane steering-arm actuator [62]. The USDA actuator causes forward motion and the steering-arm decides if the robot moves straight or turns. The USDA is $120\ \mu\text{m} \times 60\ \mu\text{m} \times 1.5\ \mu\text{m}$ and the steering-arm actuator is approximately $120\ \mu\text{m}$ to $160\ \mu\text{m}$. MicroStressBot is unicycle (can turn in one direction) and is unidirectional (can only move forward). It is not small-time locally controllable (STLC). The configuration is defined as $q = (x, y, \theta)$ and its configuration space by $\mathcal{Q} = \mathbb{R}^2 \times \mathbb{S}^1$. The kinematics of MicroStressBot is

$$\dot{q} = u \begin{bmatrix} \cos \theta \\ \sin \theta \\ 0 \end{bmatrix} + \omega \begin{bmatrix} 0 \\ 0 \\ 1 \end{bmatrix} \quad (2.1)$$

where u and ω are linear velocity and turning rate.

The MicroStressBot is fabricated from polycrystalline silicon using a MEMS foundry process [68]. Post-processing is used to curve out-of-plane (upwards) the steering arm of MicroStressBot [69]. As it has been shown in [69], a layer of high compressive stressor material such as Chromium(Cr) is patterned and deposited to provide an out-of-plane curvature. The thickness of the deposited material and the area covered by the stressor layer must be precisely defined, such that the steering arm is deflected at the preset actuation voltage. Figure 7 shows the scanning-electron microscope (SEM) image of a MicroStressBot. The microrobot

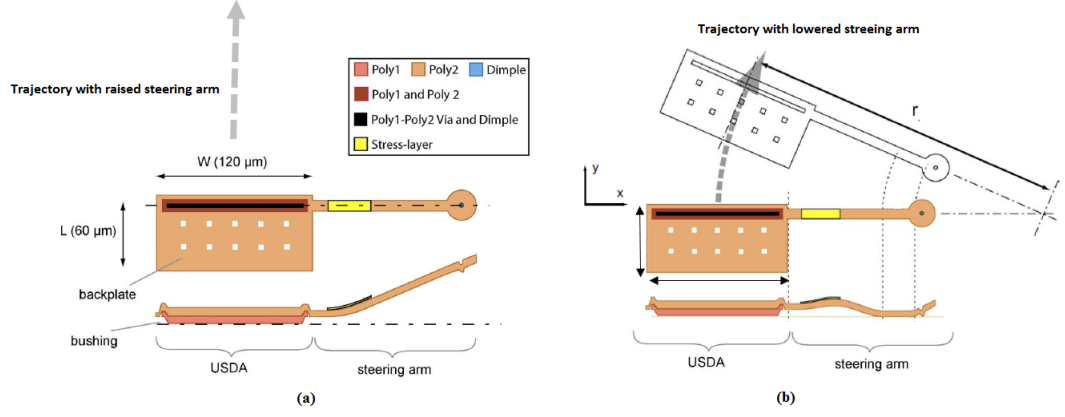


Figure 6: The kinematics of the MicroStressBots. a) Trajectory with raised steering arm, b) Trajectory with lowered steering arm [6] © [2008] IEEE.

is actuated on a special substrate. The substrate consists of a field of insulated interdigitated electrodes. A capacitive circuit is built between the body of the microrobot and the substrate by applying a voltage waveform between the pairs of electrodes. The electric potential of the formed capacitive coupling provides power for the actuation of the USDA and also controls the state of the steering arm. The voltage waveform that results in capacitive coupling of the microrobot chassis and the substrate is called the control waveform. This waveform has two parts: a) Control-cycle: the pulses that controls the hysteresis state of the steering arm, and b) Power-delivery-cycle: that results in the USDA translation. The power-delivery-cycle consists of pulses that change between a minimum V_b and a maximum V_s . In order to actuate

the USDA, V_s must be greater than the minimum voltage (V_{flex}) at which the backplate of the USDA is flexed, while V_b must be less than the maximum voltage (V_{rel}) at which the flexure in the backplate is relaxed. V_{flex} and V_{rel} are described in more detail in [70].

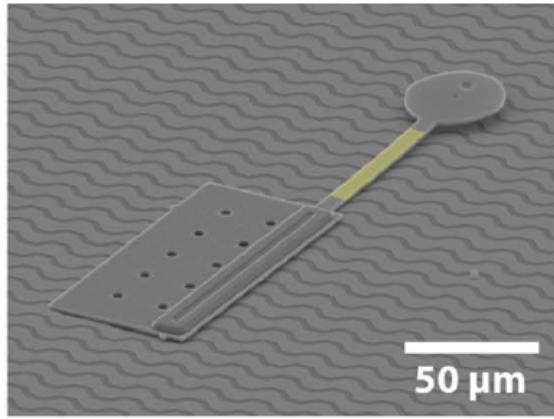


Figure 7: SEM image of a MicroStressBot [6] © [2008] IEEE.

The steering arm of MicroStressBot changes its state at two different voltage levels. The voltage level, at which the steering arm is lowered and the robot is turning, is called snap-down voltage (V_d) and the voltage level at which the arm is raised and the robot is moving straight, is called the release voltage (V_u). These voltage levels are the transition voltages of the steering arm. The steering arm is pulled into contact with the substrate if the voltage applied to the microrobot is equal or greater the snap-down transition voltage (V_d) and the steering arm is

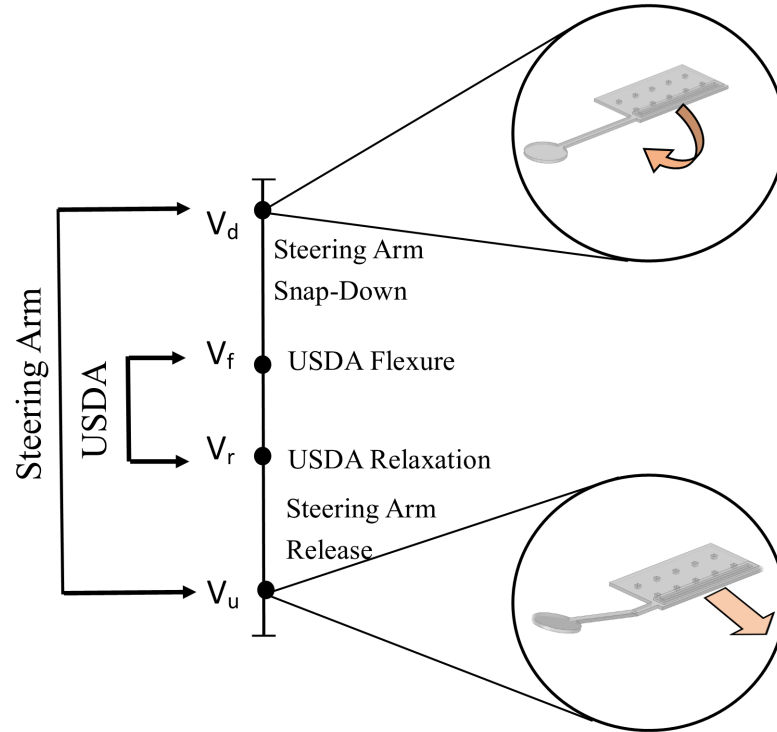


Figure 8: Snap-down and release voltages of the MicroStressBots.

released if the voltage applied to the microrobot is equal or less than the release transition voltage (V_u). The steering-arm position denotes the hysteresis state of the microrobot. When the arm is raised, the hysteresis state is 0 and when the arm is lowered, the hysteresis state is 1. Figure 8 shows the effect of snap-down and release voltages.

2.2 GCSR: A Strategy for Multi-Microrobots Control and Assembly

The waveforms that program the hysteresis states of the system are called control primitives. For a single robot, the control primitive is defined as a triple voltage pulses (V_a , V_b , V_p). The robot moves straight when a control primitive with $V_a < V_d$ or $V_b < V_u$ is applied, and the robot turns when a control primitive with $V_a > V_d$, and $V_b > V_u$ is applied to the system. $V_a > V_d$, and $V_b > V_u$ keeps the steering arm lowered through the stepping cycle while $V_a < V_d$ or $V_b < V_u$ releases the steering arm. Figure 9 shows the control and power-delivery waveform for a single MicroStressBot.

As stated in [7], in order to control n microrobots, the control primitive contains up to $2n$ control pulses. In this work, we propose a new control primitive technique that provides exactly 6 control pulses for controlling n microrobots and unlike the previous techniques relying on heterogeneity, does not increase with the population size.

Global Control-Selective Response (GCSR) [7] is a control strategy for planar microassembly of heterogeneous MicroStressBots. GCSR uses the control matrix for controlling and maneuvering the robots from their predefined initial configurations to their target goal configurations. The strategy of GCSR is utilizing the control matrix to maneuver single robot sequentially to the final configuration while the other robots turn without advancing to the final configuration. The control matrix is constructed by a mapping between the accessible control primitives and the hysteresis states of the system. The control primitives are the waveforms that encode the hysteresis states of the system and the hysteresis states of the system define the motion of the individual robots. In the control matrix, each entry contains the hysteresis states of all

microrobots during the applied control primitive. The resulting sequence of control primitives is called the control sequence, usually denoted by S . Figure 10 shows the trajectory of a microrobot D_1 from initial (a) to target (b) configuration (docking with a seed-shape (c)), during the application of control sequence $S = \{P_0, P_2, P_1, P_2, P_1, P_2, P_1, P_2, P_1\}$. During this partial assembly robot D_2 orbits without advancing to goal. This type of GCSR (STRING (STRICly Non-nested hysteresis Gap)) is designed to be sequential (i.e. one robot at a time is maneuvered towards the goal) to increase the number of controllable microrobots and enable robust collision avoidance.

In order to control n microrobots, accessing 2^n possible hysteresis states are sufficient but not necessary. As it is shown in [7], using $n + 1$ hysteresis states is enough to control n robots sequentially (control the single robot sequentially while the other robots are confined to the circular trajectories) from specific initial configurations (predefined initial configuration). For an n -microrobotic system, V_{di} and V_{ui} define the snap-down and release voltages of microrobot i . In general, an n -microrobotic system is STRING (STRICly Non-nested hysteresis Gap) system if the robots in the system have been sorted according to ascending values of V_{di} and V_{ui} . The n STRING microrobots are labeled D_i , where $i \in \{1, \dots, n\}$. It has been shown in [7] that an n -robot STRING system has exactly $n + 1$ accessible hysteresis states with the two pulses control primitive P_j . These pulses snaps down all the microrobot D_i steering arms for $i \leq j$, and releases the microrobot D_i steering arms for all $i > j$. Figure 11 shows the relation between the transition voltages and control primitives for three accessible hysteresis states of the STRING system.

The control matrix that shows the mapping between control primitives and hysteresis states in a STRING system is called a STRING control matrix. Let matrix A be a control-matrix of size $n \times m$. Each entry A_{ij} is the microrobot j th hysteresis state when the i th control primitive is applied. In the STRING control matrix, the robots start turning when the higher index i control primitives are applied. The STRING control matrix for four devices is:

$$A = \begin{matrix} & \begin{matrix} D_1 & D_2 & D_3 & D_4 \end{matrix} \\ \begin{matrix} P_1 \\ P_2 \\ P_3 \\ P_4 \\ P_5 \end{matrix} & \left(\begin{array}{cccc} 0 & 0 & 0 & 0 \\ 1 & 0 & 0 & 0 \\ 1 & 1 & 0 & 0 \\ 1 & 1 & 1 & 0 \\ 1 & 1 & 1 & 1 \end{array} \right) \end{matrix} \quad (2.2)$$

The order of the assembly is set by the STRING control matrix (it starts sequentially from applying control primitives with the highest index i down to the control primitive with $i = 1$) to reduce the parallel motion to sequential motion for single robots (while the other robots are confined to the circular trajectories). The process of assembling the target goal shape starts with maneuvering two robots (D_n and D_{n-1}) from specific initial configuration to form the seed shape while the others are confined to the circular trajectories. As an example, assembly in a system with 4 microrobots, starts with D_4 and D_3 . In order to control D_4 and D_3 simultaneously, $2^2 = 4$ hysteresis states are required while the other microrobots are confined to the circular trajectories (*hysteresisstate* = 1). As it can be seen from the last three rows of STRING matrix

For four robots, D_3 and D_4 could be exactly in three states while the others are confined to the circular trajectories ($hysteresisstate = 1$). In STRING (STRICly Non-nested hysteresis Gap) type of GCSR, only 3 out of the 4 hysteresis states for the first two robots forming the seed-shape are accessible, making their independent control challenging and accomplishing micro-assembly from an arbitrary initial configuration difficult. It is shown in [7], the first two robots (D_n and D_{n-1}) are positioned manually into particular places before the start of the assembly process in such a way that forming the seed shape does not need the full access to 4 hysteresis states. Following the assembly of the seed shape from the specific initial configuration of the first two robots, single robots (D_i where $i \in \{n-2, \dots, 1\}$) are maneuvered sequentially, progressively assembling the target shape using the STRING control matrix. It has been shown in [7] that microassembly can be implemented on a group of MicroStressBots only from specific initial configurations if a STRING matrix can be generated for such system. V_{di} and V_{ui} are the snap-down and release voltages of the microrobot i in an n microrobotic system. Let the number of independent transition voltage levels (pull-down and release voltages) of the global control signal be called the control voltage bandwidth ζ of a Multi-microStressBots system. The number of accessible hysteresis states of the system depends on the relation between the robots hysteresis gaps. Let δ_v be the maximum deviation of the transition voltage that is revealed during the operation of the microrobot. The two transition voltages are independent if they are separated by at least $2\delta_v$.

In [7], three different strategies for designing the transition voltage levels of the microrobots have been proposed. The goal of these techniques is to minimize the control bandwidth size with

respect to the population size of the robots in the system and create a highly underactuated system. Nested Hysteresis Gaps (NHG) is the first control strategy introduced in [7]. In NHG, a system of n steering arms is sorted according to ascending V_{di} and descending for V_{ui} . All 2^n hysteresis states are accessible in NHG system. However, NHG system suffers from the large control bandwidth size. In NHG, each robot needs two control voltage levels. Hence, the control voltage bandwidth in NHG system is $\zeta_n = 2n$. The other control strategy is Strictly non-nested hysteresis gaps (STRING) [7]. A system of n steering arms is STRING, if the robots are sorted corresponding to ascending values of V_{di} and V_{ui} . It has been shown in [7] that $n + 1$ hysteresis states are accessible in STRING system and the control bandwidth requirement for a STRING system is $\zeta_n = n + 1$. Because the STRING system cannot access all the 2^n states, a sequential microassembly algorithm has been deployed in [7] to complete the assembly process. The third control strategy introduced in [7] is SESat control strategy. It can access at least $n + 1$ hysteresis states which are essential for sequential microassembly algorithm and also the control bandwidth requirement is $\zeta_n = \lceil 2\sqrt{n} \rceil$. As it has been shown in [7], SESat control primitives increase linearly with the size of the population. Hence, implementing microassembly on a large number of robots is challenging.

A key contribution of the proposed work is the novel practical, reconfigurable and time efficient control strategy for GCSR that could complete multi-shapes microassembly (control strategy that could create multiple target assembly shapes) from arbitrary initial configuration with constant control primitives.

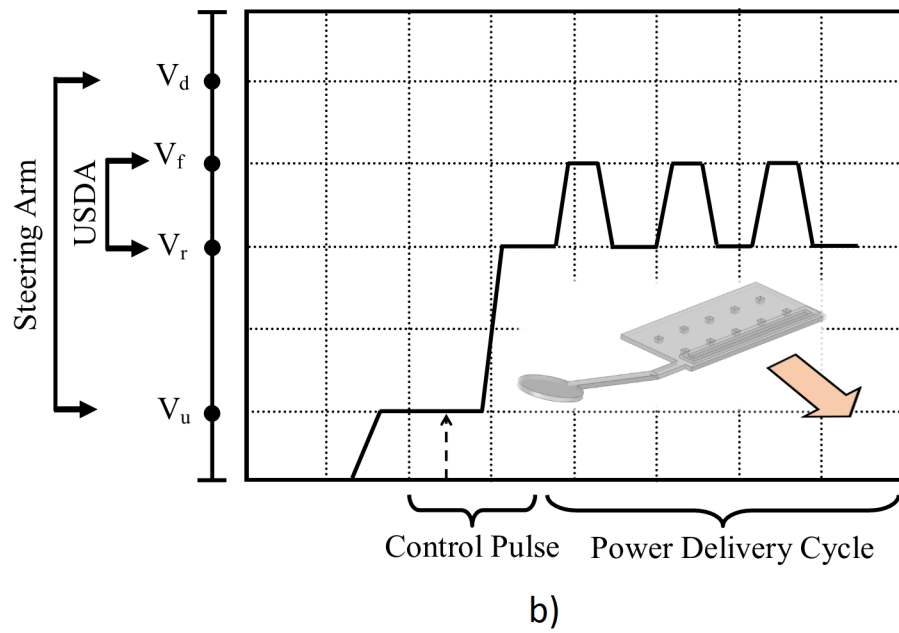
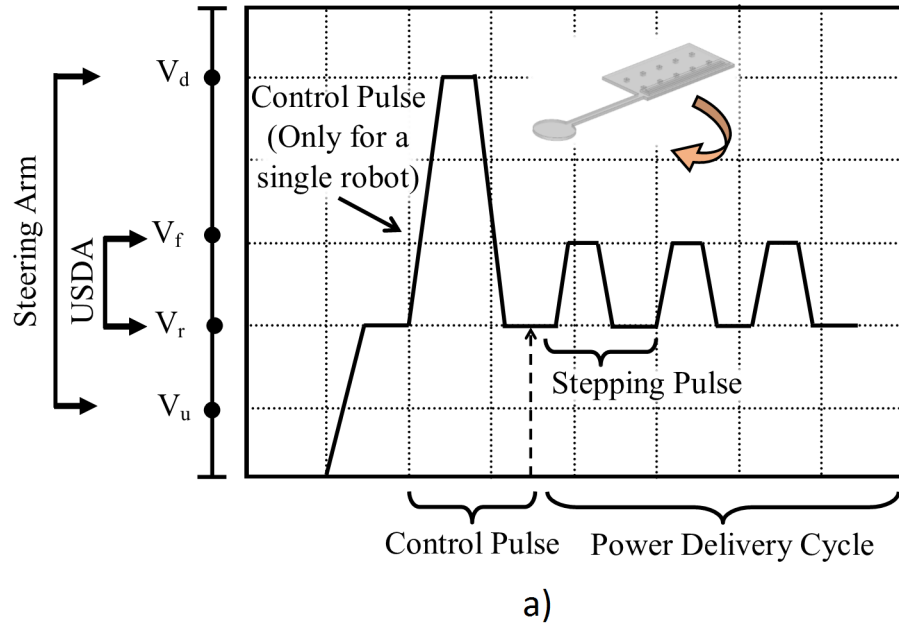


Figure 9: The control and power-delivery waveform for a single MicroStressBot. (a) Turning, (b) Straight-line motion.

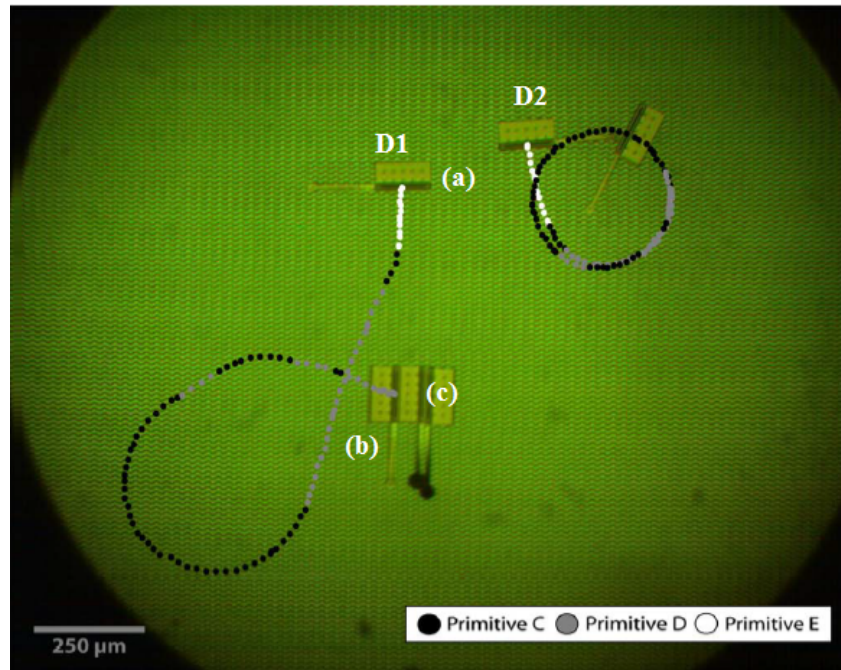


Figure 10: Trajectories of MicroStressBots D_1 and D_2 during partial microassembly [6] © [2008]

IEEE.

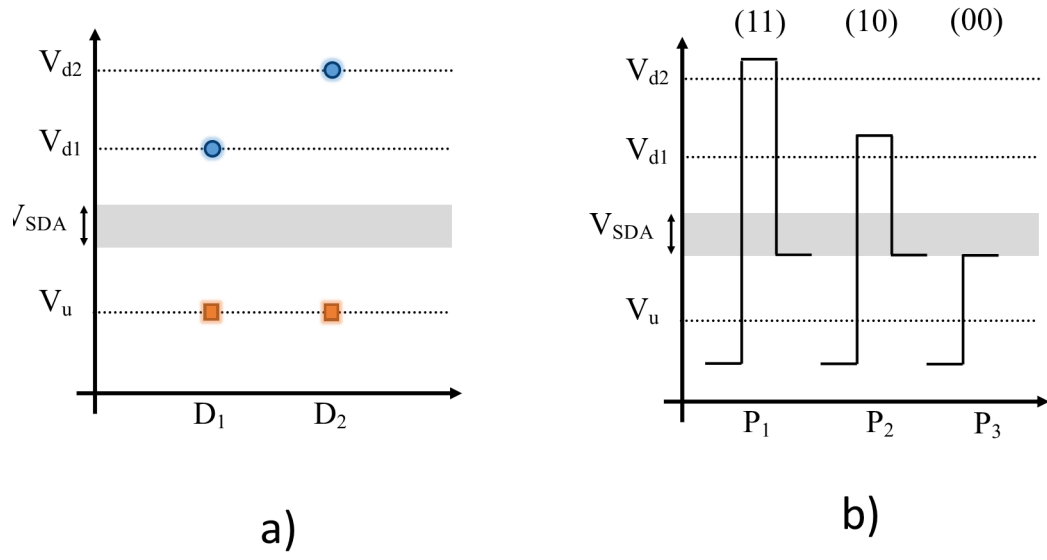


Figure 11: (a) Transition voltages for a STRING system of two microrobots, and (b) Control primitives that access three of the hysteresis states for the system.

CHAPTER 3

CLUSTER SYSTEM I: ENABLING GCSR THROUGH CONTROL SIGNAL DIFFERENTIATION

(Some parts of this chapter are copied from my paper with the following citation: Vahid Foroutan, Farhad Farzami, Danilo Erricolo, Ratul Majumdar, and Igor Paprotny, "SAT-C: An Efficient Control Strategy for Assembly of Heterogenous Stress-Engineered MEMS Microrobots," International Conference on Robotics and Automation (ICRA), 2018.

Authors contributions: Vahid Foroutan conceived the idea, proved it, developed the macroscale platform for experiments and wrote the paper; Farhad Farzami helped in setting up the experimental platform and drawing the figures; Danilo Erricolo supervised the project; Ratul Majumdar helped in drawing some figures; Igor Paprotny defined the project, supervised and led the paper writing.

3.1 String-Cluster System

In this section, we introduce a control strategy that not only have the control voltage bandwidth $\zeta_n = O(n)$ but also is capable of controlling two microrobots simultaneously. We start with the following definitions:

Definition 1. *Nested-Group-Microrobots (NGM) set:*

Set of all groups of two Microrobots that forms a *Nested-Hysteresis-Gaps (NHGs)* structure is *Nested-Group-Microrobots (NGM)*.

$$NGM = \{(D_i, D_j) | D_i, D_j \in M, V_{dj} > V_{di}, V_{ui} > V_{uj}; i, j \in \mathbb{N}\} \quad (3.1)$$

V_d and V_u are snap-down and release voltages. M is the set of all microrobots in the system.

$M = \{D_1, D_2, \dots, D_n\}$; where D_i is the i th Micorobot in the system.

Definition 2. *Nested-Group-Microrobots Cluster (Cluster):* Each member of NGM is called *Cluster*.

$$Cluster = \forall (D_i, D_j) \in NGM; i, j \in \mathbb{N} \quad (3.2)$$

In each Cluster, we define $V_{dl} = \text{Min}(V_{di}, V_{dj})$, $V_{dh} = \text{Max}(V_{di}, V_{dj})$, $V_{ul} = \text{Min}(V_{ui}, V_{uj})$ and $V_{uh} = \text{Max}(V_{ui}, V_{uj})$, respectively. Figure 12 shows the transition voltages in a Cluster.

Definition 3. *STRICtly Non-nested hysteresis-Gaps (String)-Cluster (String-Cluster) system:* This system consists of Clusters where each two microrobots in two different Clusters form a String system. This system is formed by Equation 3.3.

$$String - Cluster = \{Cluster \in NGM | \forall Cluster_k,$$

$$Cluster_m(k < m); V_{dh,k} \leq V_{dl,m}, V_{uh,k} \leq V_{ul,m}; m, k \in \mathbb{N}\} \quad (3.3)$$

In an M Clusters microrobotic system, the robots have been sorted according to ascending values of V_{dl} , V_{dh} , V_{ul} and V_{uh} . In this system, there is always non-nested hysteresis gaps

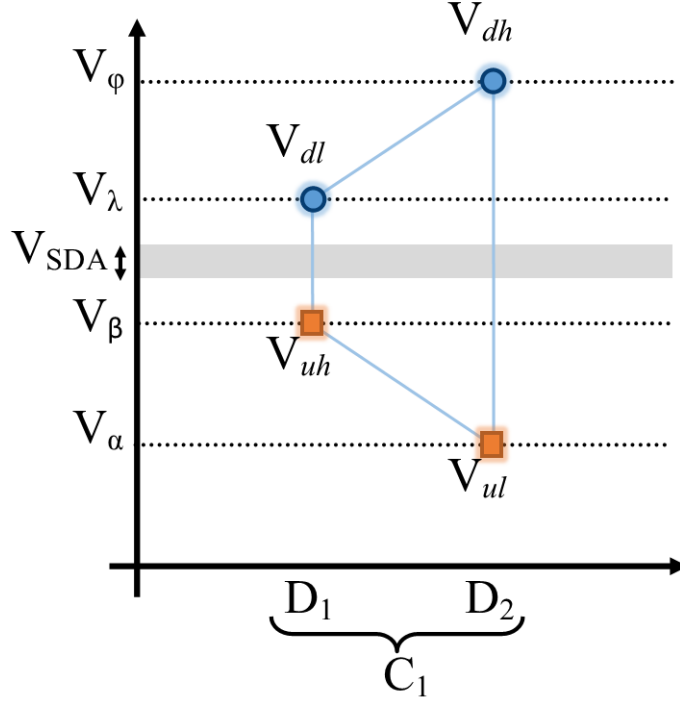


Figure 12: Cluster Structure. $V_{dl} = \text{Min}(V_{d1}, V_{d2})$, $V_{dh} = \text{Max}(V_{d1}, V_{d2})$, $V_{ul} = \text{Min}(V_{u1}, V_{u2})$ and $V_{uh} = \text{Max}(V_{u1}, V_{u2})$. Snap-down and release voltages are shown as circles and rectangles.

between each two microrobots belong to different Clusters. Figure 13 shows a String-Cluster system.

Lemma 1. *An M – String – Cluster system has exactly $\frac{3}{2}(n - 4) + 7 = 3(M - 2) + 7$ accessible hysteresis states, where $M = \text{no. Clusters}$, $n = \text{no. Microrobots}$ and $M = n/2$.*

Proof. By Induction:

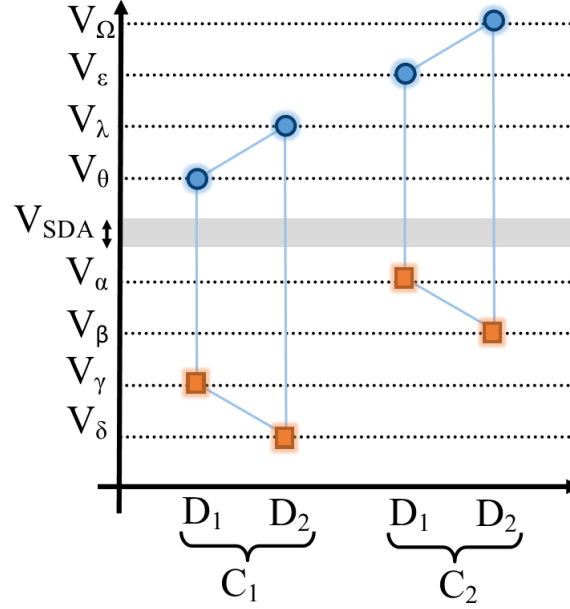


Figure 13: String-Cluster system.

Base condition: An *String – Cluster* system with $M = 2$ has seven accessible states. In each Cluster, we have two microrobots sorted in an *NHG* system format. Let $M = 2$ Clusters microrobotic system consist of two Clusters C_1 and C_2 , where each Cluster C_i consists of two microrobots $\{D_1, D_2\}$. In Cluster C_1 , the microrobots got 2 states: (0 = arm up) and (1 = arm down). Hence, we have $2^2 = 4$ states (00 = arm up, arm up), (01 = arm up, arm down), (10 = arm down, arm up) and (11 = arm down, arm down). Without loss of generality, $V_{dh,1} \leq V_{dl,2}$ and $V_{uh,1} \leq V_{dl,2}$. Figure 14 shows the ranges for transition voltages of Cluster C_2 , such that the $M = 2$ Clusters microrobotic system becomes *String – Cluster*. Let assume

that V_δ, \dots, V_ψ are the significantly independent transition voltage levels, ordered such that $V_\delta \leq V_\gamma \leq V_\beta \leq V_\alpha \leq V_\zeta \leq V_\theta \leq V_\lambda \leq V_\epsilon \leq V_\phi \leq V_\Omega \leq V_\psi$ with $|V_\Omega - V_\phi| = 2\delta_v$ and $|V_\zeta - V_\alpha| = 2\delta_v$. Let $V_{dl,1} = V_\epsilon$, $V_{dh,1} = V_\phi$ and $V_{ul,1} = V_\beta$, $V_{uh,1} = V_\alpha$. It follows that the snap-down voltage $V_{dl,2}$ can have value $V_1 \in (V_\phi, V_\Omega]$, or voltage $V_2 = V_\phi$ and the snap-down voltage $V_{dh,2}$ can have value $V_3 \in (V_\Omega, V_\psi]$, or voltage $V_4 = V_\Omega$ and $|V_{dh,2} - V_{dl,2}| \geq 2\delta_v$. Similarly, the release voltage, $V_{uh,2}$ can have the value $V_5 \in (V_\zeta, V_{rel} - 2\delta_v]$ or voltage $V_6 = V_\zeta$, and the release voltage $V_{ul,2}$ can have the value $V_7 \in (V_\alpha, V_\zeta]$ or voltage $V_8 = V_\alpha$ and $|V_{uh,2} - V_{ul,2}| \geq 2\delta_v$. Consequently, for C_1 and C_2 microrobotic system to remain *String-Cluster*, the release and snap-down voltages of C_2 could be one of the following combinations: (V_1, V_5, V_3, V_7) , (V_1, V_5, V_3, V_8) , (V_1, V_6, V_3, V_8) , (V_2, V_5, V_3, V_7) , (V_2, V_5, V_3, V_8) , (V_2, V_6, V_3, V_8) , (V_2, V_5, V_4, V_7) , (V_2, V_5, V_4, V_8) and (V_2, V_6, V_4, V_8) .

We examine each case separately.

(V_1, V_5, V_3, V_7) : because of $V_{dl,2}$, $V_{dh,2}$ are greater than the snap-down voltages of C_1 , $(V_{dl,2} > V_{dl,1})$, $(V_{dl,2} > V_{dh,1})$, and $(V_{dh,2} > V_{dl,1})$, $(V_{dh,2} > V_{dh,1})$, we can only snap down the arms of D_1 and D_2 in C_2 after we snap down the arms of C_1 . Since $V_{ul,2}, V_{uh,2}$ is greater than the release voltages of C_1 , $(V_{ul,2} > V_{ul,1})$, $(V_{ul,2} > V_{uh,1})$, and $(V_{uh,2} > V_{ul,1})$ and $(V_{uh,2} > V_{uh,1})$, we can only release the arms of C_1 after we have released the arms of D_1 and D_2 in C_2 . Because the $(V_{dh,2} > V_{dl,2} > V_{dh,1} > V_{dl,1})$, we can snap down C_1 and D_1 of C_2 while D_2 of C_2 is released. Since the $(V_{uh,2} > V_{ul,2} > V_{uh,1} > V_{ul,1})$, we can release D_1 of C_2 while D_2 and all other Clusters are snapped down. Consequently, we can change the states of C_2 to 01, 10 or 11 when C_1 is in

state 11. During all other states of the system the state of C_2 is 00. Consequently, the number of accessible hysteresis states increase by exactly 3.

(V_1, V_5, V_3, V_8) : This case is similar to (V_1, V_5, V_3, V_7) , except that the arm of D_1 of Cluster C_1 is released at the same time as the arm of D_2 of Cluster C_2 . As long as $V_{dh,2} > V_{dl,1}$, we can snap down the arm of D_2 of C_2 only after all other Clusters are in state 11. As a consequence the number of accessible hysteresis states increase by exactly 3.

(V_2, V_5, V_3, V_7) : The snap-down voltage D_1 of C_2 is equal to the snap-down voltage of D_2 of C_1 , $V_{dl,2} = V_{dh,1}$. In this case, the arm of D_1 of C_2 and the arm of D_2 of C_1 are snapped down at a same time. Since the release voltage of D_1 of C_2 is greater than the release voltages of C_1 , ($V_{uh,2} > V_{uh,1} > V_{ul,1}$), we can only release the arm D_2 of C_1 after we release the arm D_1 of C_2 . As in the (V_1, V_5, V_3, V_7) case, the state of C_2 must be 00 except when C_1 , is snapped down, then D_1 of C_2 can be either 00, 01, 10 or 11 by varying the release voltages. Consequently, the number of accessible hysteresis states increases by exactly 3.

(V_2, V_5, V_3, V_8) : This case is similar to (V_1, V_5, V_3, V_7) , except that the snap-down voltage D_1 of C_2 is equal to the snap-down voltage of D_2 of C_1 , $V_{dl,2} = V_{dh,1}$. In this case, the arm of D_1 of C_2 and the arm of D_2 of C_1 are snapped down at the same time. Since the release voltage of D_1 of C_2 is greater than the release voltages of C_1 , ($V_{uh,2} > V_{uh,1} > V_{ul,1}$), we can only release the arm D_2 of C_1 after we release the arm D_1 of C_2 . In this case, the arm of D_1 of Cluster C_1 is released at the same time as the arm of D_2 of Cluster C_2 . As long as $V_{dh,2} > V_{dl,1}$, we can snap

down the arm of D_2 of C_2 only after all other Clusters are in state 11. As in the (V_1, V_5, V_3, V_7) case, the state of C_2 is 00 except when C_1 is 11, then C_2 can be assigned to 00, 01, 10 or 11 by varying the release voltages. Hence, the hysteresis states number increases by exactly 3.

(V_2, V_6, V_3, V_8) : This case is similar to (V_2, V_5, V_3, V_8) .

(V_1, V_6, V_3, V_8) : This case is similar to (V_1, V_5, V_3, V_8) .

(V_2, V_5, V_4, V_7) : This case is similar to (V_2, V_5, V_3, V_7) .

(V_2, V_5, V_4, V_8) : This case is similar to (V_2, V_5, V_3, V_8) .

(V_2, V_6, V_4, V_8) : This case is similar to (V_2, V_5, V_3, V_8) .

We know that C_1 had four states, by adding C_2 to the system the number of states increased by exactly 3. Hence, in an *String – Cluster* system with 2 Clusters, the number of accessible hysteresis states is 7.

Inductive step: Adding a Cluster to the system will increase the number of accessible control states by exactly 3, if both M and $M + 1$ Clusters system remain *String – Cluster*.

Consider M Clusters microrobotic system, C_1, \dots, C_M , where each Cluster C_i consists of two microrobots (D_1, D_2) , to be a *String – Cluster* system sorted according to $V_{dl,i}, V_{dh,i}$ and $V_{ul,i}, V_{uh,i}$. Without loss of generality, $V_{dh,M} \leq V_{dl,M+1}$ and $V_{uh,M} \leq V_{ul,M+1}$. The transition voltages ranges of Cluster C_{M+1} are shown in Figure 15. This is the structure that causes the new $M + 1$ Clusters microrobotic system remain *String – Cluster*. Let assume that V_δ, \dots, V_ψ are the significantly independent transition voltage levels, ordered such that $V_\delta \leq V_\gamma \leq V_\beta \leq$

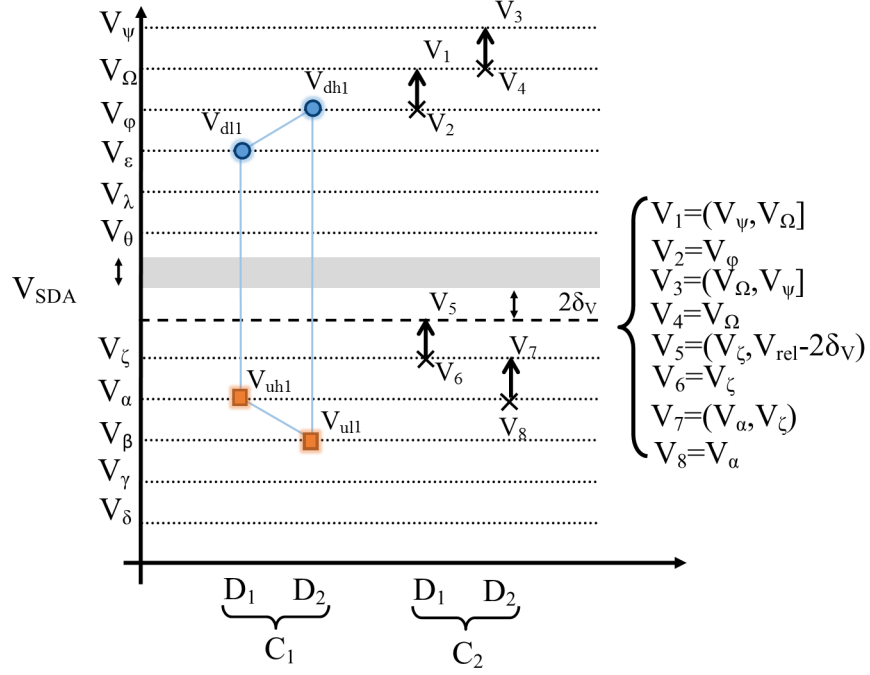


Figure 14: String-Cluster system. Showing the proof of the base condition of Lemma 1.

$V_\alpha \leq V_\zeta \leq V_\theta \leq V_\lambda \leq V_\epsilon \leq V_\phi \leq V_\Omega \leq V_\psi$ with $|V_\Omega - V_\phi| = 2\delta_v$ and $|V_\zeta - V_\alpha| = 2\delta_v$. Let $V_{dl,M} = V_\epsilon$, $V_{dh,M} = V_\phi$ and $V_{ul,M} = V_\beta$, $V_{uh,M} = V_\alpha$. It follows that the snap-down voltage $V_{dl,M+1}$ can have value $V_1 \in (V_\phi, V_\Omega]$, or voltage $V_2 = V_\phi$ and the snap-down voltage $V_{dh,M+1}$ can have value $V_3 \in (V_\Omega, V_\psi]$, or voltage $V_4 = V_\Omega$ and $|V_{dh,M+1} - V_{dl,M+1}| \geq 2\delta_v$. Similarly, the release voltage, $V_{uh,M+1}$ can have the value $V_5 \in (V_\zeta, V_{rel} - 2\delta_v]$ or voltage $V_6 = V_\zeta$, and the release voltage $V_{ul,M+1}$ can have the value $V_7 \in (V_\alpha, V_\zeta]$ or voltage $V_8 = V_\alpha$ and $|V_{uh,M+1} - V_{ul,M+1}| \geq 2\delta_v$.

Consequently, for the $M + 1$ Cluster microrobotic system to remain *String-Cluster*, the release and snap-down voltages of C_{M+1} could be one of the following combinations: (V_1, V_5, V_3, V_7) , (V_1, V_5, V_3, V_8) , (V_1, V_6, V_3, V_8) , (V_2, V_5, V_3, V_7) , (V_2, V_5, V_3, V_8) , (V_2, V_6, V_3, V_8) , (V_2, V_5, V_4, V_7) , (V_2, V_5, V_4, V_8) and (V_2, V_6, V_4, V_8) . We examine each case separately:

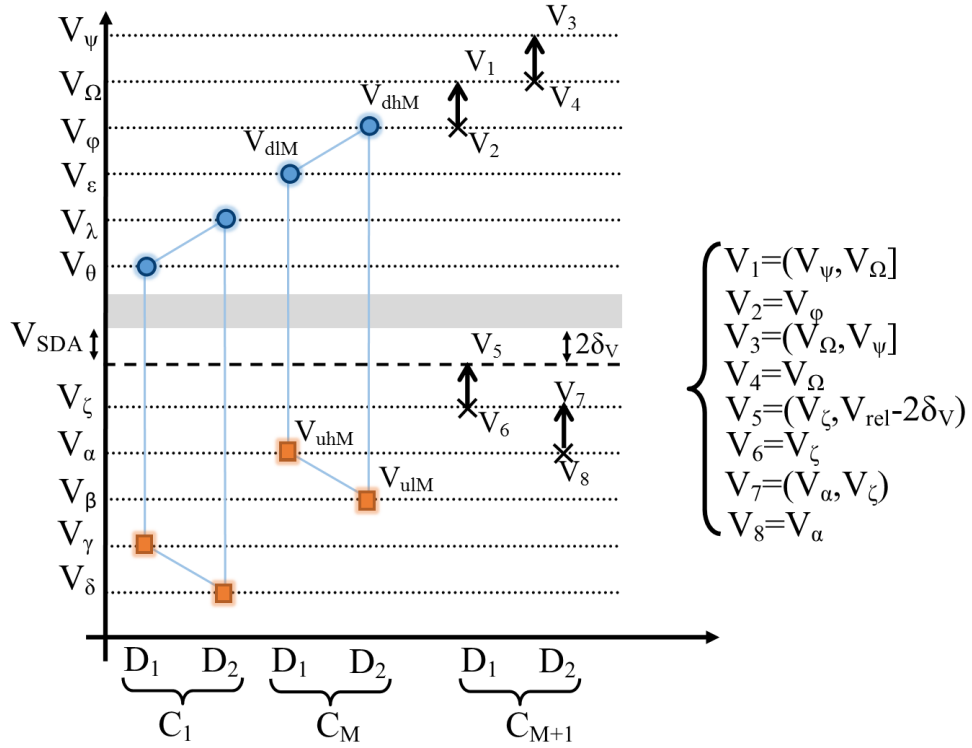


Figure 15: String-Cluster system. Showing the proof of the inductive step of Lemma 1.

(V_1, V_5, V_3, V_7): because of $V_{dl,M+1}, V_{dh,M+1}$ are greater than the snap-down voltages of C_1, \dots, C_M ; ($V_{dl,M+1} > V_{dh,i} > V_{dl,i}$) and ($V_{dh,M+1} > V_{dh,i} > V_{dl,i}$), $i \in Z_M$ where $Z_M = \{1, \dots, M\}$, we can only snap down the arm of D_1 and D_2 in C_{M+1} after we snap down the arms of all other Clusters. Since $V_{ul,M+1}$ and $V_{uh,M+1}$ is greater than the release voltages of C_1, \dots, C_M , ($V_{ul,M+1} > V_{uh,i} > V_{ul,i}$), and ($V_{uh,M+1} > V_{uh,i}, V_{ul,i}$), $i \in Z_M$ where $Z_M = \{1, \dots, M\}$, we can only release the arms of all C_1, \dots, C_M after we have released the arm of D_1 and D_2 in C_{M+1} . Because the ($V_{dh,M+1} > V_{dl,M+1} > V_{dl,i}, V_{dh,i}$), $i \in Z_M$ where $Z_M = \{1, \dots, M\}$, we can snap down all other Clusters and D_1 of C_{M+1} while D_2 of C_{M+1} is released. Since the ($V_{uh,M+1} > V_{ul,M+1} > V_{uh,i} > V_{ul,i}$), $i \in Z_M$ where $Z_M = \{1, \dots, M\}$, we can release D_1 of C_{M+1} while D_2 and all other Clusters are snapped down. Consequently, we can change the states of C_{M+1} to 01, 10 or 11 when C_1, \dots, C_M have been assigned state 11. For the other states the C_{M+1} is in state 00. As a consequence, the number of accessible hysteresis states increase by exactly 3.

(V_1, V_5, V_3, V_8): This case is similar to (V_1, V_5, V_3, V_7), except that the arm of D_1 of Cluster C_M is released at the same time as the arm of D_2 of Cluster C_{M+1} . As long as $V_{dh,M+1} > V_{dl,M}$, we can snap down the arm of D_2 of C_{M+1} only after all other Clusters are in state 11. As a consequence, the number of accessible hysteresis states increase by exactly 3.

(V_2, V_5, V_3, V_7): The snap-down voltage D_1 of C_{M+1} is as same as the snap-down voltage of D_2 of C_M , $V_{dl,M+1} = V_{dh,M}$. The arm of D_1 of C_{M+1} and the arm of D_2 of C_M are snapped down at the same time. Since the D_1 of C_{M+1} release voltage is greater than the release voltages

of C_1, \dots, C_M , $V_{uh,M+1} > V_{ul,i}, V_{uh,i}, i \in Z_M$ where $Z_M = \{1, \dots, M\}$, we can only release the arm D_2 of C_M after we release the arm D_1 of C_{M+1} . As in the (V_1, V_5, V_3, V_7) case, the state of C_{M+1} must be 00 except when C_1, \dots, C_M are all snapped down, then of D_1 of C_{M+1} can be either 00, 01, 10 or 11 by varying the release voltages. Consequently, the number of accessible hysteresis states increases by exactly 3.

(V_2, V_5, V_3, V_8) : This case is similar to (V_1, V_5, V_3, V_7) , except that The snap-down voltage D_1 of C_{M+1} is equal to the snap-down voltage of D_2 of C_M , $V_{dl,M+1} = V_{dh,M}$. The arm of D_1 of C_{M+1} and the arm of D_2 of C_M are snapped down at the same time. Since the D_1 of C_{M+1} release voltage is greater than the release voltages of C_1, \dots, C_M , $V_{uh,M+1} > V_{ul,i}, V_{uh,i}, i \in Z_M$ where $Z_M = \{1, \dots, M\}$, we can only release the arm D_2 of C_M after we release the arm D_1 of C_{M+1} . In this case, the arm of D_1 of Cluster C_M is released at the same time as the arm of D_2 of Cluster C_{M+1} . As long as $V_{dh,M+1} > V_{dl,M}$, we can snap down the arm of D_2 of C_{M+1} only after all other Clusters are in state 11. As in the (V_1, V_5, V_3, V_7) case, the state of C_{M+1} must be 00 except when C_1, \dots, C_M are all snapped down. when all C_1, \dots, C_M are snapped down C_{M+1} can be either 00, 01, 10 or 11. As a consequence, the number of accessible hysteresis states increase by exactly 3.

(V_2, V_6, V_3, V_8) : This case is similar to (V_2, V_5, V_3, V_8) .

(V_1, V_6, V_3, V_8) : This case is similar to (V_1, V_5, V_3, V_8) .

(V_2, V_5, V_4, V_7) : This case is similar to (V_2, V_5, V_3, V_7) .

(V_2, V_5, V_4, V_8) : This case is similar to (V_2, V_5, V_3, V_8) .

(V_2, V_6, V_4, V_8) : This case is similar to (V_2, V_5, V_3, V_8) .

It has been shown that by adding a Cluster to a *String – Cluster* system, we can increase the number of hysteresis states by exactly 3. By considering the base case (7 states for the first two Clusters), it follows by induction that every $M - \text{String} - \text{Cluster}$ system has exactly $\frac{3}{2}(n - 4) + 7 = 3(M - 2) + 7$ accessible hysteresis states, where M = number of Clusters, n = number of Microrobots and $M = n/2$. (Base condition = 7 states for the first two Clusters)

□

Now we can design the control primitives and also the corresponding control matrix. The $\frac{3}{2}(n - 4) + 7$ hysteresis states of an $M - \text{String} - \text{Cluster}$ system are included in the control matrix. We construct the control primitive $P_j(S)$ such that it assigns the state 11 to all Clusters C_i for $i < j$, and 00 to all Cluster C_i for $i > j$, and based on the value of S , it can assign the states 00, 01, 10 or 11 to C_j . P_j is defined by two control pulses, $P_j(S) = (V_{a,1}, V_{a,2})$ with a decision variable S . Consider the *String – Cluster* system shown in Figure 16, where $V_\delta, \dots, V_\Omega$ represent significantly independent control voltage levels. S selects the Hysteresis state of C_j :

$$C_j - \text{Hysteresis} - \text{States} = \begin{cases} "00", & \text{if } S = 0 \\ "01", & \text{if } S = 1 \\ "10", & \text{if } S = 2 \\ "11", & \text{if } S = 3 \end{cases} \quad (3.4)$$

$$P_j(S) = \begin{cases} (V_{dl,j}, V_{ul,j}^+) & \text{if } j \in Z_M, S = 0 \\ (V_{dh,j}, V_{ul,j}^+) & \text{if } j \in Z_M, S = 1 \\ (V_{dl,j}, V_{uh,j}^+) & \text{if } j \in Z_M, S = 2 \\ (V_{dh,j}, V_{uh,j}^+) & \text{if } j \in Z_M, S = 3 \end{cases} \quad (3.5)$$

where $V_{ul,j}^+ = V_{ul,j} + \delta_v$ and $V_{uh,j}^+ = V_{uh,j} + \delta_v$.

When $S = 0$, $(V_{a,1})$ snaps down the steering arms of all of the Clusters C_i , $i \in Z_{j-1}$, where $Z_{j-1} = \{1, \dots, j-1\}$, and D_1 of Cluster C_j . The second control pulse $(V_{a,2})$ keeps all the Clusters C_i , $i \in Z_{j-1}$ snapped down while all other Clusters are released.

For $S = 1$, $(V_{a,1})$ snaps down the steering arms of all of the Clusters C_i , $i \in Z_j$ where $Z_j = \{1, \dots, j\}$, and also all microrobots D_1 of C_k , $k > j$ with $V_{dl,k} = V_{dh,j}$. All the Clusters C_k , $k > j$ and the microrobot D_1 of C_j that were snapped down by the first control pulse will be released by the second control pulse $V_{a,2}$.

For $S = 2$, $(V_{a,1})$ snaps down the steering arms of all of the Clusters C_i , $i \in Z_{j-1}$, where $Z_{j-1} = 1, \dots, j-1$, and D_1 of Cluster C_j . The second control pulse $V_{a,2}$ keeps all the Clusters C_i , $i \in Z_{j-1}$ and D_1 of Cluster C_j snapped down while all other Clusters are released.

When $S = 3$, $(V_{a,1})$ snaps down the steering arms of all of the Clusters C_i , $i \in Z_j$, and also it snaps down all microrobots D_1 of C_k , $k > j$ with $V_{dl,k} = V_{dh,j}$. All the Clusters C_k , $k > j$ that were snapped down by the first control pulse will be released by the second control pulse $V_{a,2}$.

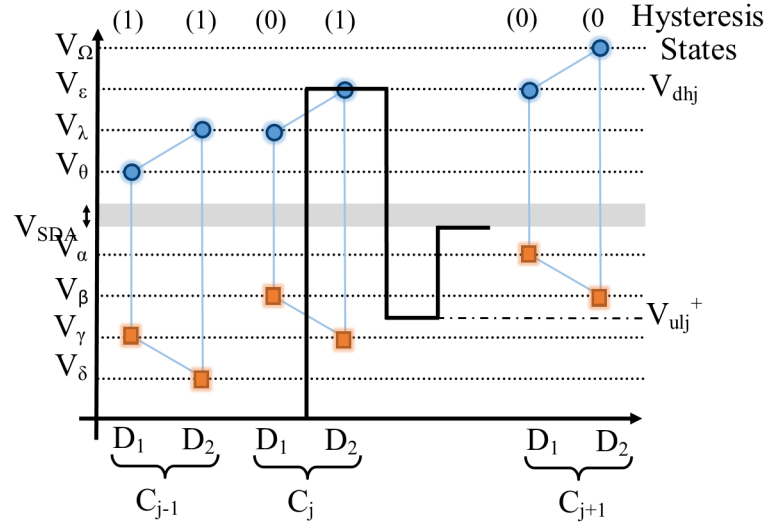


Figure 16: Illustration of control cycle in String-Cluster system. (control primitive $P_j(S)$, where $S = 1$)

The $(\frac{3}{2}(n-4)+7) \times n$ control matrix A can be formed by the $\frac{3}{2}(n-4)+7$ control primitives constructed by $P_j(S)$. As an example, Equation 3.6 shows such a control matrix for two clusters (Four robots).

$$A = \begin{matrix} & C_1(D_1) & C_1(D_2) & C_2(D_1) & C_2(D_2) \\ \begin{matrix} P_1 \\ P_2 \\ P_3 \\ P_4 \\ P_5 \\ P_6 \\ P_7 \end{matrix} & \begin{pmatrix} 0 & 0 & 0 & 0 \\ 0 & 1 & 0 & 0 \\ 1 & 0 & 0 & 0 \\ 1 & 1 & 0 & 0 \\ 1 & 1 & 0 & 1 \\ 1 & 1 & 1 & 0 \\ 1 & 1 & 1 & 1 \end{pmatrix} \end{matrix} \quad (3.6)$$

Let the Matrix A be the *String – Cluster* control matrix and let the $\frac{3}{2}(n - 4) + 7$ control primitives be the *String – Cluster* control primitives. These $\frac{3}{2}(n - 4) + 7$ control primitives create $\frac{3}{2}(n - 4) + 7$ hysteresis states and we refer to these states as the *String – Cluster* hysteresis states. The order of the assembly is set by the *String – Cluster* control matrix. In the *String – Cluster* system instead of the parallel motion of all microrobots, two robots are controlled and maneuvered toward the target shape progressively while the other robots confined to the circular trajectories. The process of assembling the target goal shape starts with maneuvering two robots ($D_n = C_n(D_2)$ and $D_{n-1} = C_n(D_1)$) from arbitrary configuration to form the seed shape while the others confined to the circular trajectories. As an example, the assembly in a system with 4 microrobots starts with D_4 and D_3 . In order to control D_4 and D_3 simultaneously, $2^2 = 4$ hysteresis states are required while the other microrobots are confined to the circular trajectories (*hysteresisstate* = 1). As it can be seen from the last 4

rows of matrix A (String-Cluster control matrix for four robots in Equation 3.6), D_4 and D_3 can be fully controlled and be in 4 states while the others are confined to the circular trajectories ($hysteresisstate = 1$). The *String-Cluster* control matrix shows that the microassembly could start from arbitrary initial configuration of robots. Following the assembly of the seed shape, two robots ($(D_i$ and D_{i-1} where $i \in \{n - 2, \dots, 1\}$) are maneuvered in parallel, progressively assembling the target shape. Because, at each iteration of the assembly process in the String-Cluster system two robots are controlled and maneuvered, creating multi-seed shapes is easy and possible. Hence, this system is capable of creating not only one shape microassembly but also multi-shapes microassembly in different regions. This system is reconfigurable because, in the case of a disassembly of the target shape due to any reason, the assembly process could be resumed again starting with the first two robots (D_n and D_{n-1}) for creating the seed-shape from an arbitrary initial configuration of microrobots. This system is time-efficient, unlike the STRING and SESat systems it maneuvers two microrobots simultaneously toward the target shape at each iteration of the assembly process. It is important to mention that the control bandwidth in a *String-Cluster* system is $\zeta_n = n + 2$, because adding a Cluster to the system will increase number the independent voltage levels by exactly 2.

3.2 SATurated-Cluster System (SAT-C)

In this section, we present a new set of control strategies that not only have the control voltage bandwidth $O(\sqrt{n})$ but also is capable of controlling two microrobots simultaneously.

Lemma 2. *Any $M - Cluster$ system can be sorted such that all $\frac{3}{2}(n - 4) + 7$ String-Cluster hysteresis states are accessible, where $M = \text{number of Clusters}$, $n = \text{number of Microrobots}$ and $M = n/2$.*

Proof:By Construction:

Let an $M - Cluster$ system be a system with (H) independent release voltages and (P) independent snap-down voltages. It follows that $n = 2M \leq PH$, where $M = \text{no. Clusters}$, $n = \text{no. Microrobots}$ and $M = n/2$. Consider a system, sorted primarily according to snap-down voltages $V_{dl,i}$, $V_{dh,i}$ and secondarily sorted according to increasing release voltages $V_{ul,i}$ and $V_{uh,i}$. Figure 17 shows the system when $P = 4$ and $H = 4$. We call such a system SATurated-Cluster system (SAT-C). In this system $n = 2(P - 1)(H/2)$ or $n = 2(H - 1)(P/2)$. For this system, the control primitives $P_j(S)$ could be constructed that can access all the $(\frac{3}{2}(n - 4) + 7)$ String-Cluster control primitives. Let $P_j(S)$ be a control cycle with six control pulses, $P_j(S) = (V_{a,1}, V_{a,2}, V_{a,3}, V_{a,4}, V_{a,5}, V_{a,6})$ with a decision variable S . Unlike the previous techniques, the new control primitives do not increase with population size, enabling the implementation of the proposed control system. The control cycle for each control primitive defined by Equation 3.7 contains a sequence exactly 6 control pulses. Again (S) selects the hysteresis state of C_j in Equation 3.8. We construct the control primitive $P_j(S)$ in Equation 3.7, Where $V_{max} = \text{MAX}\{V_{dh,j}\}$, $1 \leq j \leq n$; $V_{ul,j}^+ = V_{ul,j} + \delta_v$, $V_{uh,j}^+ = V_{uh,j} + \delta_v$, $V_{ul,j}^- = V_{ul,j} - \delta_v$ and $V_{dl,j}^- = V_{dl,j} - \delta_v$. $P_j(S)$ generates $\frac{3}{2}(n-4)+7$ control primitives that construct a *String-Cluster* matrix, that assigns all Clusters C_i ($i < j$) the state 11, and all Cluster C_i ($i > j$) the state 00,

while based on the value of (S) it assigns the states 01, 10 or 11 to C_j . Consider the base case, where all C_j , ($j \in Z_M$) are in state 00.

$$P_j(S) = \begin{cases} (V_{max}, V_{ul,j}^-, V_{dl,j}, V_{ul,j}^+, V_{dl,j}^-, V_{uh,j}^+) & \text{if } j \in Z_M, S = 0 \\ (V_{max}, V_{ul,j}^-, V_{dh,j}, V_{ul,j}^+, V_{dl,j}^-, V_{uh,j}^+) & \text{if } j \in Z_M, S = 1 \\ (V_{max}, V_{ul,j}^-, V_{dl,j}, V_{uh,j}^+, V_{uh,j}^+, V_{uh,j}^+) & \text{if } j \in Z_M, S = 2 \\ (V_{max}, V_{ul,j}^-, V_{dh,j}, V_{ul,j}^+, V_{dl,j}^+, V_{uh,j}^+) & \text{if } j \in Z_M, S = 3 \end{cases} \quad (3.7)$$

$$C_j - Hysteresis - States = \begin{cases} "00", & \text{if } S = 0 \\ "01", & \text{if } S = 1 \\ "10", & \text{if } S = 2 \\ "11", & \text{if } S = 3 \end{cases} \quad (3.8)$$

Proof. We define Group (G_i) , $i \in \mu = \{1, \dots, M/(K-1)\}$, (Where M is the number of Clusters and K is the number of independent snap-down voltages) to be the set of all Clusters C_j , ($j \in Z_M$) with equal $V_{ul,j}$ and $V_{uh,j}$.

$$G_i = \{Cluster \in NGM | \forall Cluster_k, Cluster_m, V_{ul,j} = V_{ul,k}, V_{uh,j} = V_{uh,k}; m, k \in Z_M\} \quad (3.9)$$

We make the inductive argument:

Base condition: Base case keeps all Cluster C_j , ($j \in Z_M$) in state 00.

Inductive step: after applying of the first two control pulses $(V_{max}, V_{ul,j}^-)$, all Groups (G_1, \dots, G_{j-1}) are in state 11 and all Groups G_i , $(i > j - 1)$ are in state 00. We will show that by applying the sequence of four more primitive control voltages shown in Equation 3.7, the system will be in one of the four states of String-Cluster system, where Cluster (C_j) will be in state 00, 01, 10 or 11 based on the value of (S) while all Clusters (C_1, \dots, C_{j-1}) are in state 11 and all Cluster C_i , $(i > j)$ are in state 00. The $V_{ul,i}$, $V_{uh,i}$ and $V_{dl,i}$, $V_{dh,i}$, $i \in Z_M$ are sorted in such way that for a Cluster C_k , $(k > j)$, only six different cases could be considered and possible with respect to its transition voltages:

1. $V_{dl,j} < V_{dh,j} < V_{dl,k} < V_{dh,k}$ and $V_{ul,j} = V_{ul,k} < V_{uh,j} = V_{dh,k}$ (e.g., $j = 4$ and $k = 6$ in Figure 17).
2. $V_{dl,j} < V_{dh,j} < V_{dl,k} < V_{dh,k}$ and $V_{ul,j} < V_{uh,j} < V_{ul,k} < V_{uh,k}$ (e.g., $j = 1$ and $k = 6$ in Figure 17).
3. $V_{dl,j} < V_{dh,j} = V_{dl,k} < V_{dh,k}$ and $V_{ul,j} = V_{ul,k} < V_{uh,j} = V_{uh,k}$ (e.g., $j = 2$ and $k = 3$ in Figure 17).
4. $V_{dl,j} < V_{dh,j} = V_{dl,k} < V_{dh,k}$ and $V_{ul,j} < V_{uh,j} < V_{ul,k} < V_{uh,k}$ (e.g., $j = 2$ and $k = 6$ in Figure 17).
5. $V_{dl,k} < V_{dh,k} \leq V_{dl,j} < V_{dh,j}$ and $V_{ul,j} < V_{uh,j} < V_{ul,k} < V_{uh,k}$ (e.g., $j = 2$ and $k = 4$ in Figure 17).
6. $V_{dl,j} = V_{dl,k} < V_{dh,j} = V_{dh,k}$ and $V_{ul,j} < V_{uh,j} < V_{ul,k} < V_{uh,k}$ (e.g., $j = 1$ and $k = 4$ in Figure 17).

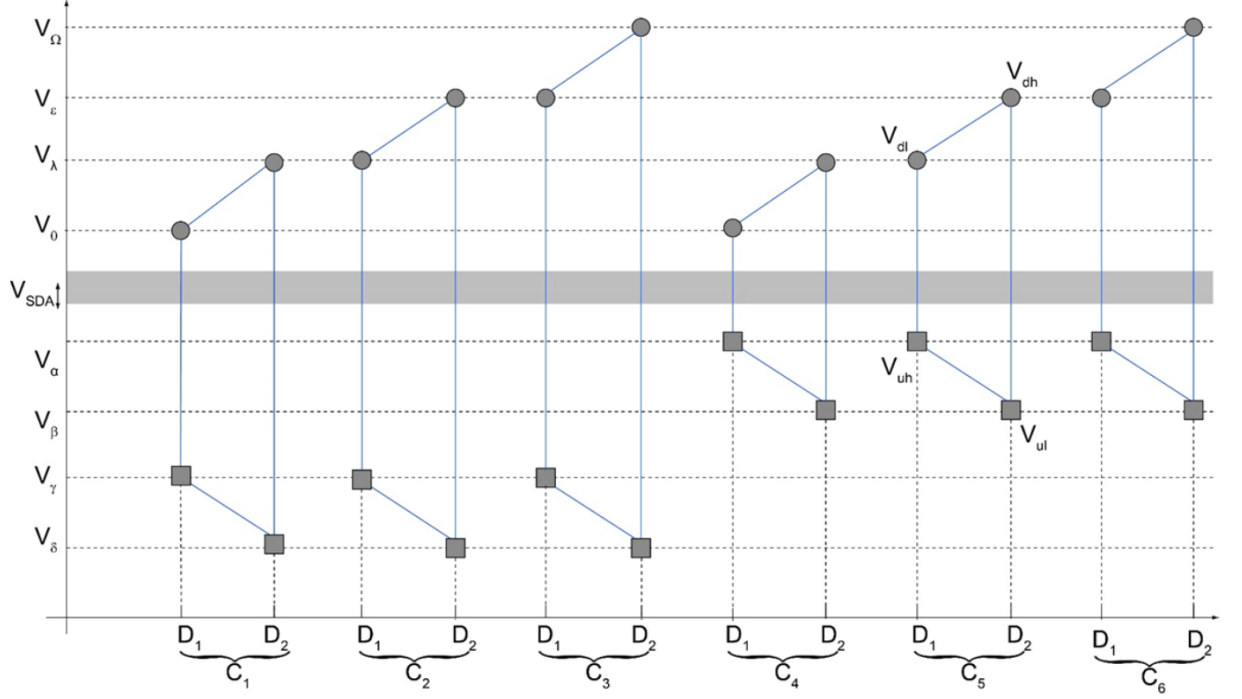


Figure 17: Example of an SAT-C system with $k = 4$ and $l = 4$.

if $S = 0$ then

$$P_j(S) = (V_{max}, V_{ul,j}^-, V_{dl,j}, V_{ul,j}^+, V_{dl,j}^-, V_{uh,j}^+):$$

Case (a), (b): $V_{dl,j}$ sets Cluster C_j to state 10, while C_k , $k > j$ is in state 00. $V_{ul,j}^+$ will set C_j to state 00 and will release D_1 of all Clusters C_i ($i \leq j$) with $V_{uh,i} = V_{uh,j}$. By applying the remaining control primitives $V_{dl,j}^-, V_{uh,j}^+$, all D_1 of all Clusters C_i ($i \leq j$) with $V_{uh,i} = V_{uh,j}$ will be snapped down while keeping the state of C_j in 00. Case (c), (d): $V_{dl,j}$ sets Cluster C_j to state 10, while C_k , $k > j$ is in state 00. $V_{ul,j}^+$ will set C_j to state 00 and will release D_1 of

all Clusters C_i ($i \leq j$) with $V_{uh,i} = V_{uh,j}$. With the remaining control primitives $V_{dl,j}^-$, $V_{uh,j}^+$, all D_1 of all Clusters C_i ($i \leq j$) with $V_{uh,i} = V_{uh,j}$ will be snapped down while keeping the state of C_j in 00. Case (e), (f): $V_{dl,j}$ sets Cluster C_j to state 10, while C_k , $k > j$ is in state 11. $V_{ul,j}^+$ will set C_j to state 00 and will release C_k , $k > j$ and D_1 of all Clusters C_i ($i \leq j$) with $V_{uh,i} = V_{uh,j}$. With the remaining control primitives $V_{dl,j}^-$, $V_{uh,j}^+$, all D_1 of all Clusters C_i ($i \leq j$) with $V_{uh,i} = V_{uh,j}$ will be snapped down and C_k , ($k > j$) will be in state 00 while keeping the state of C_j in 00.

if $S = 1$ then

$$P_j(S) = (V_{max}, V_{ul,j}^-, V_{dh,j}, V_{ul,j}^+, V_{dl,j}^-, V_{uh,j}^+):$$

In case (a) and (b): $V_{dh,j}$ assigns Cluster C_j to state 11, and assigns C_k , $k > j$ to be in state 00. Consequently, $V_{ul,j}^+$ will set C_j to state 01 and will release D_1 of all Clusters C_i ($i \leq j$) with $V_{uh,i} = V_{uh,j}$. By applying the remaining control primitives $V_{dl,j}^-$, $V_{uh,j}^+$, all D_1 of all Clusters C_i ($i \leq j$) with $V_{uh,i} = V_{uh,j}$ will be snapped down while keeping the state of C_j in 01. Case (c), (d): $V_{dh,j}$ sets Cluster C_j to state 11 and C_k , $k > j$ to 10. Consequently, $V_{ul,j}^+$ will set C_j to state 01 and $C_k = 00$ and will release D_1 of all Clusters C_i ($i \leq j$) with $V_{uh,i} = V_{uh,j}$. By applying the remaining control primitives $V_{dl,j}^-$, $V_{uh,j}^+$, all D_1 of all Clusters C_i ($i \leq j$) with $V_{uh,i} = V_{uh,j}$ will be snapped down while keeping the state of C_j in 01. Case (e), (f): $V_{dh,j}$ sets Clusters C_j and C_k , $k > j$ to state 11. Consequently, $V_{ul,j}^+$ will set C_j to state 01 and $C_k = 00$ and will release D_1 of all Clusters C_i ($i \leq j$) with $V_{uh,i} = V_{uh,j}$. By applying the remaining control primitives $V_{dl,j}^-$, $V_{uh,j}^+$, all D_1 of all Clusters C_i ($i \leq j$) $V_{uh,i} = V_{uh,j}$ will be snapped down while keeping the state of C_j in 01.

if $S = 2$ then

$$P_j(S) = (V_{max}, V_{ul,j}^-, V_{dl,j}, V_{uh,j}^+, V_{uh,j}^+, V_{uh,j}^+)$$

Case (a), (b): $V_{dl,j}$ sets Cluster C_j to state 10, while $C_k, k > j$ is in state 00. Consequently, $V_{uh,j}^+$ will keep C_j in state 01. Case (c), (d): $V_{dl,j}$ sets Cluster C_j to state 10, while $C_k, k > j$ is in state 00. Consequently, $V_{uh,j}^+$ will keep C_j in state 01. Case (e), (f): $V_{dl,j}$ sets Cluster C_j to state 10, while $C_k, (k > j)$ is in state 11. Consequently, $V_{uh,j}^+$ will keep C_j in state 01 and release Cluster C_k .

if $S = 3$ then

$$P_j(S) = (V_{max}, V_{ul,j}^-, V_{dh,j}, V_{ul,j}^+, V_{dl,j}^+, V_{uh,j}^+):$$

Case (a), (b): $V_{dh,j}$ sets Cluster C_j to state 11, while $C_k, k > j$ is in state 00. Consequently, $V_{ul,j}^+$ will set C_j to state 01 and will release D_1 of all Clusters C_i ($i \leq j$) with $V_{uh,i} = V_{uh,j}$. Finally, by applying $V_{dl,j}^+, V_{uh,j}^+, C_j$ will be in state 11 and all Clusters C_i ($i \leq j$) will be snapped down. Case (c), (d): $V_{dh,j}$ sets Cluster C_j to state 11 and $C_k, (k > j)$ to 10. Consequently, $V_{ul,j}^+$ will set C_j to state 01 and $C_k = 00$ and will release D_1 of all Clusters C_i ($i \leq j$) with $V_{uh,i} = V_{uh,j}$. Finally, $V_{dl,j}^+$ and $V_{uh,j}^+$ will set C_j to state 11 again while keeping C_k in state 00. Case (e), (f): $V_{dh,j}$ sets Cluster C_j to state 11 and $C_k, k > j$ to 11. By applying $V_{ul,j}^+, V_{dl,j}^+, V_{uh,j}^+, C_j$ will be in 11 while C_k is released. \square

Theorem 1. *Any planning algorithm for the String-Cluster system can be deployed to construct the control sequence for motion planning the (SAT-C) system.*

Proof. Based on Lemma 2, we can construct a *String-Cluster* control matrix for any (SAT-C) microrobotic system.

TABLE I: COMPARISON OF THE CONTROL VOLTAGE BANDWIDTH REQUIREMENTS AND CONTROL PULSE EFFICIENCY OF NHG, STRING, SESAT, STRING-CLUSTER AND SAT-C SYSTEMS

Control Strategies					
	NHG	STRING	String-Cluster	SESat	SAT-C
ζ_n	$2n$	$n + 1$	$n + 2$	$\lceil 2\sqrt{n} \rceil$	$\lceil 1 + 2\sqrt{n} \rceil$
No. control pulses	$O(n)$	2	2	$O(n)$	$O(1)$

□

Further reduction in the control bandwidth requirements ζ_n is possible with Theorem 2. For a microrobotic system with H independent release and P independent snap-down voltage levels, the control control voltage bandwidth is $\zeta_n = P + H$. In an SATurated-Cluster system (SAT-C), the number of microrobots, is $n = (P - 1)(H)$ or $n = (P)(H - 1)$. It follows that n is maximized when $H = P = \zeta_n/2$, and $\zeta_n = \lceil 1 + \sqrt{1 + 4n} \rceil \approx \lceil 1 + \sqrt{4n} \rceil = \lceil 1 + 2\sqrt{n} \rceil$. We call such a system symmetric SATurated-Cluster system (SAT-C). Table I compares the control voltage bandwidth requirements and the number of control pulses in the control cycle of the five classes of microrobotic systems: a) NHG, b) STRING, c) SESat, d) String-Cluster and e) SAT-C.

3.3 Hardware Experiments

In this chapter, we explain our hardware platform, experimental process and the results.

3.3.1 Robots with two direct-drive wheels

We have implemented the SAT-C algorithm on macroscale robots, which were designed to emulate the behavior of stress-engineered MEMS microrobots. Our robots have two direct-drive wheels that can only move forward and can only turn in one direction. Figure 18 shows the kinematics of the robot. The size of the robot is $18 \text{ cm} \times 13 \text{ cm}$. Let L and W be the length and width of the robot, respectively. The configuration is defined as $q = (x, y, \theta)$ and its configuration space by $\mathcal{Q} = \mathbb{R}^2 \times \mathbb{S}^1$. The kinematics of our robot is given by

$$\dot{q} = u \begin{bmatrix} \cos \theta \\ \sin \theta \\ 0 \end{bmatrix} + \omega \begin{bmatrix} 0 \\ 0 \\ 1 \end{bmatrix} \quad (3.10)$$

3.3.2 Hardware system

Our robots are commanded to turn in one direction or to move forward. These commands are broadcast over 2.4 GHz using XBee 2mW wire antenna. Figure 19 shows the block diagram of our hardware system.

The control strategies described in previous sections have been tested on groups of robots. We define two virtual snap-down and release points for each robot. As it was stated before, δ_v is the maximum deviation of the transition voltage manifested during the microrobot operation. The two transition voltages (snap-down or release points) are separated by at least $2\delta_v$. We

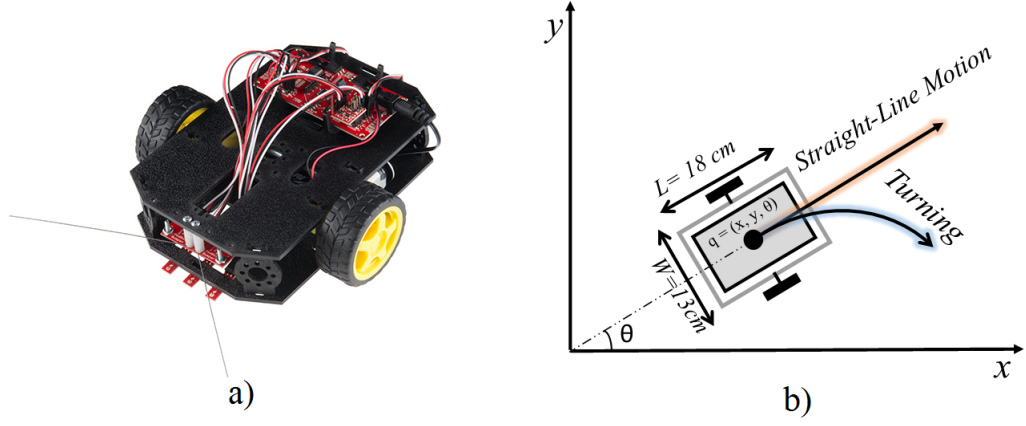


Figure 18: a) Schematic of the Robot, b) Kinematics of the Robot.

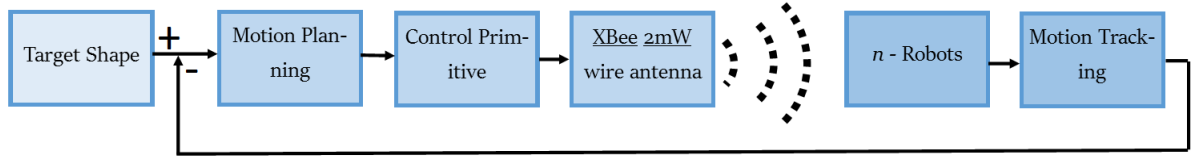


Figure 19: Block diagram of the system.

chose δ_v to be 0.5 for our experiments and consequently the transition points are separated by 1. Snap-down point results in turning while the release point causes the robot to move forward. As it was stated before, SATurated-Cluster system (SAT-C) needs exactly six pulses. These pulses are broadcast using XBee 2mW wire antenna and each robot reacts to it based on its

snap-down and release points. Figure 20 shows our eight robots (four Clusters) snap-down and release points.

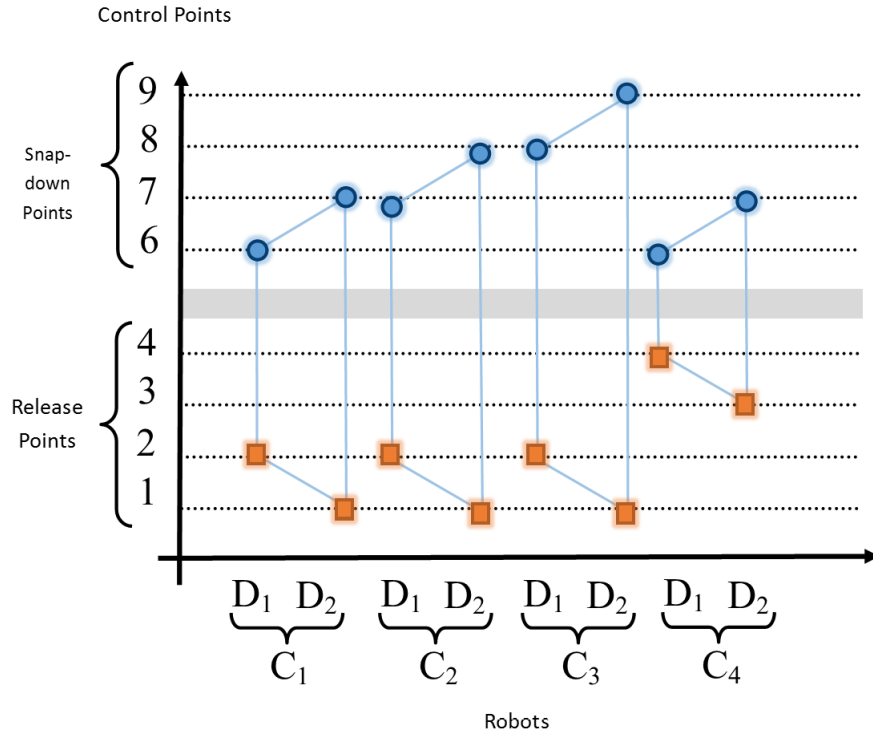


Figure 20: Transition control points (snap-down and release points).

We have four Clusters C_i , $i \in \{1, 2, 3, 4\}$. In each Cluster, we have two robots D_1 and D_2 . All D_1 s in Clusters C_i , $i \in \{1, 2, 3, 4\}$ are left handed, hence they turn counter-clockwise and

all D_2 s in Clusters C_i , $i \in \{1, 2, 3, 4\}$, are right handed, and they turn clockwise. Figure 21 shows our four Clusters (eight robots).

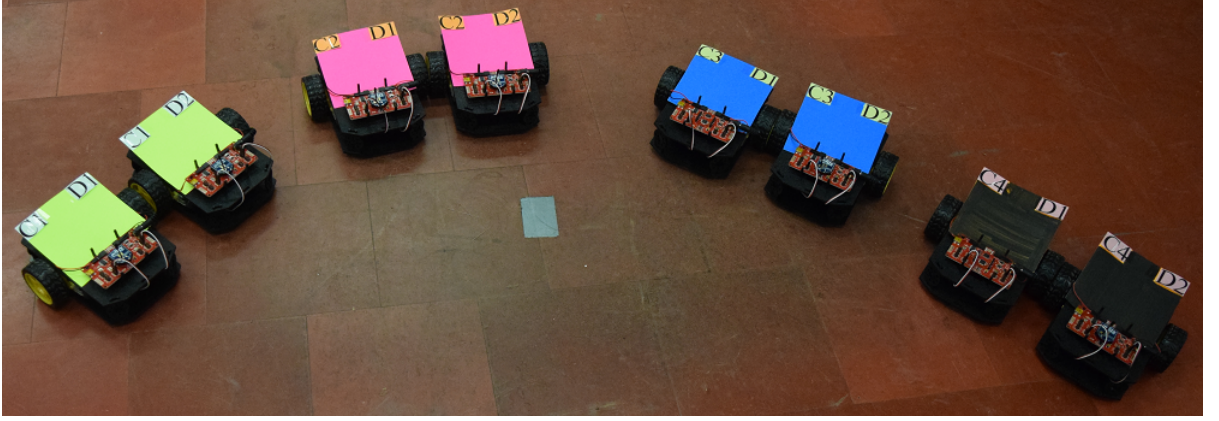


Figure 21: Four Clusters: C_1 (yellow), C_2 (pink), C_3 (blue) and C_4 (black) in the system.

We assigned equal linear and turning velocities to all robots but we experimentally recorded different speeds due to the system noise. Figure II shows experimentally recorded averages of the forward speed and the turning rate for each robot in the system.

3.3.3 Single-shape assembly

We applied our proposed control and planning strategies to a group four Clusters (eight robots). The target shape could be any shape that could be created with our robots. As an example, we chose a cross shape to be our target shape. Figure 22 shows the target shape.

Robots	D_1	D_2	D_3	D_4	D_5	D_6	D_7	D_8
Turning rate (rad/sec)	0.7457	0.7551	0.7340	0.7036	0.7897	0.7754	0.7263	0.7515
Forward speed (m/sec)	0.089	0.094	0.096	0.082	0.091	0.098	0.086	0.093

TABLE II: EXPERIMENTALLY RECORDED AVERAGES OF THE FORWARD SPEED AND THE TURNING RATE FOR EACH ROBOT IN THE SYSTEM. $(D_1, D_2) = (C_1(D_1), C_1(D_2))$, $(D_3, D_4) = (C_2(D_1), C_2(D_2))$, $(D_5, D_6) = (C_3(D_1), C_3(D_2))$ and finally $(D_7, D_8) = (C_4(D_1), C_4(D_2))$.

The robots were operated in $330\text{cm} \times 330\text{cm}$ environment. We recorded their position using a digital video camera. The control waveform pulses for the control primitives were broadcast using XBee 2mW wire antenna from a local PC. The duration of each control primitive was controlled manually during the execution of the control sequence S .

We conducted a series of experiments to show that our control policy can create the cross target shape. Figure 23 and Figure 24 show two experiments for our assembly process. These two assembly experiments were started from two arbitrary initial configurations. As it was stated, this system is time-efficient, unlike the STRING and SESat systems it maneuvers two

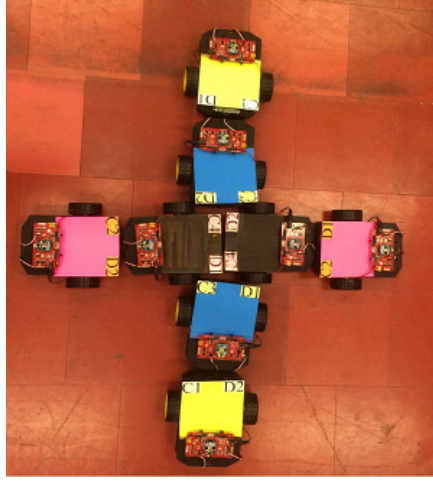


Figure 22: Cross type of target shapes.

microrobots simultaneously toward the target shape at each iteration of the assembly process. The time for completing the assembly is shown in Figure III.

3.3.4 Robustness against disturbance

Our proposed control strategy is robust against disturbance because, in the case of a disassembly of the target shape due to any reason, the assembly process could be resumed again starting with the first two robots (D_n and D_{n-1}) for creating the seed-shape from an arbitrary initial configuration of microrobots. Following the construction of the seed shape, two robots (D_i and D_{i-1} where $i \in \{n-2, n-3, \dots, 1\}$) are maneuvered in parallel, progressively assembling the target shape.

We applied our proposed control strategy to a group of two Clusters (four robots). We chose a cross shape to be our target shape. The control waveform pulses for the control primitives were broadcast using XBee 2mW wire antenna from a local PC. The duration of each control primitive was controlled manually during the execution of the control sequence S .

As it was stated in chapter 3, δ_v is the maximum deviation of the transition voltage manifested during the microrobot operation. The two transition voltages (snap-down or release points) are separated by at least $2\delta_v$. We chose δ_v to be 0.5 for our experiments and consequently the transition points are separated by 1.

To model the process noise, we apply Gaussian noise to snap-down and release points of each robot. For each snap-down point, the mean (μ) of the noise is the snap-down point itself and the standard deviation (σ) is 0.15. Similarly, for each release point, the mean (μ) of the noise is the release point itself and also the standard deviation (σ) is 0.15.

We conducted an experiment to show that in the case of a disassembly, our control policy can create the assembly shape again. Figure 25 shows the robustness against disturbance in our assembly process. Our experiments showed, by sweeping the standard deviation (σ) of the noise from 0.15 to 0.5, the system is still controllable. By increasing the standard deviation of the noise beyond 0.5, we will lose the controllability of the whole system. Hence, the system is not controllable with the standard deviation beyond 0.5 for the applied Gaussian noise.

3.3.5 multiple-shapes assembly

We applied our proposed control and planning strategies to a group four Clusters (eight robots). The target shape could be any shape that could be created with our robots. In our

String-Cluster system, the maximum number of target shapes $N = \frac{n}{2}$ where n is the number of the robots in the system. We conducted two experiments with a different number of target shapes. In our first experiment, we chose $N = 4$ target shapes that each target shape consists of two robots. The control waveform pulses for the control primitives were broadcast using XBee 2mW wire antenna from a local PC. The duration of each control primitive was controlled manually during the execution of the control sequence S . Figure 26 shows the experiment for our assembly process.

In our second experiment, we chose two target shapes that each target shape consists of four robots (cross shape). The robots were operated in $330\text{cm} \times 330\text{cm}$ environment. We recorded their position using a digital video camera. The control waveform pulses for the control primitives were broadcast using XBee 2mW wire antenna from a local PC. The duration of each control primitive was controlled manually during the execution of the control sequence S . Figure 27 shows the experiment for our multiple-shapes assembly process. The assembly time is shown in Table III. Movies of these assembly experiments are available online at <https://www.youtube.com/watch?v=LwUEuM8vSSs>.

Experiments	Single Shape 1	Single Shape 2	Multi-Shapes 1	Multi-Shapes 2
Assembly Time (<i>min : sec</i>)	5 : 05	3 : 51	6 : 02	4 : 48

TABLE III: EXPERIMENTALLY RECORDED TIME FOR THE ASSEMBLY.

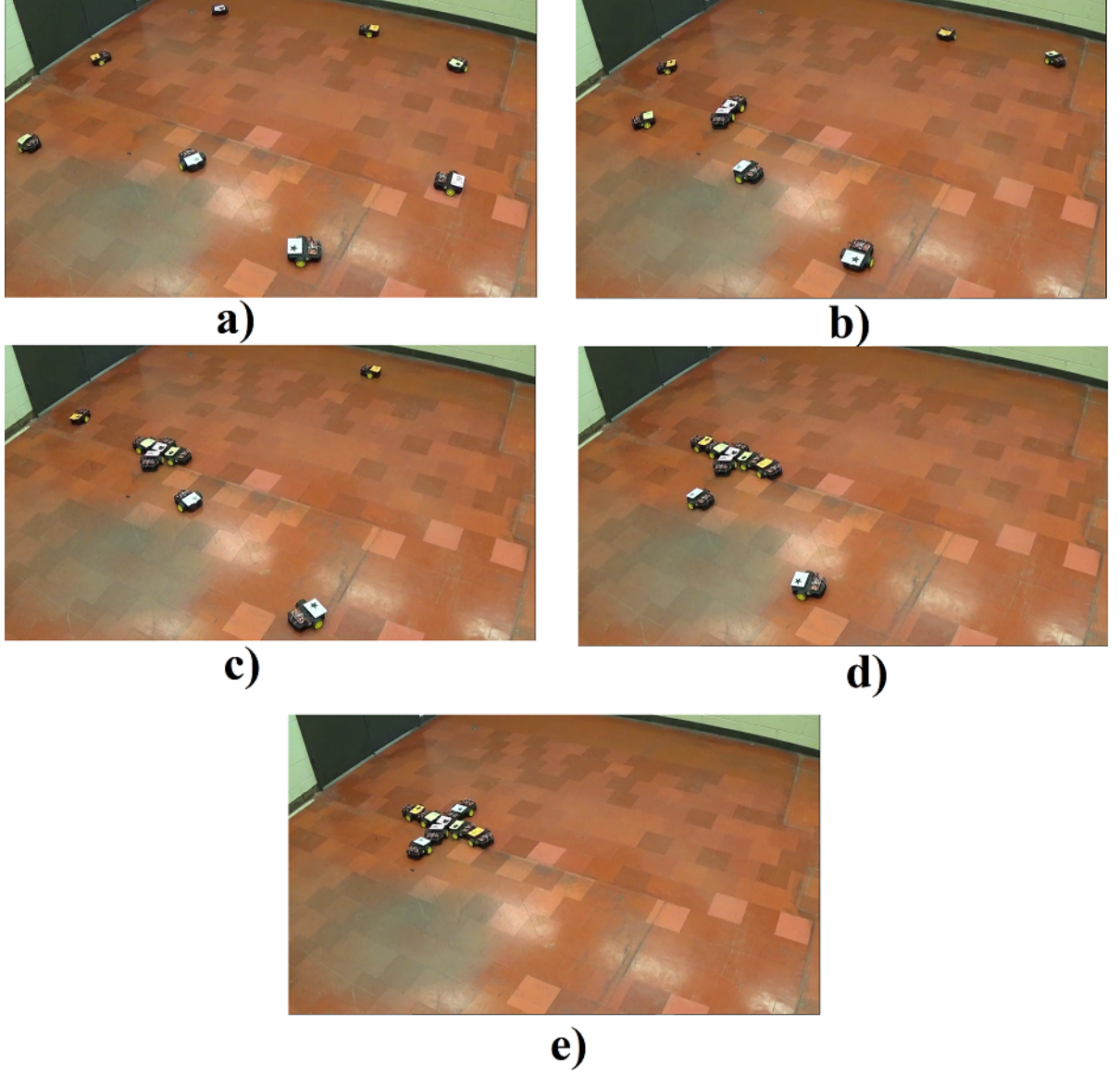


Figure 23: Experimental assembly data using four Clusters (eight robots). (a) Arbitrary initial configuration. (b) Forming the seed shape (ϕ_{k1}) using $C_4(D_1)$ and $C_4(D_2)$ while the rest are confined to the circular trajectories. (c) Forming the second intermediate shape (ϕ_{k2}) using $C_3(D_1)$ and $C_3(D_2)$ while the rest are confined to the circular trajectories, (d) Generating the third intermediate shape (ϕ_{k3}) using $C_2(D_1)$ and $C_2(D_2)$ while the rest are confined to the circular trajectories, and finally (e) Generating the final shape ($\phi_{k4} = \phi_k$) using the $C_1(D_1)$ and $C_1(D_2)$.

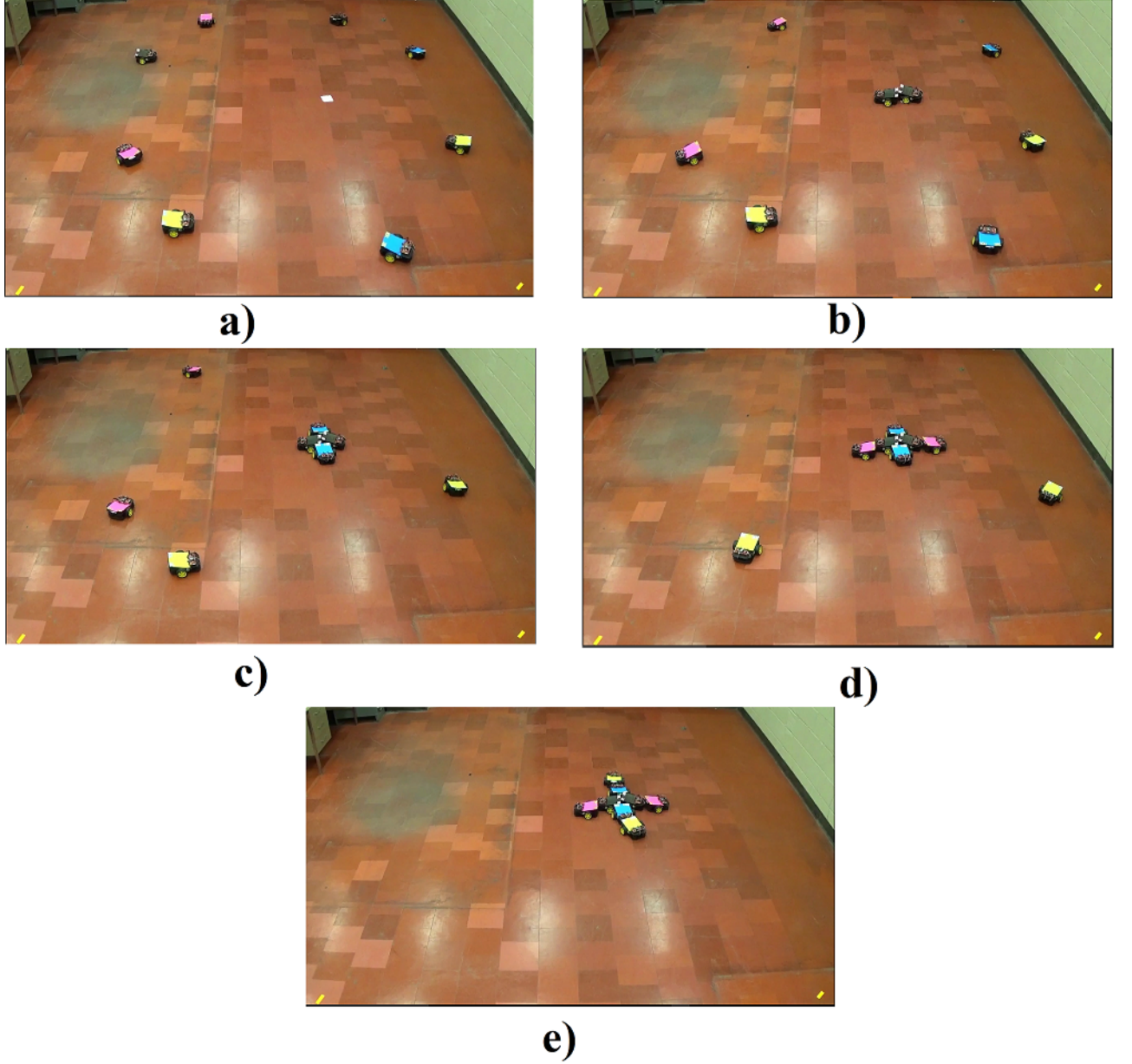


Figure 24: Experimental assembly data using four Clusters (eight robots). (a) Arbitrary initial configuration, (b) Forming the seed shape (ϕ_{k1}) using $C_4(D_1)$ and $C_4(D_2)$ while the rest are confined to the circular trajectories, (c) Forming the second intermediate shape (ϕ_{k2}) using $C_3(D_1)$ and $C_3(D_2)$ while the rest are confined to the circular trajectories, (d) Generating the third intermediate shape (ϕ_{k3}) using $C_2(D_1)$ and $C_2(D_2)$ while the rest are confined to the circular trajectories, and finally (e) Generating the final shape ($\phi_{k4} = \phi_k$) using the $C_1(D_1)$ and $C_1(D_2)$.

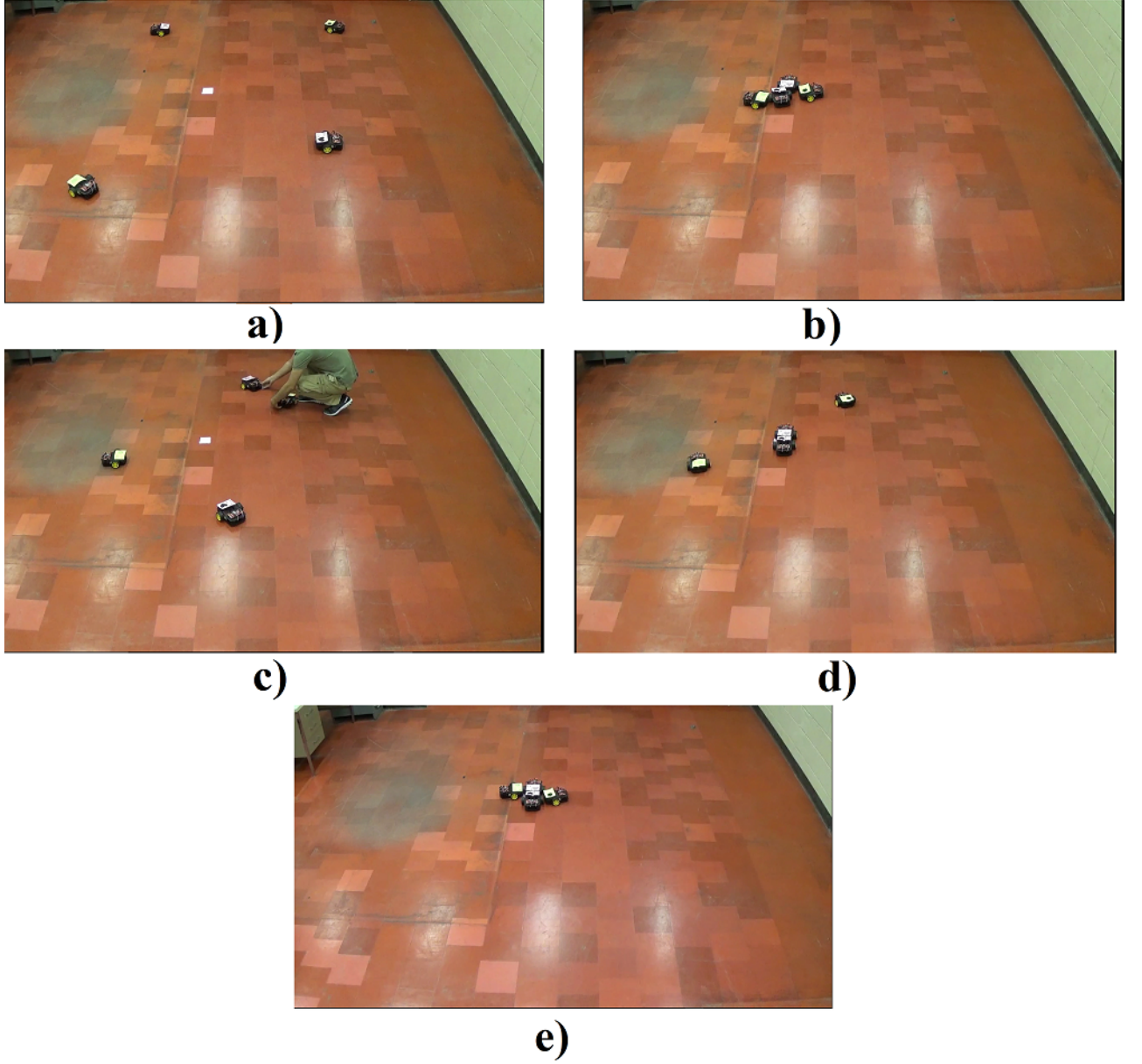


Figure 25: Robustness against disturbance experiment using two Clusters (four robots). (a) Arbitrary initial configuration, (b) Generating the final shape ($\phi_{k4} = \phi_k$) using the $C_2(D_1)$ and $C_2(D_2)$ followed by $C_1(D_1)$ and $C_1(D_2)$, (c) Disassembly due to disturbance, (d) Forming the seed shape (ϕ_{k1}) using $C_2(D_1)$ and $C_2(D_2)$ while the rest are confined to the circular trajectories, and finally (e) Generating the final shape ($\phi_{k2} = \phi_k$) using the $C_1(D_1)$ and $C_1(D_2)$.

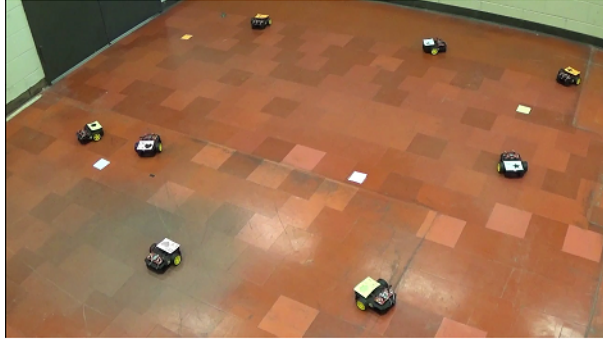
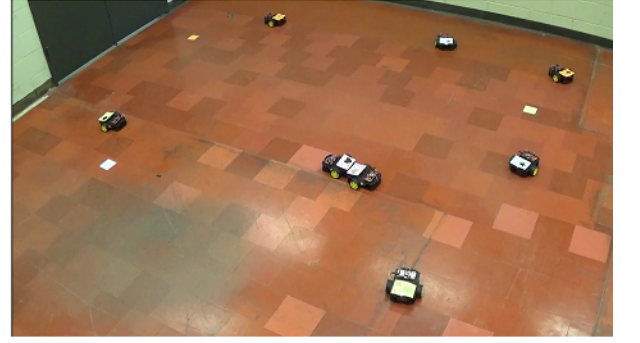
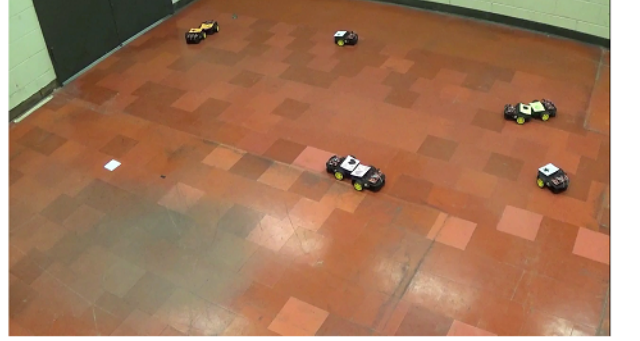
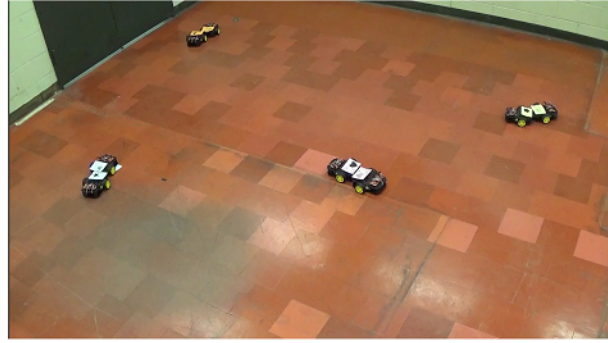
**a)****b)****c)****d)****e)**

Figure 26: Multiple shapes assembly (four shapes) using four Clusters (eight robots). (a) Arbitrary initial configuration. (b) Forming the first target shape (ϕ_{k1}) using $C_4(D_1)$ and $C_4(D_2)$ while the rest are confined to the circular trajectories, (c) Forming the second target shape (ϕ_{k2}) using $C_3(D_1)$ and $C_3(D_2)$ while the rest are confined to the circular trajectories, (d) Generating the third target shape (ϕ_{k3}) using $C_2(D_1)$ and $C_2(D_2)$ while the rest are confined to the circular trajectories, and finally (e) Generating the fourth final shape (ϕ_{k4}) using the $C_1(D_1)$ and $C_1(D_2)$.

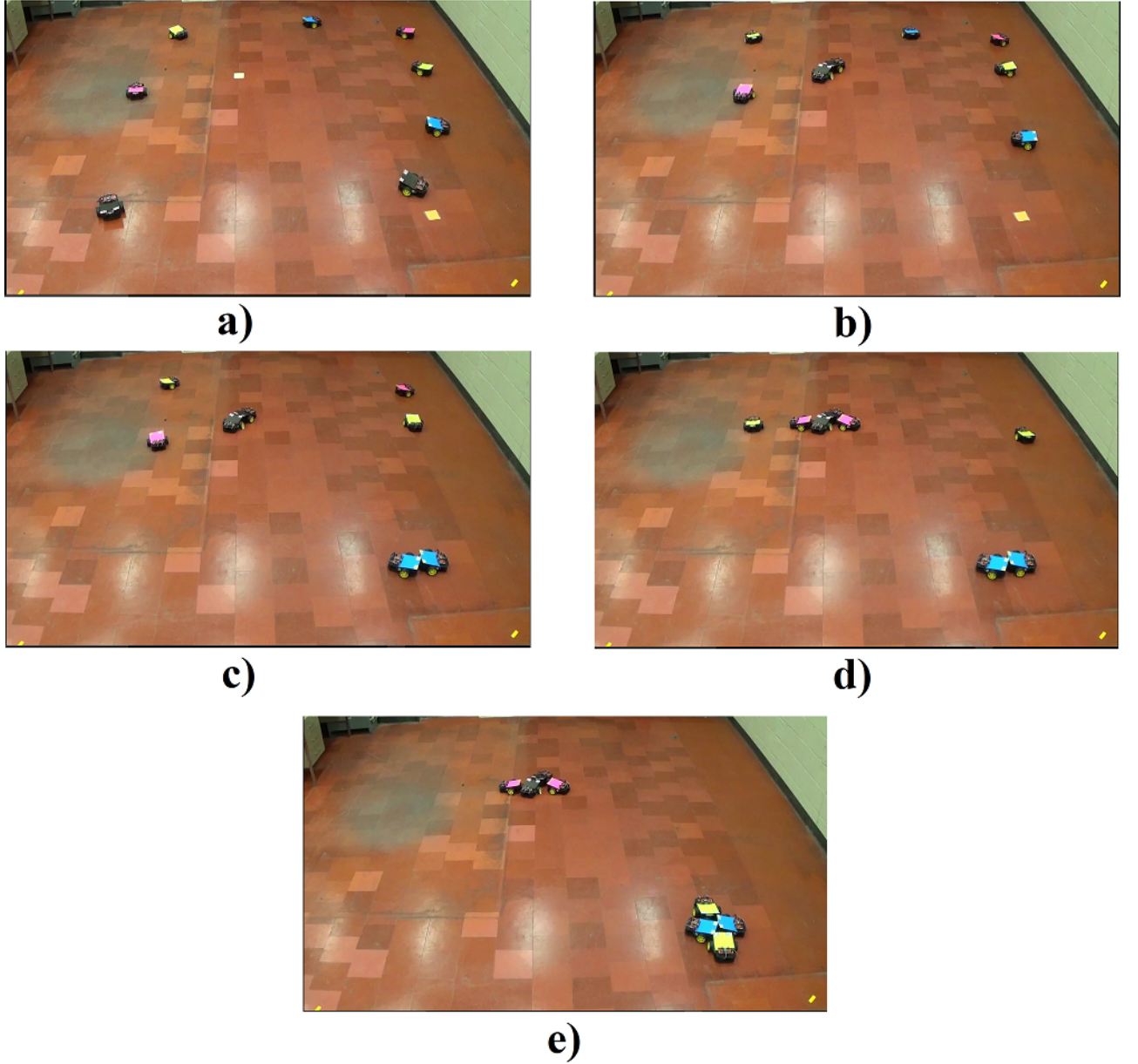


Figure 27: Multiple shapes assembly (two cross shapes) using four Clusters (eight robots).

(a) Arbitrary initial configuration. (b) Forming the first seed shape (ϕ_{k1}) using $C_4(D_1)$ and $C_4(D_2)$ while the rest are confined to the circular trajectories, (c) Forming the second seed shape (ϕ_{k2}) using $C_3(D_1)$ and $C_3(D_2)$ while the rest are confined to the circular trajectories, (d) Generating the first target shape (ϕ_{k3}) using $C_2(D_1)$ and $C_2(D_2)$ while the rest are confined to the circular trajectories, and finally (e) Generating the second final shape (ϕ_{k4}) using the $C_1(D_1)$ and $C_1(D_2)$.

CHAPTER 4

CLUSTER SYSTEM II: ENABLING GCSR THROUGH CONTROL SIGNAL DIFFERENTIATION

(Some parts of this chapter are copied from my paper with the following citation: Vahid Foroutan, Farhad Farzami, Danilo Erricolo, and Igor Paprotny, "Efficient Constant-Time Addressing Scheme for Parallel-Controlled Assembly of Stress-Engineered MEMS Microrobots," International Conference on Control, Automation and Robotics (ICCAR), 2018.

Authors contributions: Vahid Foroutan conceived the idea, proved it, developed the macroscale platform for experiments and wrote the paper; Farhad Farzami helped in setting up the experimental platform and drawing the figures; Danilo Erricolo supervised the project; Igor Paprotny supervised the paper writing.

4.1 Cluster-String System

In this section, we introduce a control strategy that is robust against disturbance and capable to control and complete the assembly process from arbitrary initial configuration.

We start with the following definitions:

Definition 4. *Reversed-Nested-Hysteresis-Gaps (RNHG) structure:*

Reversed-Nested-Hysteresis-Gaps (RNHG) is the system of n steering arms, sorted according to descending V_{di} , ($V_{di} - 2\delta_v \geq V_{dj}$) and ascending V_{ui} , ($V_{ui} + 2\delta_v \leq V_{uj}$), for all $i < j$.

Definition 5. *Reversed-Nested-Group-Microrobots (RNGM) set:*

Set of all groups of two Microrobots that forms a *Reversed-Nested-Hysteresis-Gaps (RNHG)* structure is *Reversed-Nested-Group-Microrobots (RNGM)*.

$$RNGM = \{(D_i, D_j) | D_i, D_j \in M, V_{dj} < V_{di}, V_{uj} > V_{ui}; (i < j); i, j \in \mathbb{N}\} \quad (4.1)$$

V_d and V_u are snap-down and release voltages. M is the set of all microrobots in the system. $M = \{D_1, D_2, \dots, D_n\}$; where D_i is i th Microrobot in the system.

Definition 6. *Reversed-Nested-Group-Microrobots Cluster (R-Cluster):* Each member of $RNGM$ is called *R-Cluster*.

$$R - Cluster = \forall (D_i, D_j) \in RNGM; i, j \in \mathbb{N} \quad (4.2)$$

In each R-Cluster, $V_{dl} = \text{Min}(V_{di}, V_{dj})$, $V_{dh} = \text{Max}(V_{di}, V_{dj})$, $V_{ul} = \text{Min}(V_{ui}, V_{uj})$ and $V_{uh} = \text{Max}(V_{ui}, V_{uj})$, respectively. Figure 28 Shows the transition voltages in a R-Cluster.

Definition 7. *Reversed Cluster-STRICtly Non-nested hysteresis-Gaps (R-Cluster-String) system:*

This system consists of one R-Cluster for the first two microrobots in the system. The snap-down and release voltages of the third microrobot are as same as V_{dl} and V_{ul} of the first R-Cluster in the system. The rest of the microrobots sorted according to descending values of V_d , and secondarily sorted according to descending values of V_u . A *R-Cluster-String*

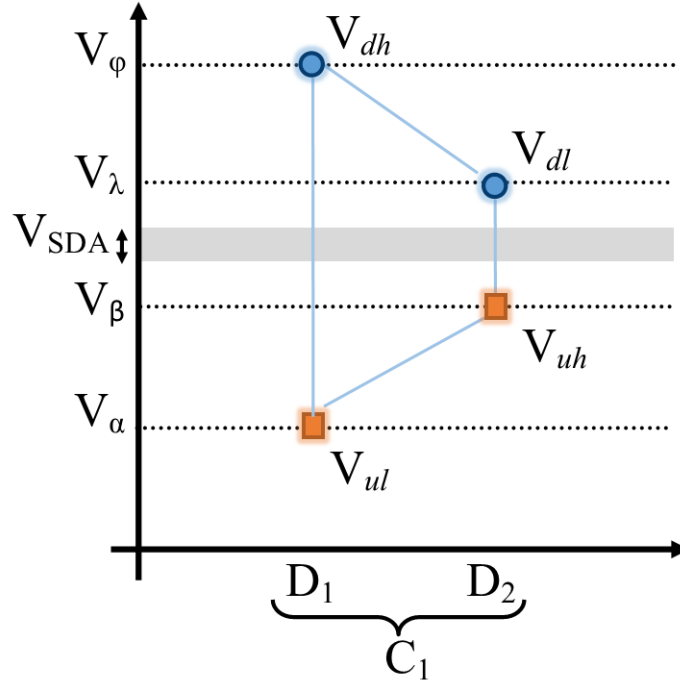


Figure 28: R-Cluster Structure. $V_{dl} = \text{Min}(V_{d1}, V_{d2})$, $V_{dh} = \text{Max}(V_{d1}, V_{d2})$, $V_{ul} = \text{Min}(V_{u1}, V_{u2})$ and $V_{uh} = \text{Max}(V_{u1}, V_{u2})$. Snap-down and release voltages are shown as circles and rectangles.

microrobotic system has non-nested hysteresis gaps between every two microrobots except the first two microrobots in the first R-Cluster. If $V_{dj} - V_{di} \leq 2\delta_v$, and $V_{uj} - V_{ui} \leq 2\delta_v$ then those two microrobots cannot be controlled independently. Figure 29 shows the *R-Cluster-String* system.

Lemma 3. *An R-Cluster-String system has exactly $n + 2$ accessible hysteresis states, where n = no. Microrobots in the system.*

Proof. By Induction:

Base condition: An *R-Cluster-String* system with one R-Cluster has four accessible states. In an R-Cluster, we have two microrobots sorted in an *RNHG* system format. Consider the R-Clusters C_1 consists of two microrobots $\{D_1, D_2\}$. In the R-Cluster C_1 , each microrobot has 2 states: (0 = arm up) and (1 = arm down). Hence, we have $2^2 = 4$ states (00 = arm up, arm up), (01 = arm up, arm down), (10 = arm down, arm up) and (11 = arm down, arm down).

Inductive step: Increasing the size of the system by exactly one microrobot (changing an n microrobotic system to an $n + 1$ microrobotic system), adds exactly 1 accessible hysteresis state to the system if both n and $n + 1$ microrobotic systems are *R-Cluster-String*.

Consider an n *R-Cluster-String* microrobotic system. Let D_1, \dots, D_n , be the microrobots in the system. Figure 29 shows the ranges for control voltages of Microrobot D_{n+1} , in such a way that the new $n + 1$ microrobotic system remain *R-Cluster-String* ($V_{d,n+1} \leq V_{d,n}$ and $V_{u,n+1} \leq V_{u,n}$). Assume $V_\delta, \dots, V_\Omega$ are significantly independent transition voltage levels. Consider $V_\delta \leq V_\gamma \leq V_\beta \leq V_\alpha \leq V_\theta \leq V_\lambda \leq V_\epsilon \leq V_\Omega$. Let $V_{d,n} = V_\lambda$ and $V_{u,n} = V_\gamma$. The snap-down voltage $V_{d,n+1}$ can have value $V_1 = V_\lambda$, or voltage $V_2 \in (V_\lambda, V_\theta]$. The release voltage, $V_{u,n+1}$ can have the value $V_3 = V_\gamma$ or voltage $V_4 \in (V_\gamma, V_\delta]$. Consequently, the $n + 1$ microrobotic system will be remained *R-Cluster-String*, if the release and snap-down voltages for D_{n+1} are one the following combinations: (V_2, V_4) , (V_1, V_4) and (V_2, V_3) . We examine each case:

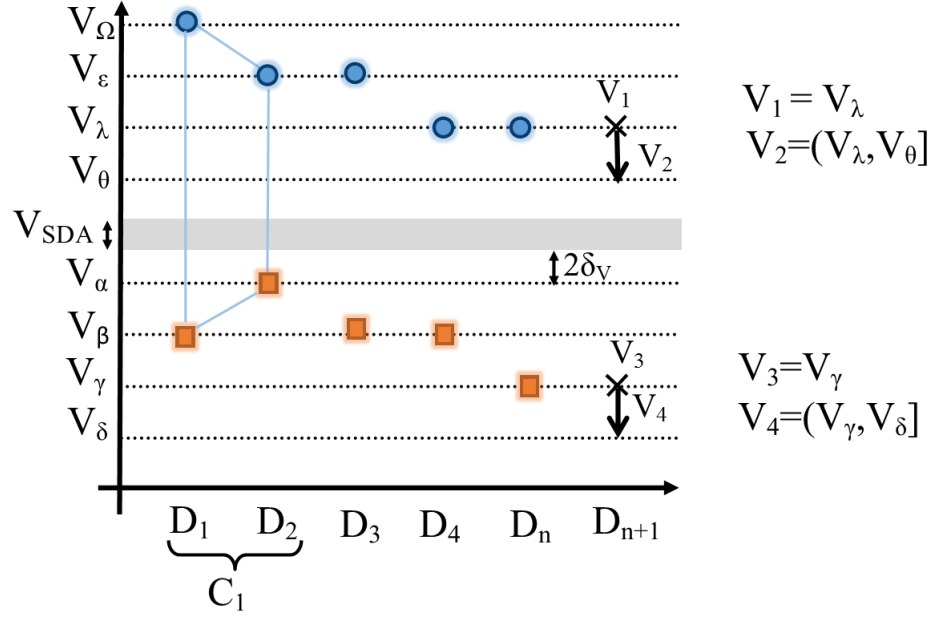


Figure 29: R-Cluster-String system. Showing the proof of the inductive step of Lemma 1.

(V_2, V_4) : because of $V_{d,n+1}$, is less than the snap-down voltages of D_1, \dots, D_n ; ($V_{d,n+1} < V_{d,i}$), $i \in Z_n$ where $Z_n = \{1, \dots, n\}$, we can snap down the arm of D_{n+1} before the arms of all other robots. Since $V_{u,n+1}$, is less than the release voltages of D_1, \dots, D_n ; ($V_{u,n+1} < V_{u,i}$), $i \in Z_n$ where $Z_n = \{1, \dots, n\}$, we can only release the arm of D_{n+1} while the arms of all other robots are released. During all other states of the system, the state of D_{n+1} is 1. As a consequence the number of accessible hysteresis states increases by exactly one.

(V_1, V_4) : In this case, the arm of D_n and D_{n+1} are snapped down at the same time. Because $V_{u,n+1} < V_{u,i}$, $i \in Z_n$ where $Z_n = \{1, \dots, n\}$, we can release the arm of D_{n+1} only after all other

devices are release (hysteresis state = 0) which means D_{n+1} is in state 1 if at least one of the other robots is snapped down. D_{n+1} could 0 or 1 when the other robots are in state 0. Hence, the number of accessible hysteresis states increases by one.

(V_2, V_3) : This case is similar to (V_2, V_4) but the arm of D_{n+1} and D_n are released at the same time. Since $V_{d,n+1}$, is less than the snap-down voltages of D_1, \dots, D_n ; ($V_{d,n+1} < V_{d,i}$), $i \in Z_n$ where $Z_n = \{1, \dots, n\}$, we can snap down the arm of D_{n+1} when all robots are at state 0. Hence, D_{n+1} could 0 or 1 when the other robots are in state 0 and during all other states D_{n+1} is in state 1. Hence, the accessible hysteresis states number increases by one.

It has been shown that the addition of one microrobot to a *R-Cluster-String* system, increases the accessible hysteresis states number by exactly one. We know that the base condition with $n = 2$ has four states. Hence, *R-Cluster-String* can access exactly $n + 2$ hysteresis states.

□

Now we construct the control primitives for accessing the $n + 2$ hysteresis states and based on the constructed the control primitives, we will form the $(n + 2) \times n$ control matrix for the *R-Cluster-String* system. We define two different control primitives $P_{12}(S)$ and $P_i(S)$ where $i \in \{3, \dots, n\}$.

We construct the control primitive $P_{12}(S)$ such that it assigns the state 1 to all D_i for $i \in \{3, \dots, n\}$, and based on the value of S , it can assign the states 00, 01, 10 or 11 to D_1 and D_2 . $P_{12}(S)$ consists a control cycle with two control pulses, $P_{12}(S) = (V_{a,1}, V_{a,2})$ with a decision variable S . Equation 4.4 shows $P_{12}(S)$. Consider the *R-Cluster-String* system shown in Figure

30, where $V_\delta, \dots, V_\Omega$ represent significantly independent control voltage levels. S selects the Hysteresis state of C_1 .

$$(D_1, D_2) - \text{Hysteresis} - \text{States} = \begin{cases} \text{"00"}, & \text{if } S = 0 \\ \text{"01"}, & \text{if } S = 1 \\ \text{"10"}, & \text{if } S = 2 \\ \text{"11"}, & \text{if } S = 3 \end{cases} \quad (4.3)$$

$$P_{12}(S) = \begin{cases} (V_{dl}, V_{ul}^+) & \text{if } S = 0 \\ (V_{dl}, V_{uh}^+) & \text{if } S = 1 \\ (V_{dh}, V_{ul}^+) & \text{if } S = 2 \\ (V_{dh}, V_{uh}^+) & \text{if } S = 3 \end{cases} \quad (4.4)$$

where $V_{ul,j}^+ = V_{ul,j} + \delta_v$ and $V_{uh,j}^+ = V_{uh,j} + \delta_v$.

When $S = 0$, the steering arms of all the microrobots D_i , $i \in \{3, \dots, n\}$, and D_2 of the R-Cluster C_1 are snapped-down with the first control pulse ($V_{a,1}$). The second control pulse ($V_{a,2}$) keeps all the microrobots D_i , $i \in \{3, \dots, n\}$ snapped down while releasing D_2 of the R-Cluster C_1 . Hence, D_1 and D_2 are in state "00". Figure 30 a) shows the control primitive.

For $S = 1$, the steering arms of all the microrobots D_i , $i \in \{3, \dots, n\}$, and D_2 of the R-Cluster C_1 are snapped-down with the first control pulse ($V_{a,1}$). The second control pulse ($V_{a,2}$)

keeps all the microrobots $D_i, i \in \{2, \dots, n\}$ snapped down. Hence, D_1 and D_2 are in state "01".

Figure 30 b) illustrates the control primitive.

For $S = 2$, the steering arms of all the microrobots $D_i, i \in \{1, \dots, n\}$ are snapped-down with the first control pulse ($V_{a,1}$). The second control pulse ($V_{a,2}$) keeps all the microrobots $D_i, i \in \{3, \dots, n\}$ and D_1 of the R-Cluster C_1 snapped down while releasing D_2 of the R-Cluster C_1 . Hence, D_1 and D_2 are in state "10". Figure 30 c) illustrates the control primitive.

For $S = 3$, the steering arms of all the microrobots $D_i, i \in \{1, \dots, n\}$ are snapped-down with the first control pulse ($V_{a,1}$). the second control pulse ($V_{a,2}$) keeps all the micrororobts snapped down. Hence, D_1 and D_2 are in state "11". Figure 30 d) illustrates the control primitive.

We now construct the control primitive $P_i, i \in \{3, \dots, n\}$ such that it assigns the state 1 to all $D_j, j \in \{1, \dots, n\}$ for $j > i$ and 0 to all $D_j, j < i$ and finally, based on the value of S it can assign 0 or 1 to D_i .

$P_i(S)$ is defined by a control cycle of two control pulses, $P_i = (V_{a,1}, V_{a,2})$ with a decision variable S . Equation 4.6 shows $P_i(S)$. Consider the *R-Cluster-String* system shown in Figure 31.

$$D_i - Hysteresis - States = \begin{cases} "0", & \text{if } S = 0 \\ "1", & \text{if } S = 1 \end{cases} \quad (4.5)$$

$$P_i(S) = \begin{cases} (V_{d,i+1}, V_{u,i+1}^+) & \text{if } S = 0, i \in \{1, \dots, n-1\} \\ (V_{d,i}^-, V_{u,i}) & \text{if } S = 0, i = n \\ (V_{d,i}, V_{u,i}^+) & \text{if } S = 1 \end{cases} \quad (4.6)$$

where $V_{u,i}^+ = V_{u,i} + \delta_v$ and $V_{d,i}^- = V_{d,i} - \delta_v$.

When $S = 0$, $(V_{a,1})$ snaps down the steering arms of all of the microrobots D_j , $(j > i)$ while keeps all microrobots D_j , $(j < i)$ released. The second control pulse $(V_{a,2})$ keeps all the microrobots D_j , $(j > i)$ snapped down while releases all microrobots D_j , $(j \leq i)$. Figure 31 a) shows the control primitive.

When $S = 1$, $(V_{a,1})$ snaps down the steering arms of all of the microrobots D_j , $(j > i)$ while keeps all microrobots D_j , $(j < i)$ released. Because $(V_{a,1}) = V_{d,i}$, the first control pulse snaps down the D_i . The second control pulse $(V_{a,2})$ keeps all the microrobots D_j , $(j \geq i)$ snapped down while keeps all microrobots D_j , $(j < i)$ released. Figure 31 b) shows the control primitive.

The $n + 2$ control primitives generated by $P_{12}(S)$ and $P_i(S)$ construct a $(n + 2) \times n$ control matrix A . Equation 4.7 shows the control matrix for four microrobots.

$$A = \begin{matrix} & C_1(D_1) & C_1(D_2) & D_3 & D_4 \\ \begin{matrix} P_{12}(S=11) \\ P_{12}(S=10) \\ P_{12}(S=01) \\ P_{12}(S=00)=P_3(S=1) \\ P_3(S=0)=P_4(S=1) \\ P_4(S=0) \end{matrix} & \begin{pmatrix} 1 & 1 & 1 & 1 \\ 1 & 0 & 1 & 1 \\ 0 & 1 & 1 & 1 \\ 0 & 0 & 1 & 1 \\ 0 & 0 & 0 & 1 \\ 0 & 0 & 0 & 0 \end{pmatrix} \end{matrix} \quad (4.7)$$

We call A , the *R-Cluster-String* control matrix and these $n + 2$ hysteresis states that are addressable through $P_{12}(S)$ and $P_i(S)$ control primitives are the *R-Cluster-String* hysteresis states. The order of the assembly is set by the *R-Cluster-String* control matrix to reduce the parallel motion to parallel motion for two robots in the first step and then sequential motion of one robot (while the other robots confined to the circular trajectories). The process of assembling the target goal shape starts with maneuvering two robots ($D_1 = C_1(D_1)$ and $D_2 = C_1(D_2)$) from any arbitrary configuration to form the initial shape while the others confined to the circular trajectories. As an example, the assembly in a system with 4 microrobots starts with D_1 and D_2 . In order to control D_1 and D_2 simultaneously, $2^2 = 4$ hysteresis states are required while the other microrobots are confined to the circular trajectories (hysteresis state = 1). As it can be seen from *R-Cluster-String* control matrix for four robots in Equation

4.7, the first 4 rows of matrix A shows D_1 and D_2 can be fully controlled and be in 4 states while the others are confined to the circular trajectories (hysteresis state = 1). The *R-Cluster-String* control matrix shows that microassembly could start from any arbitrary initial configuration of robots. Following the assembly of the initial shape from an arbitrary initial configuration of the first two robots, one robot (D_i where $i \in \{3, 4, \dots, n\}$) is maneuvered sequentially, assembling the target shape. This system is reconfigurable because, in the case of a disassembly of the target shape due to any reason, the assembly process could be resumed again starting with the first two robots (D_1 and D_2) for creating the initial shape from an arbitrary initial configuration of microrobots.

The control bandwidth in *R-Cluster-String* system is $\zeta_n = n + 1$. As it was shown in Lemma 3, in order to add exactly one more hysteresis state to the *R-Cluster-String* system, we need to add one microrobot with exactly one independent voltage level.

4.2 Symmetric Electromechanical SATurated - 1 System (SeSAT-1)

Consider a Microrobotic system with (K) independent snap-down and (L) independent release voltages.

Definition 8. *Complete Group:* We define the Complete Group (CG), to be all microrobots sorted according to descending value of V_d with equal release voltages V_u .

Definition 9. *Diminished Group:* We define the Diminished Group (DG), to be all microrobots sorted according to descending value of V_d with equal release voltages V_u . In this group, the microrobot with the maximum snap-down voltage is removed. Hence, DG is as same as CG but the number of the robots is reduced by exactly one.

Definition 10. *Nested Group:*

This group Nested Group (NG) consists of one R-Cluster and the rest of the microrobots sorted according to the descending value of V_d with equal release voltages V_u . Figure 32 shows the Nested Group (NG).

Lemma 4. *Any n - microrobotic system can be sorted in such a way that the required $n + 2$ R-Cluster-String hysteresis states are addressable.*

Proof: By Construction:

Let an n - microrobotic system be a system with (L) independent release voltages and (K) independent snap-down voltages. We know that $n \leq KL$. Consider a system constructed by one Nested Group (NG), followed by one Diminished Group (DG), and finally followed by Complete Groups (CG)s for the rest of the microrobots in the system. Figure 33 shows such a system when $K = 4$ and $L = 4$. We call such a system Symetric Electromechanical SATurated - 1 (SeSAT-1). In this system, $n = KL - 1$. For this system, there exists control primitives $P_{12}(S)$, $P_i(S)$ and $P_j(S)$, shown in Equation 4.8, Equation 4.10 and Equation 4.12 which generates all $n + 2$ R-Cluster-String control primitives. $P_{12}(S)$, $P_i(S)$ and $P_j(S)$ are defined by a control cycle containing six, six and four control pulses with a decision variable S , respectively. $P_{12}(S)$ is the equation for creating required control primitives for the first two microrbots (D_1 and D_2) inside the R-Cluster. $P_i(S)$ is the equation for creating required control primitives for the rest of the microrobots in the Nested Group (NG) and finally $P_j(S)$ is the equation for creating required control primitives for the rest of the microrobots. Unlike the previous techniques [7], the new control primitives do not increase with population size, enabling the implementation

of the proposed control system. We construct the control primitives , $P_{12}(S)$, $P_i(S)$ and $P_j(S)$.

$V_{max} = MAX\{V_{d,k}\}$, $1 \leq k \leq n$; $V_{u,i}^+ = V_{u,i} + \delta_v$, $V_{u,i}^- = V_{u,i} - \delta_v$ and $V_{d,i}^- = V_{d,i} - \delta_v$ where $i \in Z_{NG} = \{3, \dots, K\}$. $V_{u,j}^+ = V_{u,j} + \delta_v$, $V_{u,j}^- = V_{u,j} - \delta_v$ and $V_{d,j}^- = V_{d,j} - \delta_v$ where $j \in Z_n = \{(K+1), \dots, n\}$.

$P_{12}(S)$, $P_i(S)$ and $P_j(S)$ generate $n+2$ control primitives that form a *R-Cluster-String* matrix.

$$P_{12}(S) = \begin{cases} (V_{max}, V_{u,1}^-, V_{d,2}, V_{u,1}^+, V_{d,2}^-, V_{u,2}^+) & \text{if } S = 0 \\ (V_{max}, V_{u,1}^-, V_{d,2}, V_{u,2}^+) & \text{if } S = 1 \\ (V_{max}, V_{u,1}^-, V_{d,1}, V_{u,1}^+, V_{d,2}^-, V_{u,2}^+) & \text{if } S = 2 \\ (V_{max}, V_{u,1}^-, V_{d,1}, V_{u,2}^+) & \text{if } S = 3 \end{cases} \quad (4.8)$$

$$(D_1, D_2) - Hysteresis - States = \begin{cases} "00", & \text{if } S = 0 \\ "01", & \text{if } S = 1 \\ "10", & \text{if } S = 2 \\ "11", & \text{if } S = 3 \end{cases} \quad (4.9)$$

$$P_i(S) = \begin{cases} (V_{max}, V_{u,1}^-, V_{d,2}, V_{u,1}^+, V_{d,i}^-, V_{u,i}^+) & \text{if } i \in Z_{NG}, S = 0 \\ (V_{max}, V_{u,1}^-, V_{d,2}, V_{u,1}^+, V_{d,i}^+, V_{u,i}^+) & \text{if } i \in Z_{NG}, S = 1 \end{cases} \quad (4.10)$$

$$(D_i) - Hysteresis - States = \begin{cases} "0", & \text{if } S = 0 \\ "1", & \text{if } S = 1 \end{cases} \quad (4.11)$$

$$P_j(S) = \begin{cases} (V_{max}, V_{u,j}^-, V_{d,j}^-, V_{u,j}^+) & \text{if } j \in Z_n, S = 0 \\ (V_{max}, V_{u,j}^-, V_{d,j}^+, V_{u,j}^+) & \text{if } j \in Z_n, S = 1 \end{cases} \quad (4.12)$$

$$(D_j) - Hysteresis - States = \begin{cases} "0", & \text{if } S = 0 \\ "1", & \text{if } S = 1 \end{cases} \quad (4.13)$$

Proof. By Induction:

Base condition: All Microrobots D_i , ($i \in \{1, \dots, n\}$) are in state 0.

Inductive step:

First, we will show that after applying $P_{12}(S)$, the first two microrobots inside the R-Cluster (D_1, D_2) will be in states 00, 01, 10, 11 based on the value of (S) while all other microrobots are in state 1. In the next step, we will show that by applying $P_i(S)$, microrobot D_i , $i \in Z_{NG} = \{3, \dots, K\}$ (e.g. $i \in \{3, 4\}$ in Figure 33 will be in state 0 or 1 based on the value of (S) while all microrobots (D_1, \dots, D_{i-1}) are in state 0 and all microrobots D_k , $(k > i)$ $k \in \{1, \dots, n\}$ are in state 1. Finally, we will prove that $P_j(S)$ causes D_j , $j \in \{(K+1), \dots, n\}$ (e.g. $j \in \{4, 5, \dots, 15\}$ in Figure 33 to be in state 0 or 1 based on the value of (S) while all microrobots (D_1, \dots, D_{j-1}) are in state 0 and all microrobots $D_k, (k > j)$ $k \in \{1, \dots, n\}$ are in state 1.

$P_{12}(S)$:

if $S = 0$ then $P_{12}(S) = (V_{max}, V_{u,1}^-, V_{d,2}, V_{u,1}^+, V_{d,2}^-, V_{u,2}^+)$.

By applying V_{max} and $V_{u,1}^-$, the Nested Group (NG) and Diminished Group (DG) will be in state 0 while all Complete Groups (CG)s will be in state 1. $V_{d,2}$ and $V_{u,1}^+$ set the Diminished Group (DG) to state 1 and release the Nested Group (NG) (state = 0) while keeping all the Complete Groups (CG)s in state 1. Finally, $V_{d,2}^-$ and $V_{u,2}^+$ set D_1 and D_2 to state 00 while keeping all other microrobots in state 1.

if $S = 1$ then $P_{12}(S) = (V_{max}, V_{u,1}^-, V_{d,2}, V_{u,2}^+)$.

By applying V_{max} and $V_{u,1}^-$, the Nested Group (NG) and Diminished Group (DG) will be in state 0 while all Complete Groups (CG)s will be in state 1. $V_{d,2}$ sets all the microrobots except D_1 to state 1 and finally $V_{u,2}^+$ sets D_1 and D_2 to state 01 while keeping all other microrobots in state 1.

if $S = 2$ then $P_{12}(S) = (V_{max}, V_{u,1}^-, V_{d,1}, V_{u,1}^+, V_{d,2}^-, V_{u,2}^+)$.

By applying V_{max} and $V_{u,1}^-$, the Nested Group (NG) and Diminished Group (DG) will be in state 0 while all Complete Groups (CG)s will be in state 1. $V_{d,1}$ and $V_{u,1}^+$ set D_1 and the Diminished Group (DG) to state 1 and release all other robots in the Nested Group (NG) (state = 0) while keeping all the Complete Groups (CG)s in state 1. Finally, $V_{d,2}^-$ and $V_{u,2}^+$ set D_1 and D_2 to state 10 while keeping all other microrobots in state 1.

if $S = 3$ then $P_{12}(S) = (V_{max}, V_{u,1}^-, V_{d,1}, V_{u,2}^+)$.

By applying V_{max} and $V_{u,1}^-$, the Nested Group (NG) and Diminished Group (DG) will be in state 0 while all Complete Groups (CG)s will be in state 1. $V_{d,1}$ sets R-Cluster to state 11 and $V_{u,2}^+$ will keep R-Cluster at state 11 while all other microrobots are in state 11.

$P_i(S)$, $i \in \{3, \dots, K\}$ (e.g. $i \in \{3, 4\}$ in Figure 33) :

if $S = 0$ then $P_i(S) = (V_{max}, V_{u,1}^-, V_{d,2}, V_{u,1}^+, V_{d,i}^-, V_{u,i}^+)$

After Applying V_{max} and $V_{u,1}^-$ the Nested Group (NG) and Diminished Group (DG) will be in state 0 while all Complete Groups (CG)s will be in state 1. $V_{d,2}$ and $V_{u,1}^+$ snap down the Diminished Group (DG) and release the Nested Group (NG). $V_{d,i}^-$ and $V_{u,i}^+$ set microrobot D_i to state 0 while all microrobots (D_1, \dots, D_{i-1}) are in state 0 and all microrobots $D_k, (k > i)$ $k \in \{1, \dots, n\}$ are in state 1.

if $S = 1$ then $P_i(S) = (V_{max}, V_{u,1}^-, V_{d,2}, V_{u,1}^+, V_{d,i}^+, V_{u,i}^+)$

After Applying V_{max} and $V_{u,1}^-$ the Nested Group (NG) and Diminished Group (DG) will be in state 0 while all Complete Groups (CG)s will be in state 1. $V_{d,2}$ and $V_{u,1}^+$ snap down the Diminished Group (DG) and release the Nested Group (NG). $V_{d,i}^+$ and $V_{u,i}^+$ set microrobot D_i

to state 1 while all microrobots (D_1, \dots, D_{i-1}) are in state 0 and all microrobots $D_k, (k > i)$ $k \in \{1, \dots, n\}$ are in state 1.

$P_j(S), j \in \{(K+1), \dots, n\}$ (e.g. $j \in \{4, 5, \dots, 15\}$ in Figure 33):

if $S = 0$ then $P_j(S) = (V_{max}, V_{u,j}^-, V_{d,j}^-, V_{u,j}^+)$

After Applying V_{max} and $V_{u,j}^-$, the group that contains D_j and all the groups before it are in state 0 while all the groups after it are in state 1. $V_{d,j}^-$ and $V_{u,j}^+$ set D_j to state 0 while all microrobots (D_1, \dots, D_{j-1}) are in state 0 and all microrobots $D_k, (k > i)$ are in state 1.

if $S = 1$ then $P_j(S) = (V_{max}, V_{u,j}^-, V_{d,j}^+, V_{u,j}^+)$

After Applying V_{max} and $V_{u,j}^-$, the group that contains D_j and all the groups before it are in state 0 while all the groups after it are in state 1. $V_{d,j}^+$ and $V_{u,j}^+$ set D_j to state 1 while all microrobots (D_1, \dots, D_{j-1}) are in state 0 and all microrobots $D_k, (k > i)$ are in state 1.

□

Theorem 2. *Any planning algorithm for the R-Cluster-String system can be deployed to construct the control sequence for motion planning the SeSAT-1 system.*

Proof. As it was shown in Lemma 4, we can construct the R-Cluster-String control matrix for the SeSAT-1 system.

□

We have shown that we can reduce the control bandwidth requirements ζ_n . For a micro-robotic system with L independent release and K independent snap-down voltage levels. The control voltage bandwidth is $\zeta_n = K + L$. The number of microrobots in the SeSAT-1 system is

TABLE IV: COMPARISON OF THE CONTROL VOLTAGE BANDWIDTH REQUIREMENTS OF NHG, STRING, SESAT, R-CLUSTER-STRING AND SESAT-1 SYSTEMS

	Control Strategies				
	NHG	STRING	SESat	R-Cluster-String	SeSAT-1
ζ_n	$2n$	$n + 1$	$\lceil 2\sqrt{n} \rceil$	$n + 1$	$\lceil 2\sqrt{n + 1} \rceil$
No. control pulses	$O(n)$	2	$O(n)$	2	$O(1)$
Number of controllable robots with $\zeta_n = 20$	10	19	100	19	99

$n = (KL - 1)$. We know that n is maximized when $L = K = \zeta_n/2$, and $\zeta_n = \lceil 2\sqrt{n + 1} \rceil$. Table IV compares the control voltage bandwidth requirements and the number of control pulses in the control cycle of the five classes of microrobotic systems: a) NHG, b) STRING, c) SESat, d) R-Cluster-String and e) SeSAT-1.

4.3 Hardware Experiments

In this section, we explain our hardware platform, experimental process and the results.

4.3.1 Robots with two direct-drive wheels

We have applied the SeSAT-1 control strategy on a group of macroscale robots. These robots were designed in such a way that could mimic the behavior of stress-engineered MEMS

microrobots. These robots have two direct-drive wheels that are unidirectional and unicycle. The kinematics of the robot is shown in Figure 34. $L = 18$ cm and $W = 13$ cm shows the length and width of the robot, respectively. The configuration is defined as $q = (x, y, \theta)$ and its configuration space by $\mathcal{Q} = \mathbb{R}^2 \times \mathbb{S}^1$. The kinematics of our robot is given by

$$\dot{q} = u \begin{bmatrix} \cos \theta \\ \sin \theta \\ 0 \end{bmatrix} + \omega \begin{bmatrix} 0 \\ 0 \\ 1 \end{bmatrix} \quad (4.14)$$

4.3.2 Hardware system

For each robot, two virtual snap-down and release points are defined. snap-down point results in turning while the release point causes the robot to move forward. In order to complete the assembly process using SeSAT-1 control strategy, we need 4 - 6 control pulses to be applied to the system for each control primitive. These pulses are broadcast over 2.4 GHz using XBee 2 mW wire antenna and every robot receives exactly the same control pulses. Each robot reacts to these control pulses based on its snap-down and releases points. Our system consists of eight robots. We assigned equal linear and turning velocities to all robots but we experimentally recorded different speeds due to the system noise.

4.3.3 Assembly

Our control strategies have been implemented on a group of eight robots. The target shape could be any shape that could be created with our robots. The robots were operated in 330 cm \times 330 cm environment. We recorded the position of the robots with a digital video camera.

As it was mentioned, the control waveform pulses for the control primitives were broadcast using XBee 2 mW wire antenna from a local PC. The duration of each control primitive was controlled manually during the execution of the control sequence S .

As our experimental results show, our control strategies were able to accomplish the assembly process and make the cross target shape. Figure 35 shows our experiment for the assembly process.

4.3.3.1 Robustness against disturbance

Our proposed control strategy is robust against disturbance because, in the case of a disassembly of the target shape due to any reason, the assembly process could be resumed again starting with the first two robots (D_1 and D_2) for creating the seed-shape from an arbitrary initial configuration of microrobots. Following the construction of the seed shape, robot D_i where $i \in \{3, 4, \dots, n\}$ are maneuvered sequentially, completing the assembly of the target shape.

We applied our proposed control strategy to a group of four robots. We chose a cross shape to be our target shape. As it was stated before, δ_v is the maximum deviation of the transition voltage manifested during the microrobot operation. The two transition voltages (snap-down or release points) are separated by at least $2\delta_v$. We chose δ_v to be 0.5 for our experiments and consequently, the transition points are separated by 1. We conducted an experiment to show that in the case of a disassembly, our control policy can create the assembly shape again. Figure 36 shows the robustness against disturbance in our assembly process. Movies of these assembly experiments are available online at <https://www.youtube.com/watch?v=eknPV5qFIbc>.

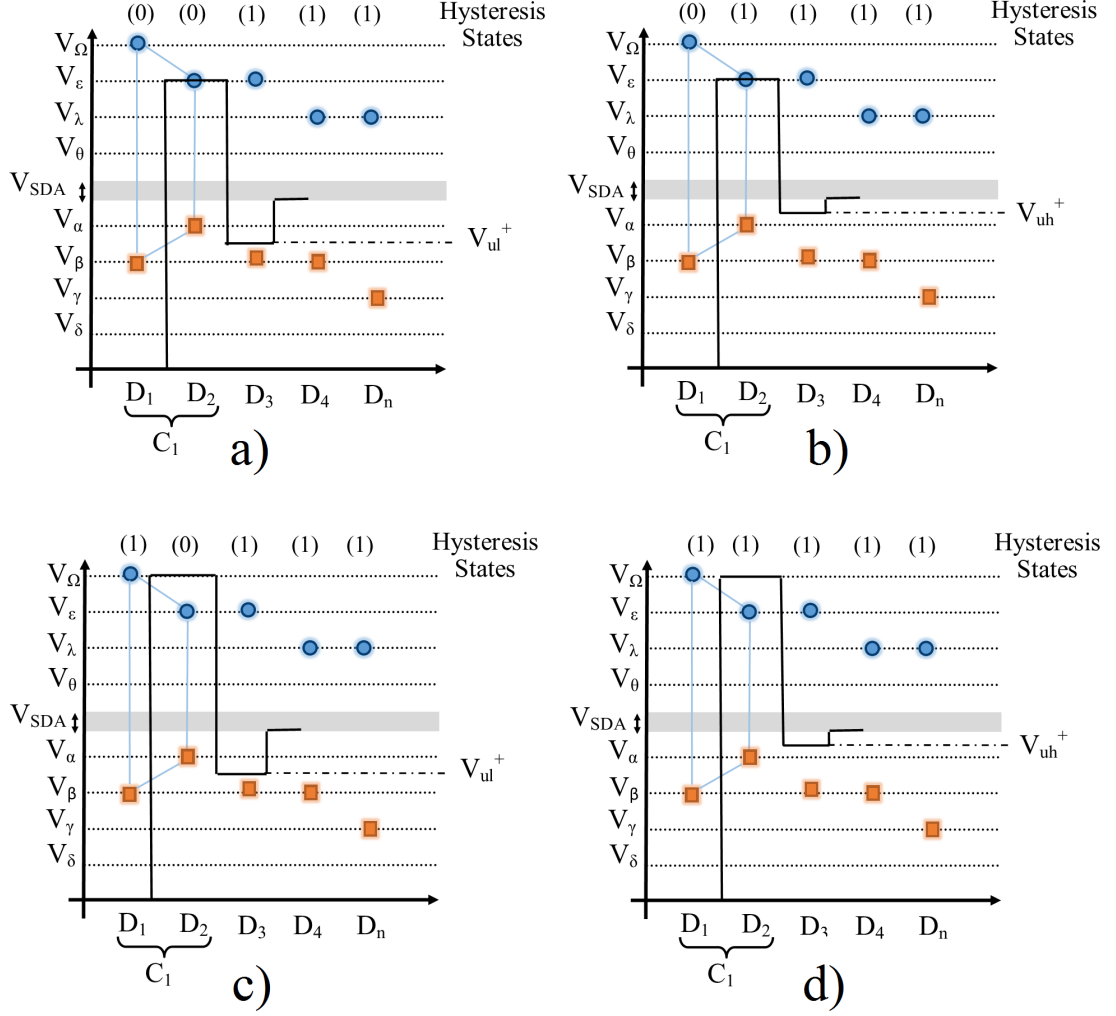


Figure 30: Illustration of control cycle in R-Cluster-String system. a) Control primitive $P_{12}(S)$, where $S = 0$, b) Control primitive $P_{12}(S)$, where $S = 1$, c) Control primitive $P_{12}(S)$, where $S = 2$, and d) Control primitive $P_{12}(S)$, where $S = 3$.

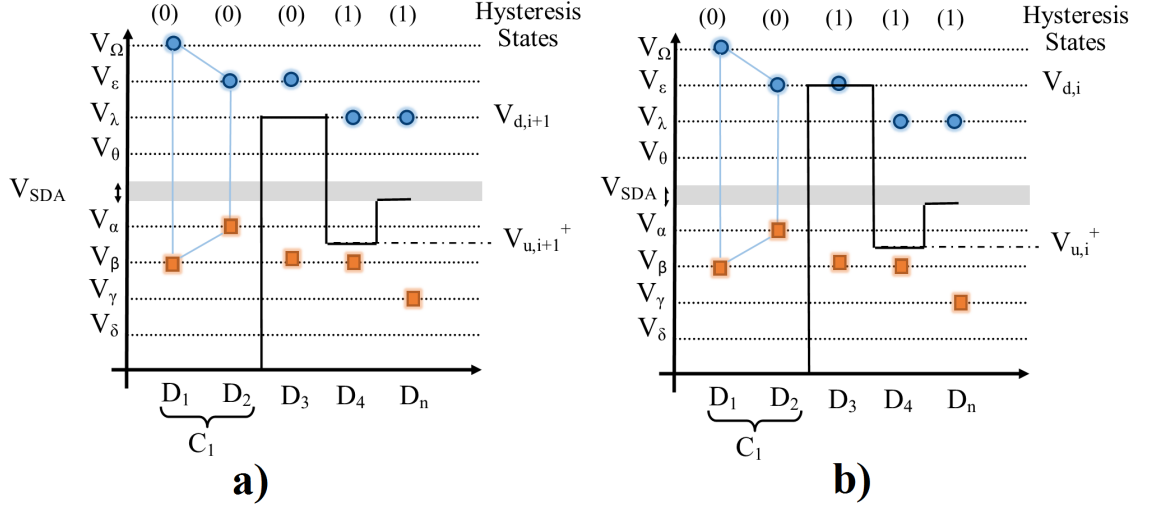


Figure 31: Illustration of control cycle in *R-Cluster-String* system. a) Control primitive $P_i(S)$, where $S = 0$ and $i = 3$, and b) Control primitive $P_i(S)$, where $S = 1$ and $i = 3$.

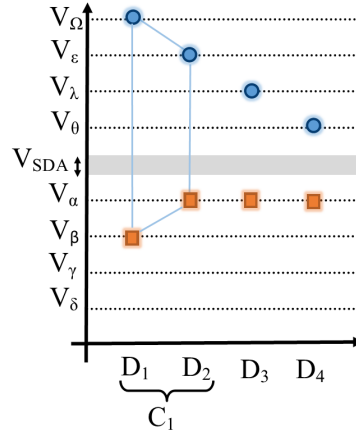


Figure 32: Illustration of Nested Group (NG)

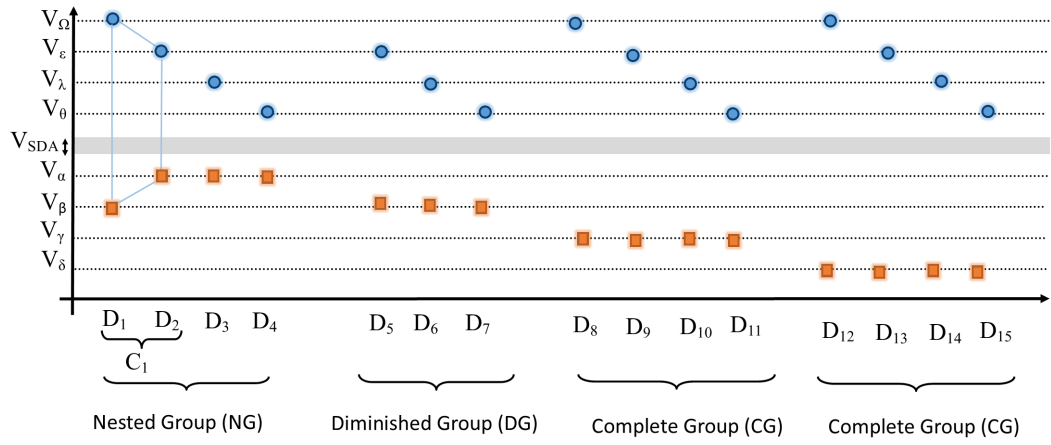


Figure 33: Example of a SeSAT-1 system with $K = 4$ and $L = 4$.

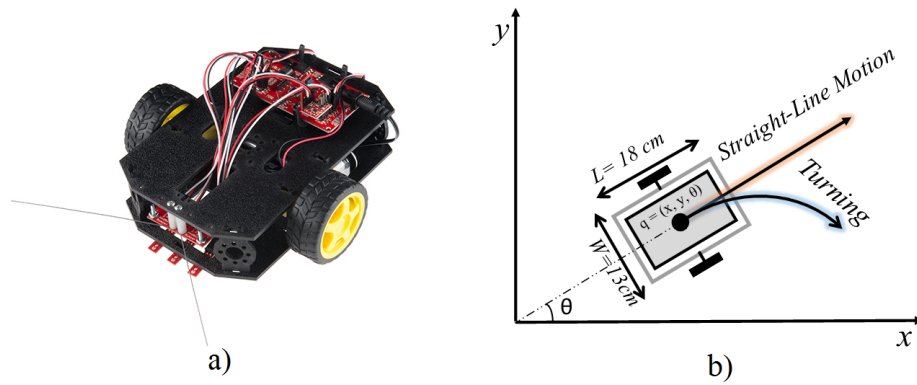


Figure 34: a) Schematic of the Robot, b) Kinematics of the Robot.

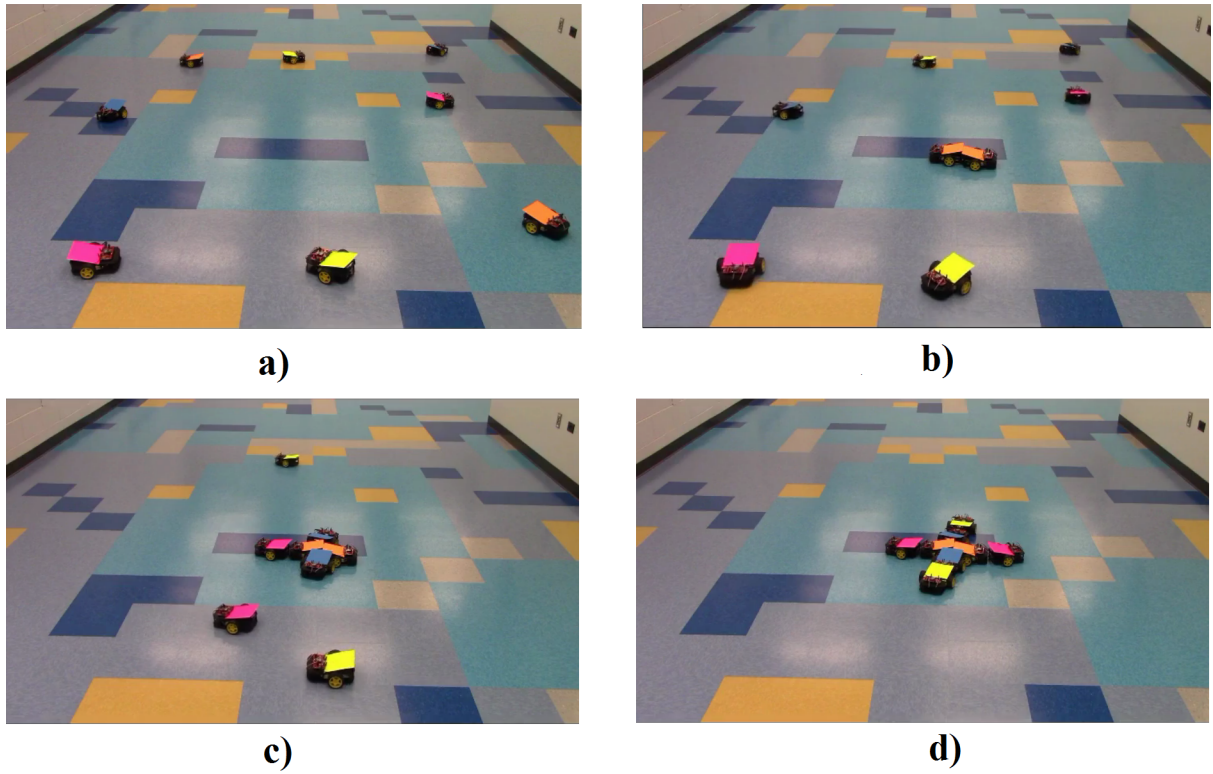


Figure 35: Experimental assembly data using eight robots. a) Arbitrary initial configuration, b) Forming the seed shape, c) Forming the intermediate shape, and finally d) Generating the final shape.

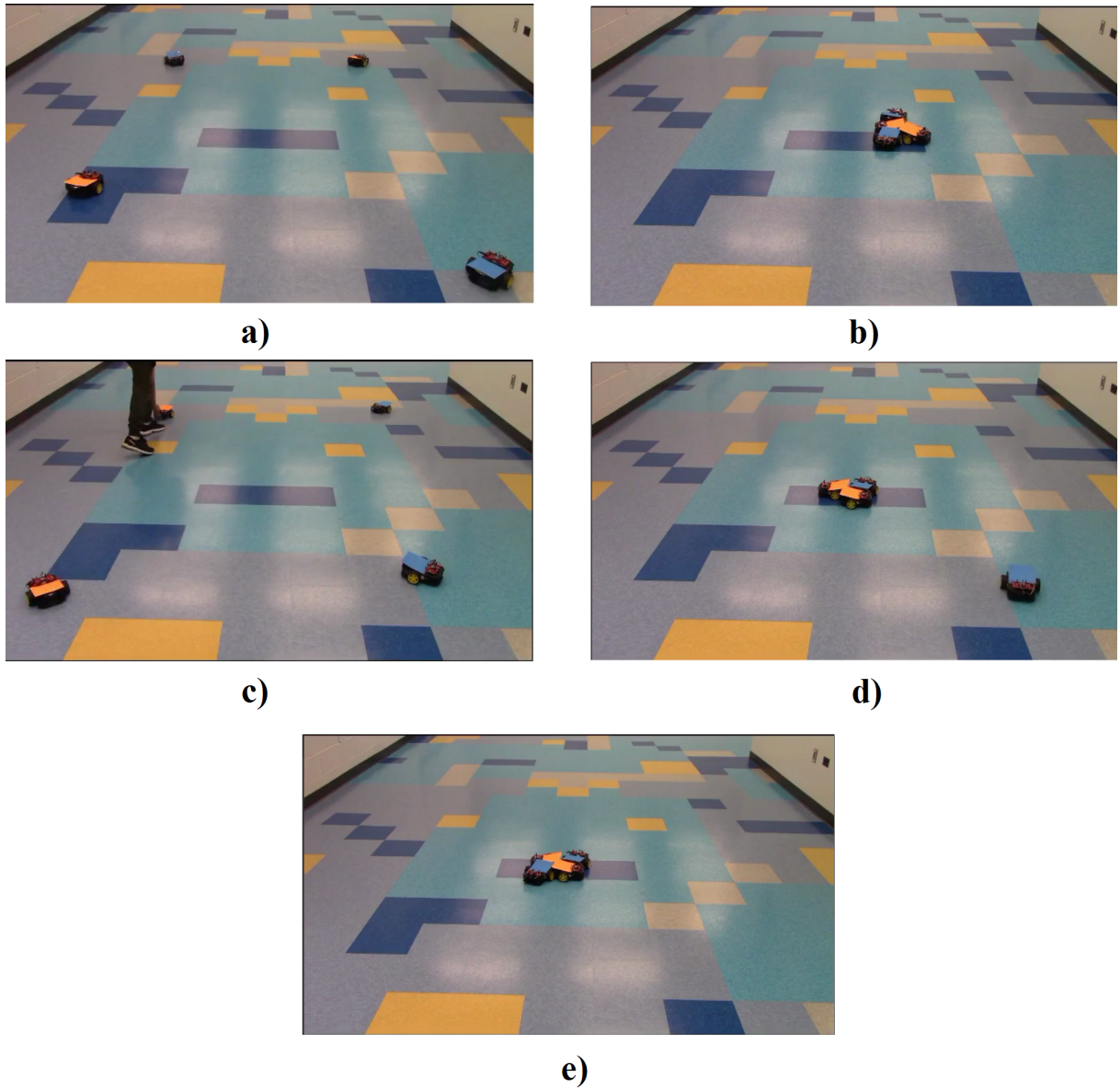


Figure 36: Robustness against disturbance experiment using four robots. a) Arbitrary initial configuration, b) Generating the final shape, c) Disassembly due to disturbance, d) Forming the intermediate shape, and finally e) Generating the final shape.

CHAPTER 5

CONCLUSION

This dissertation proposed a theoretical control framework for completing the micro-assembly for multi-stress-engineered MEMS microrobotic system. The stress-engineered MEMS micro-robot (MicroStressBots) are fabricated using surface micromachining PolyMUMPS foundry process [68]. The MicroStressBots operation mechanism, can be found in detail in [62]. This robot includes an untethered scratch drive actuator (USDA) and an out-of-plane steering-arm actuator [62]. The USDA actuator is responsible for the translation of the MicroStressBots and the steering-arm decides if the robot moves straight or turns. The USDA is $120\text{ }\mu\text{m} \times 60\text{ }\mu\text{m} \times 1.5\text{ }\mu\text{m}$ and the steering-arm actuator is approximately $120\text{ }\mu\text{m}$ to $160\text{ }\mu\text{m}$. The MicroStressBot is fabricated from polycrystalline silicon using a MEMS foundry process [68]. Post-processing is used to curve out-of-plane (upwards) the steering arm of MicroStressBot [69]. The microrobot is actuated on a special substrate. The substrate consists of a field of insulated interdigitated electrodes. A capacitive circuit is built between the body of the microrobot and the substrate by applying a voltage waveform between the pairs of electrodes. The electric potential of the formed capacitive coupling provides power for the actuation of the USDA and also controls the state of the steering arm. The voltage waveform that results in capacitive coupling of the microrobot chassis and the substrate is called the control waveform. This waveform has two parts: *a)* Control-cycle: the pulses that control the hysteresis state of the steering arm, and *b)* Power-delivery-cycle: that results in USDA translation. The power-delivery-cycle consists

of pulses that change between a minimum V_b and a maximum V_s . In order to actuate the USDA, V_s must be greater than the minimum voltage (V_{flex}) at which the backplate of the USDA is flexed, while V_b must be less than the maximum voltage (V_{rel}) at which the flexure in the backplate is relaxed. V_{flex} and V_{rel} are described in more detail in [70]. The steering arm of MicroStressBot changes its state at two different voltage levels. The voltage level, at which the steering arm is lowered and the robot is turning, is called snap-down voltage (V_d) and the voltage level at which the arm is raised and the robot is moving straight, is called the release voltage (V_u). These voltage levels are the transition voltages of the steering arm. Nathanson [71] lumped model for the snap-down voltage of a cantilever is shown in Equation 5.1.

$$V_{SD} \approx \sqrt{\frac{8Kg_0^3}{27\epsilon_0 A}} \quad (5.1)$$

Where g_0 is the zero-voltage gap between the electrode and the cantilever, K is the cantilever beam spring constant, and A is the cantilever area. Similarly, the release voltage lumped model [62] is

$$V_R \approx \sqrt{\frac{2Kg_1^2(g_0 - g_1)}{\epsilon_0 A}} \quad (5.2)$$

where g_1 is the air gap between the cantilever and the electrodes.

As it is stated in [62], in order to have a high snap-down voltage and low release voltage, the ratio of the snap-down voltage to the release voltage must be increased. Equation 5.3 shows the (snap-down / release) voltage ratio.

$$\frac{V_{SD}}{V_R} \approx \sqrt{\frac{4g_0^3}{27g_1^2(g_0 - g_1)}} \quad (5.3)$$

The (snap-down / release) voltage ratio does not depend on the cantilever beams spring constant and area, but it mainly depends on g_0 and g_1 . Hence, g_0 and g_1 (the parameters along the z-axis) are the design parameters for independent control of the steering arm. In order to adjust the z-axis parameters, they have done special post-processing stress engineering for curving out the steering arm by depositing chromium stress layer on top of the steering arm [62]. Stress engineering can be found in detail in [62] and [6]. In [6], independent microrobots with different snap-down and release voltages have been designed using Equation 5.3, finite element models, and empirical data.

This dissertation proposed a time-efficient control strategy that could complete multiple-shapes microassembly from arbitrary initial configuration with a constant number of control primitives. We have shown that by the proposed control strategies we will have an efficient control system to implement planar microassembly for the highly underactuated system. As it was mentioned, all the manipulative control primitives consist of the constant number of control pulses $O(1)$ and do not increase with population size. the proposed control strategy is robust against disturbance and in the case of a disassembly of the target shape due to any reason, the assembly process could be resumed again.

We have implemented the proposed control strategies on macroscale robots, which were designed to emulate the behavior of stress-engineered MEMS microrobots. We have defined two ideal snap-down and release points for each robot. The robots have two direct-drive wheels that can only turn in one direction and can only move forward. These commands are broadcast over 2.4 GHz using XBee 2 mW wire antenna. These results lay the foundation for developing new methods to control of a large number of MEMS microrobots.

Appendices

4/16/2018

Rightslink® by Copyright Clearance Center



The screenshot shows the RightsLink interface. At the top left is the Copyright Clearance Center logo. Next to it is the RightsLink logo. On the right are buttons for Home, Create Account, and Help, along with a chat icon. Below the logo is a purple box with the IEEE logo and the text "Requesting permission to reuse content from an IEEE publication". To the right of this box, the following information is displayed:

Title: Polymer-Based Wireless Resonant Magnetic Microrobots
Author: Hsi-Wen Tung; Massimo Maffioli; Dominic R. Frutiger; Kartik M. Sivaraman; Salvador Pané; Bradley J. Nelson
Publication: Robotics, IEEE Transactions on
Publisher: IEEE
Date: Feb. 2014
 Copyright © 2014, IEEE

To the right of this information is a "LOGIN" box. It contains the text: "If you're a copyright.com user, you can login to RightsLink using your copyright.com credentials. Already a RightsLink user or want to [learn more?](#)"

Thesis / Dissertation Reuse

The IEEE does not require individuals working on a thesis to obtain a formal reuse license, however, you may print out this statement to be used as a permission grant:

Requirements to be followed when using any portion (e.g., figure, graph, table, or textual material) of an IEEE copyrighted paper in a thesis:

- 1) In the case of textual material (e.g., using short quotes or referring to the work within these papers) users must give full credit to the original source (author, paper, publication) followed by the IEEE copyright line © 2011 IEEE.
- 2) In the case of illustrations or tabular material, we require that the copyright line © [Year of original publication] IEEE appear prominently with each reprinted figure and/or table.
- 3) If a substantial portion of the original paper is to be used, and if you are not the senior author, also obtain the senior author's approval.

Requirements to be followed when using an entire IEEE copyrighted paper in a thesis:

- 1) The following IEEE copyright/ credit notice should be placed prominently in the references: © [year of original publication] IEEE. Reprinted, with permission, from [author names, paper title, IEEE publication title, and month/year of publication]
- 2) Only the accepted version of an IEEE copyrighted paper can be used when posting the paper or your thesis on-line.
- 3) In placing the thesis on the author's university website, please display the following message in a prominent place on the website: In reference to IEEE copyrighted material which is used with permission in this thesis, the IEEE does not endorse any of [university/educational entity's name goes here]'s products or services. Internal or personal use of this material is permitted. If interested in reprinting/republishing IEEE copyrighted material for advertising or promotional purposes or for creating new collective works for resale or redistribution, please go to http://www.ieee.org/publications_standards/publications/rights/rights_link.html to learn how to obtain a License from RightsLink.

If applicable, University Microfilms and/or ProQuest Library, or the Archives of Canada may supply single copies of the dissertation.

BACK

CLOSE WINDOW

Copyright © 2018 Copyright Clearance Center, Inc. All Rights Reserved. [Privacy statement](#). [Terms and Conditions](#). Comments? We would like to hear from you. E-mail us at customercare@copyright.com

Figure 37: Permission for Chapter 1 Reference 2

4/16/2018

Rightslink® by Copyright Clearance Center



The screenshot shows the RightsLink interface. At the top, there are logos for the Copyright Clearance Center and RightsLink, along with navigation buttons for Home, Create Account, and Help. A chat bubble is also visible. On the left, a blue box contains the IEEE logo and the text 'Requesting permission to reuse content from an IEEE publication'. The main content area displays the following information:

- Title:** Holonomic 5-DOF magnetic control of 1D nanostructures
- Conference Proceedings:** 2012 IEEE International Conference on Robotics and Automation
- Author:** S. Schürle; K. E. Peyer; B. E. Kratochvil; B. J. Nelson
- Publisher:** IEEE
- Date:** 14-18 May 2012

Below this information, it says 'Copyright © 2012, IEEE'. On the right, there is a 'LOGIN' section with the text: 'If you're a copyright.com user, you can login to RightsLink using your copyright.com credentials. Already a RightsLink user or want to [learn more?](#)'

Thesis / Dissertation Reuse

The IEEE does not require individuals working on a thesis to obtain a formal reuse license, however, you may print out this statement to be used as a permission grant:

Requirements to be followed when using any portion (e.g., figure, graph, table, or textual material) of an IEEE copyrighted paper in a thesis:

- 1) In the case of textual material (e.g., using short quotes or referring to the work within these papers) users must give full credit to the original source (author, paper, publication) followed by the IEEE copyright line © 2011 IEEE.
- 2) In the case of illustrations or tabular material, we require that the copyright line © [Year of original publication] IEEE appear prominently with each reprinted figure and/or table.
- 3) If a substantial portion of the original paper is to be used, and if you are not the senior author, also obtain the senior author's approval.

Requirements to be followed when using an entire IEEE copyrighted paper in a thesis:

- 1) The following IEEE copyright/ credit notice should be placed prominently in the references: © [year of original publication] IEEE. Reprinted, with permission, from [author names, paper title, IEEE publication title, and month/year of publication]
- 2) Only the accepted version of an IEEE copyrighted paper can be used when posting the paper or your thesis on-line.
- 3) In placing the thesis on the author's university website, please display the following message in a prominent place on the website: In reference to IEEE copyrighted material which is used with permission in this thesis, the IEEE does not endorse any of [university/educational entity's name goes here]'s products or services. Internal or personal use of this material is permitted. If interested in reprinting/republishing IEEE copyrighted material for advertising or promotional purposes or for creating new collective works for resale or redistribution, please go to http://www.ieee.org/publications_standards/publications/rights/rights_link.html to learn how to obtain a License from RightsLink.

If applicable, University Microfilms and/or ProQuest Library, or the Archives of Canada may supply single copies of the dissertation.

[BACK](#)
[CLOSE WINDOW](#)

Copyright © 2018 Copyright Clearance Center, Inc. All Rights Reserved. [Privacy statement](#). [Terms and Conditions](#). Comments? We would like to hear from you. E-mail us at customercare@copyright.com

Figure 38: Permission for Chapter 1 Reference 4

TRF
TRANSDUCER RESEARCH FOUNDATION

Submission Date: 4/23/2018 TRF Permission Number: TRF18 HH14473

Reprint Request Form
Submit by fax to 1-619-232-0799

I am preparing a manuscript that is to be published by: University of Illinois at Chicago (UIC)

The estimated date of publication is May/2019 and the approximate number of page(s): 110

I request permission of TRF to include the following material in this and in all subsequent editions of the publication listed above, including versions made by nonprofit organizations for use of physically handicapped persons, and in all foreign-language translations and other derivative works.

Requesting Publication's Author(s) and/or editor(s): Vahid Foroutan *MEMS Micro robots through Common Control signed*

Title of requesting publication: My Thesis (Control for Micro-Assembly of Heterogeneous)

Title, Author(s), Source and year of TRF publication material: Levitation of untethered stress-engineered microflyers using thermophoretic (KNØDSEN, Force, (Vahid Foroutan, R. Majumdar, O. Mahdizadeh, S.P. Ward, Igor Paprotny) Hilton Head Workshop - 2019/6

Data Location:

A. From page 105, line 1, beginning with the words In this paper to page 106, line last line, ending with the words microscale robots

B. Figure number 1, 3, 4, 5 on page 105, 106

C. Table number 1 on page 106. If necessary, attach continuation sheets.

I have secured agreement for this requested permission from the author(s) of this material as indicated and have appended their approval letter with this form. I have read and accept the conditions for this permission and have attached copies of requested work as stated in the Policy for Grant of Reprint Permission by the Transducer Research Foundation dated August 2005.

Signature: [Signature] Date: 4/18/2018

Type or Print Name of Signator Vahid Foroutan

E-mail address: vforou2@uic.edu Fax#: _____

Agreed to, and accepted on behalf of The Transducer Research Foundation by:


TRF Representative: Katharine L. Clin Date: April 18, 2018
Ex. Director


Transducers Research Foundation
c/o Preferred Meeting Management
307 Laurel Street, San Diego, CA. 92101-1630
Phone: 1-619-232-9489 Fax: 1-619-232-0799
info@transducer-research-foundation.org http://www.transducer-research-foundation.org


Figure 39: Permission for Chapter 1 Reference 5

4/17/2018

Rightslink® by Copyright Clearance Center



[Home](#)
[Create Account](#)
[Help](#)




Title: Planar Microassembly by Parallel Actuation of MEMS Microrobots

Author: Bruce R. Donald

Publication: Microelectromechanical Systems, IEEE/ASME Journal of

Publisher: IEEE

Date: Aug. 2008

Copyright © 2008, IEEE

LOGIN

If you're a copyright.com user, you can login to RightsLink using your copyright.com credentials. Already a **RightsLink user** or want to [learn more?](#)

Thesis / Dissertation Reuse

The IEEE does not require individuals working on a thesis to obtain a formal reuse license, however, you may print out this statement to be used as a permission grant:

Requirements to be followed when using any portion (e.g., figure, graph, table, or textual material) of an IEEE copyrighted paper in a thesis:

- 1) In the case of textual material (e.g., using short quotes or referring to the work within these papers) users must give full credit to the original source (author, paper, publication) followed by the IEEE copyright line © 2011 IEEE.
- 2) In the case of illustrations or tabular material, we require that the copyright line © [Year of original publication] IEEE appear prominently with each reprinted figure and/or table.
- 3) If a substantial portion of the original paper is to be used, and if you are not the senior author, also obtain the senior author's approval.

Requirements to be followed when using an entire IEEE copyrighted paper in a thesis:

- 1) The following IEEE copyright/ credit notice should be placed prominently in the references: © [year of original publication] IEEE. Reprinted, with permission, from [author names, paper title, IEEE publication title, and month/year of publication]
- 2) Only the accepted version of an IEEE copyrighted paper can be used when posting the paper or your thesis on-line.
- 3) In placing the thesis on the author's university website, please display the following message in a prominent place on the website: In reference to IEEE copyrighted material which is used with permission in this thesis, the IEEE does not endorse any of [university/educational entity's name goes here]'s products or services. Internal or personal use of this material is permitted. If interested in reprinting/republishing IEEE copyrighted material for advertising or promotional purposes or for creating new collective works for resale or redistribution, please go to http://www.ieee.org/publications_standards/publications/rights/rights_link.html to learn how to obtain a License from RightsLink.

If applicable, University Microfilms and/or ProQuest Library, or the Archives of Canada may supply single copies of the dissertation.

[BACK](#)
[CLOSE WINDOW](#)

Copyright © 2018 Copyright Clearance Center, Inc. All Rights Reserved. [Privacy statement](#). [Terms and Conditions](#). Comments? We would like to hear from you. E-mail us at customercare@copyright.com

Figure 40: Permission for Chapter 1 and Chapter 2 Reference 6

CITED LITERATURE

1. Jing, W. and Cappelleri, D.: A magnetic microrobot with in situ force sensing capabilities. Robotics, 3(2):106–119, 2014.
2. Tung, H.-W., Maffioli, M., Frutiger, D. R., Sivaraman, K. M., Pané, S., and Nelson, B. J.: Polymer-based wireless resonant magnetic microrobots. IEEE Transactions on Robotics, 30(1):26–32, 2014.
3. Steager, E. B., Sakar, M. S., Kim, D. H., Kumar, V., Pappas, G. J., and Kim, M. J.: Electrokinetic and optical control of bacterial microrobots. Journal of Micromechanics and Microengineering, 21(3):035001, 2011.
4. Schürle, S., Peyer, K. E., Kratochvil, B., and Nelson, B. J.: Holonomic 5-dof magnetic control of 1d nanostructures. In Robotics and Automation (ICRA), 2012 IEEE International Conference on, pages 1081–1086. IEEE, 2012.
5. Foroutan, V., Majumdar, R., Mahdavi pour, O., Ward, S., and Paprotny, I.: Levitation of untethered stress engineered microflyers using thermophoretic (knudsen) force. In Tech. Dig. Hilton Head Workshop 2014: A Solid-State Sensors, Actuators and Microsystems Workshop, pages 105–106, 2014.
6. Donald, B. R., Levey, C. G., and Paprotny, I.: Planar microassembly by parallel actuation of mems microrobots. Journal of Microelectromechanical Systems, 17(4):789–808, 2008.
7. Donald, B. R., Levey, C. G., Paprotny, I., and Rus, D.: Planning and control for microassembly of structures composed of stress-engineered mems microrobots. The International journal of robotics research, 32(2):218–246, 2013.
8. Dario, P., Valleggi, R., Carrozza, M., Montesi, M., and Cocco, M.: Microactuators for microrobots: a critical survey. Journal of Micromechanics and microengineering, 2(3):141, 1992.
9. Kahn, J. M., Katz, R. H., and Pister, K. S.: Next century challenges: mobile networking for smart dust. In Proceedings of the 5th annual ACM/IEEE international conference on Mobile computing and networking, pages 271–278. ACM, 1999.

10. Popa, D. O. and Stephanou, H. E.: Micro and mesoscale robotic assembly. Journal of manufacturing processes, 6(1):52–71, 2004.
11. Diller, E., Miyashita, S., and Sitti, M.: Magnetic hysteresis for multi-state addressable magnetic microrobotic control. In Intelligent Robots and Systems (IROS), 2012 IEEE/RSJ International Conference on, pages 2325–2331. IEEE, 2012.
12. Diller, E., Floyd, S., Pawashe, C., and Sitti, M.: Control of multiple heterogeneous magnetic microrobots in two dimensions on nonspecialized surfaces. IEEE Transactions on Robotics, 28(1):172–182, 2012.
13. Ward, S., Foroutan, V., Majumdar, R., Mahdavi-pour, O., Hussain, S. A., and Paprotny, I.: Towards microscale flight: Fabrication, stability analysis, and initial flight experiments for $300\mu m \times 300\mu m \times 1.5\mu m$ sized untethered mems microfliers. IEEE transactions on nanobioscience, 14(3):323–331, 2015.
14. Bouabdallah, S., Murrieri, P., and Siegwart, R.: Design and control of an indoor micro quadrotor. In Robotics and Automation, 2004. Proceedings. ICRA'04. 2004 IEEE International Conference on, volume 5, pages 4393–4398. IEEE, 2004.
15. Bouabdallah, S., Murrieri, P., and Siegwart, R.: Towards autonomous indoor micro vtol. Autonomous robots, 18(2):171–183, 2005.
16. Bouabdallah, S., Becker, M., Perrot, V., and Siegwart, R.: Toward obstacle avoidance on quadrotors. In Proceedings of the XII International Symposium on Dynamic Problems of Mechanics (DINAME 2007), pages 20–30. Citeseer, 2007.
17. Long, Y., Gelardos, A., and Cappelleri, D. J.: A novel micro aerial vehicle design: The evolution of the omnicopter mav. In ASME 2014 International Design Engineering Technical Conferences and Computers and Information in Engineering Conference, pages V05AT08A092–V05AT08A092. American Society of Mechanical Engineers, 2014.
18. Donald, B. R., Levey, C. G., McGray, C. D., Rus, D., and Sinclair, M.: Power delivery and locomotion of untethered microactuators. Journal of Microelectromechanical Systems, 12(6):947–959, 2003.
19. Hasegawa, T., Ogawa, N., Oku, H., and Ishikawa, M.: A new framework for microrobotic control of motile cells based on high-speed tracking and focusing. In Robotics and

- Automation, 2008. ICRA 2008. IEEE International Conference on, pages 3964–3969. IEEE, 2008.
20. Hasegawa, T., Ogawa, N., Oku, H., and Ishikawa, M.: A new framework for microrobotic control of motile cells based on high-speed 3-d tracking and galvanotaxis control. Journal of the Robotics Society of Japan, 26(6):575–582, 2008.
21. Felfoul, O., Mohammadi, M., Gaboury, L., and Martel, S.: Tumor targeting by computer controlled guidance of magnetotactic bacteria acting like autonomous micro-robots. In Intelligent Robots and Systems (IROS), 2011 IEEE/RSJ International Conference on, pages 1304–1308. IEEE, 2011.
22. Ou, Y., Kim, D. H., Kim, P., Kim, M. J., and Julius, A. A.: Motion control of tetrahymena pyriformis cells with artificial magnetotaxis: Model predictive control (mpc) approach. In Robotics and Automation (ICRA), 2012 IEEE International Conference on, pages 2492–2497. IEEE, 2012.
23. Estana, R. and Woern, H.: The micron robot project. In Autonome Mobile Systeme 2007, pages 334–340. Springer, 2007.
24. Rubenstein, M., Cornejo, A., and Nagpal, R.: Programmable self-assembly in a thousand-robot swarm. Science, 345(6198):795–799, 2014.
25. Seyfried, J., Szymanski, M., Bender, N., Estana, R., Thiel, M., and Wörn, H.: The i-swarm project: Intelligent small world autonomous robots for micro-manipulation. In International Workshop on Swarm Robotics, pages 70–83. Springer, 2004.
26. Cappelleri, D., Efthymiou, D., Goswami, A., Vitoroulis, N., and Zavlanos, M.: Towards mobile microrobot swarms for additive micromanufacturing. International Journal of Advanced Robotic Systems, 11(9):150, 2014.
27. Banerjee, A., Chowdhury, S., and Gupta, S. K.: Optical tweezers: autonomous robots for the manipulation of biological cells. IEEE Robotics & Automation Magazine, 21(3):81–88, 2014.
28. Thakur, A., Chowdhury, S., Švec, P., Wang, C., Losert, W., and Gupta, S. K.: Indirect pushing based automated micromanipulation of biological cells using optical tweezers. The International Journal of Robotics Research, 33(8):1098–1111, 2014.

29. Chowdhury, S., Jing, W., and Cappelleri, D. J.: Independent actuation of multiple micro-robots using localized magnetic fields. In Manipulation, Automation and Robotics at Small Scales (MARSS), International Conference on, pages 1–6. IEEE, 2016.
30. Chowdhury, S., Jing, W., and Cappelleri, D. J.: Towards independent control of multiple magnetic mobile microrobots. Micromachines, 7(1):3, 2015.
31. Ebefors, T., Mattsson, J. U., Kälvesten, E., and Stemme, G.: A walking silicon micro-robot. In Proc. Transducers 99, pages 1202–1205, 1999.
32. Mohebbi, M. H., Terry, M. L., Bohringer, K. F., Kovacs, G. T., and Suh, J. W.: Omni-directional walking microrobot realized by thermal microactuator arrays. In Proc. ASME. Int. Mechanical Engineering Congress and Exposition, pages 1–7, 2001.
33. Linderman, R. J. and Bright, V. M.: Optimized scratch drive actuator for tethered nanometer positioning of chip-sized components. In Proc. Transducers, pages 214–217, 2000.
34. Miura, H., Yasuda, T., and Shimoyama, I.: Insect-model based microrobot. Robotics and autonomous systems, 21(3):317–322, 1997.
35. Baglio, S., Castorina, S., Fortuna, L., and Savalli, N.: Development of autonomous, mobile micro-electro-mechanical devices. In Circuits and Systems, 2002. ISCAS 2002. IEEE International Symposium on, volume 4, pages IV–IV. IEEE, 2002.
36. Kummer, M. P., Abbott, J. J., Kratochvil, B. E., Borer, R., Sengul, A., and Nelson, B. J.: Octomag: An electromagnetic system for 5-dof wireless micromanipulation. IEEE Transactions on Robotics, 26(6):1006–1017, 2010.
37. Steager, E. B., Selman Sakar, M., Magee, C., Kennedy, M., Cowley, A., and Kumar, V.: Automated biomanipulation of single cells using magnetic microrobots. The International Journal of Robotics Research, 32(3):346–359, 2013.
38. Floyd, S., Pawashe, C., and Sitti, M.: An untethered magnetically actuated micro-robot capable of motion on arbitrary surfaces. In Robotics and Automation, 2008. ICRA 2008. IEEE International Conference on, pages 419–424. IEEE, 2008.
39. Jing, W., Chen, X., Lyttle, S., Fu, Z., Shi, Y., and Cappelleri, D. J.: A magnetic thin film microrobot with two operating modes. In Robotics and Automation (ICRA), 2011 IEEE International Conference on, pages 96–101. IEEE, 2011.

40. Jing, W., Pagano, N., and Cappelleri, D. J.: A tumbling magnetic microrobot with flexible operating modes. In Robotics and Automation (ICRA), 2013 IEEE International Conference on, pages 5514–5519. IEEE, 2013.
41. Jing, W., Pagano, N., and Cappelleri, D. J.: A novel micro-scale magnetic tumbling microrobot. Journal of Micro-Bio Robotics, 8(1):1–12, 2013.
42. Jing, W., Pagano, N., and Cappelleri, D. J.: A micro-scale magnetic tumbling micro-robot. In ASME 2012 International Design Engineering Technical Conferences and Computers and Information in Engineering Conference, pages 187–196. American Society of Mechanical Engineers, 2012.
43. Banerjee, A. G., Chowdhury, S., Losert, W., and Gupta, S. K.: Real-time path planning for coordinated transport of multiple particles using optical tweezers. IEEE Transactions on automation science and engineering, 9(4):669–678, 2012.
44. Chowdhury, S., Švec, P., Wang, C., Seale, K. T., Wikswo, J. P., Losert, W., and Gupta, S. K.: Automated cell transport in optical tweezers-assisted microfluidic chambers. IEEE Transactions on Automation Science and Engineering, 10(4):980–989, 2013.
45. Hu, S. and Sun, D.: Automatic transportation of biological cells with a robot-tweezer manipulation system. The International Journal of Robotics Research, 30(14):1681–1694, 2011.
46. Ju, T., Liu, S., Yang, J., and Sun, D.: Apply rrt-based path planning to robotic manipulation of biological cells with optical tweezer. In Mechatronics and Automation (ICMA), 2011 International Conference on, pages 221–226. IEEE, 2011.
47. Wu, Y., Sun, D., Huang, W., and Xi, N.: Dynamics analysis and motion planning for automated cell transportation with optical tweezers. IEEE/ASME Transactions on Mechatronics, 18(2):706–713, 2013.
48. Khalil, I. S., van den Brink, F., Sukas, O. S., and Misra, S.: Microassembly using a cluster of paramagnetic microparticles. In Robotics and Automation (ICRA), 2013 IEEE International Conference on, pages 5527–5532. IEEE, 2013.
49. Khalil, I. S., Magdanz, V., Sanchez, S., Schmidt, O. G., Abelmann, L., and Misra, S.: Magnetic control of potential microrobotic drug delivery systems: nanoparticles, magnetotactic bacteria and self-propelled micro-

- jets. In Engineering in Medicine and Biology Society (EMBC), 2013 35th Annual International Conference of the IEEE, pages 5299–5302. IEEE, 2013.
50. Mathieu, J.-B. and Martel, S.: Steering of aggregating magnetic microparticles using propulsion gradients coils in an mri scanner. Magnetic Resonance in Medicine, 63(5):1336–1345, 2010.
51. DeVon, D. and Bretl, T.: Control of many robots moving in the same direction with different speeds: a decoupling approach. In American Control Conference, 2009. ACC’09., pages 1794–1799. IEEE, 2009.
52. Kei Cheang, U., Lee, K., Julius, A. A., and Kim, M. J.: Multiple-robot drug delivery strategy through coordinated teams of microswimmers. Applied physics letters, 105(8):083705, 2014.
53. Kim, D., Liu, A., Diller, E., and Sitti, M.: Chemotactic steering of bacteria propelled microbeads. Biomedical microdevices, 14(6):1009–1017, 2012.
54. De Lanauze, D., Felfoul, O., Turcot, J.-P., Mohammadi, M., and Martel, S.: Three-dimensional remote aggregation and steering of magnetotactic bacteria microrobots for drug delivery applications. The International Journal of Robotics Research, 33(3):359–374, 2014.
55. Behkam, B. and Sitti, M.: Bacterial flagella-based propulsion and on/off motion control of microscale objects. Applied Physics Letters, 90(2):023902, 2007.
56. Martel, S., Mohammadi, M., Felfoul, O., Lu, Z., and Pouponneau, P.: Flagellated magnetotactic bacteria as controlled mri-trackable propulsion and steering systems for medical nanorobots operating in the human microvasculature. The International journal of robotics research, 28(4):571–582, 2009.
57. Becker, A., Ou, Y., Kim, P., Kim, M. J., and Julius, A.: Feedback control of many magnetized: *Tetrahymena pyriformis* cells by exploiting phase inhomogeneity. In Intelligent Robots and Systems (IROS), 2013 IEEE/RSJ International Conference on, pages 3317–3323. IEEE, 2013.
58. Sudsang, A., Rothganger, F., and Ponce, J.: Motion planning for disc-shaped robots pushing a polygonal object in the plane. IEEE Transactions on Robotics and Automation, 18(4):550–562, 2002.

59. Chiang, P.-T., Mielke, J., Godoy, J., Guerrero, J. M., Alemany, L. B., Villagomez, C. J., Saywell, A., Grill, L., and Tour, J. M.: Toward a light-driven motorized nanocar: Synthesis and initial imaging of single molecules. ACS nano, 6(1):592–597, 2011.
60. Becker, A., Onyuksel, C., Bretl, T., and McLurkin, J.: Controlling many differential-drive robots with uniform control inputs. The international journal of Robotics Research, 33(13):1626–1644, 2014.
61. Becker, A., Onyuksel, C., and Bretl, T.: Feedback control of many differential-drive robots with uniform control inputs. In Intelligent Robots and Systems (IROS), 2012 IEEE/RSJ International Conference on, pages 2256–2262. IEEE, 2012.
62. Donald, B. R., Levey, C. G., McGray, C. D., Paprotny, I., and Rus, D.: An untethered, electrostatic, globally controllable mems micro-robot. Journal of microelectromechanical systems, 15(1):1–15, 2006.
63. Paprotny, I., Levey, C., Wright, P., and Donald, B.: Turning-rate selective control: A new method for independent control of stress-engineered mems microrobots. Robotics: Science and Systems VIII, 2012.
64. Floyd, S., Diller, E., Pawashe, C., and Sitti, M.: Control methodologies for a heterogeneous group of untethered magnetic micro-robots. The International Journal of Robotics Research, 30(13):1553–1565, 2011.
65. Frutiger, D. R., Kratochvi, B. E., Vollmers, K., and Nelson, B. J.: Magmites-wireless resonant magnetic microrobots. In Robotics and Automation, 2008. ICRA 2008. IEEE International Conference on, pages 1770–1771. IEEE, 2008.
66. Becker, A., Habibi, G., Werfel, J., Rubenstein, M., and McLurkin, J.: Massive uniform manipulation: Controlling large populations of simple robots with a common input signal. In Intelligent Robots and Systems (IROS), 2013 IEEE/RSJ International Conference on, pages 520–527. IEEE, 2013.
67. Dubins, L. E.: On curves of minimal length with a constraint on average curvature, and with prescribed initial and terminal positions and tangents. American Journal of mathematics, 79(3):497–516, 1957.
68. Koester, D., Cowen, A., Mahadevan, R., Stonefield, M., and Hardy, B.: Polymumps design handbook. MEMSCAP Inc, 2003.

69. Majumdar, R., Foroutan, V., and Paprotny, I.: Post-release stress-engineering of surface-micromachined mems structures using evaporated chromium and in-situ fabricated reconfigurable shadow masks. In Micro Electro Mechanical Systems (MEMS), 2015 28th IEEE International Conference on, pages 296–299. IEEE, 2015.
70. Akiyama, T. and Shono, K.: Controlled stepwise motion in polysilicon microstructures. Journal of Microelectromechanical Systems, 2(3):106–110, 1993.
71. Nathanson, H. C., Newell, W. E., Wickstrom, R. A., and Davis, J. R.: The resonant gate transistor. IEEE Transactions on Electron Devices, 14(3):117–133, 1967.
72. Graham, R. L., Knuth, D. E., Patashnik, O., and Liu, S.: Concrete mathematics: A foundation for computer science. Computers in Physics, 3(5):106–107, 1989.

VITA

Vahid Foroutan

Education	B.S., Computer Engineering (Hardware)	2001 – 2006
	Central Tehran Branch, Islamic Azad University, Tehran, Iran	
	M.S., Computer Engineering (Computer Architecture)	2006 – 2008
	Science and Research Branch, Islamic Azad University, Tehran, Iran	
Publications	Ph.D., Computer Engineering (Computer Architecture)	2008 – 2011
	Science and Research Branch, Islamic Azad University, Tehran, Iran	
	Ph.D., Electrical and Computer Engineering	2012 – 2018
	University of Illinois at Chicago	
Publications	Ward, S., Foroutan, V. , Majumdar, R., Mahdavi pour, O., Hussain, S. A., and Paprotny, I., “Towards Microscale Flight: Fabrication, Stability Analysis and Initial Flight Experiments for $300\mu m \times 300\mu m$ Sized Untethered Microfliers”, IEEE Transaction on NanoBioscience, 14(3): 323-331, 2015.	
	Foroutan, V. , Taheri, M., Navi, K., Azizi Mazreah, A., “Design of Two Low-Power Full Adder Cells Using GDI Structure and Hybrid CMOS Logic Style”, Integration, the VLSI Journal, 47(1): 48-61, 2014.	
	Navi, K., Foroutan, V. , Rahimi Azghadi, M., Maeen. M., Ebrahim-pour, M., Kaveh, M., Kavehei, O., “A novel low-power full-adder cell with new technique in designing logical gates based on static CMOS in-verter”, Integration, the VLSI Journal, 40(10): 1441-1448, 2009.	
	Navi, K., Maeen. M., Foroutan, V. , Timarchi, S., Ebrahimpour, M., Kavehei, O., “A Novel low-power full-adder cell for low voltage”, Integration, the VLSI Journal, 42(4): 457-467, 2009.	
	Maeen. M., Foroutan, V. , Mazloomnejad, B., and Navi, K., Bahrololoumi, Sh., Hashempour, O., Haghparast, M., “A six transistors full adder”, IE-	

ICE Electronics Express, 6(16): 1148-1154, 2009.

Navi, K., **Foroutan, V.**, and Navi, K., “On the design of low power 1-bit full adder cell”, World Applied Sciences Journal, 4(1): 142-149, 2008.

Foroutan, V., Farzami, F., Erricolo, D., Majumdar, R., and Paprotny, I., “SAT-C: An Efficient Control Strategy for Assembly of Heterogeneous Stress-Engineered MEMS Microrobots”, International Conference on Robotics and Automation (ICRA), 2018.

Foroutan, V., Farzami, F., Erricolo, D., and Paprotny, I., “Efficient Constant-Time Addressing Scheme for Parallel-Controlled Assembly of Stress-Engineered MEMS Microrobots”, International Conference on Control, Automation and Robotics (ICCAR), 2018.

Foroutan, V., Majumdar, R., Mahdavi-pour, O., Ward, S., and Paprotny, I., “Levitation of Untethered Stress-Engineered Microflyers using Thermophoretic (Knudsen) Force”, Solid-State Sensors, Actuators and Microsystems Workshop, Hilton Head Island, 2014.

Majumdar, R., **Foroutan, V.**, and Paprotny, I., “Post-Release Stress-Engineering of Surface-Micromachined MEMS Structures using Evaporated Chromium and In-Situ Fabricated Reconfigurable Shadow Masks”, IEEE International Conference on Micro Electro Mechanical Systems, 2015.

Majumdar, R., **Foroutan, V.**, and Paprotny, I., “Tactile Sensing and Compliance in MicroStressbot Assemblies”, SPIE Defence Security and Sensing, 2014.

Awards

Winner of 2016-2017 Provost’s Award for graduate research, November 2016.

Winner of 2015-2016 FMC Technologies, Inc., March 2015.

Best Paper in Top 25 Hottest Articles in 2014. (Integration, the VLSI Journal), December 2014.

Recipient of Hilton Head Solid-state, Actuators and Microsystems Workshop travel Award 2014, June 2014.

Recipient of Graduate Student Presenter Award by the University of Illinois at Chicago 2014, September 2014.

Best Paper in Top 25 Hottest Articles in July to September 2009. (Integration, the VLSI Journal), September 2009.

First rank in Computer Engineering Ph.D. entrance exam (IRAN), 2006.

Presentations Conference Presentations at Solid-Sate Sensors, Actuators and Microsystems Workshop, Hilton Head Island, 2014

Poster Presentations at International Conference on Control, Automation and Robotics (ICCAR), Auckland, New Zealand, 2018

Memberships IEEE Member

Services Journal Article Referee at IEEE Transactions on Very Large Scale Integration (VLSI) Systems

Journal Article Referee at IEEE Transaction on Circuit and Systems I (TCAS)

Journal Article Referee at IET: The Journal of Engineering (JOE)

Journal Article Referee at Elsevier International Journal of Electrical Power and Energy Systems (IJEPES)

Journal Article Referee at Journal of Circuits, Systems, and Computers (JCSC)

Journal Article Referee at Arabian Journal for Science and Engineering (AJSE)

Experience Research Assistant at University of Illinois at Chicago 2012 – 2018
Summer Intern at Intel PSG (Altera) May 2016 – Aug 2016
Adjunct Lecturer at Islamic Azad University 2008 – 2010

VITA (Continued)

106

Teaching Assistant at University of Illinois at Chicago	2012 – 2018
---	-------------